HVOF Thermal Spray TiC/TiB_2 Coatings for AUSC Boiler/Turbine Components for Enhanced Corrosion Protection

Final Scientific/Technical Report

Report Start Date – 9/1/2012

Report End Date – 8/31/2016

Authors:

Kanchan Mondal
Rasit Koc

Date Issued:

December 7th 2016

DOE Award Number:

DE-FE0008864

Name and Address of Submitting Organization

Board of Trustees, Southern Illinois University, Carbondale
Office of Sponsored Projects Administration, MC 4709
Carbondale, IL 62901

Subcontractor

Chinbay Fan
Gas Technology Institute
1700 S Mt Prospect Rd, Des Plaines, IL 60018

DISCLAIMER

ABSTRACT

The high temperatures of operations still pose significant risk of degradation and fatigue from oxidizing, corroding and eroding environment. In addition to unused O_2, water from combustion and SO_x from the coal sulfur oxidation that result in highly corrosive environment, acid gases such as HCl and other sulfur compounds may also be present. These adverse effects are further accelerated due to the elevated temperatures. In addition, ash particulates and unburnt carbon and pyritic sulfur can cause erosion of the surface and thus loss of material. Unburnt carbon and pyritic sulfur may also cause localized reduction sites. Thus, fireside corrosion protection and steam oxidation protection alternatives to currently used Ni-Cr overlays need to be identified and evaluated. Titanium carbide (TiC) is a suitable alternative on account of the material features such as the high hardness, the high melting point, the high strength and the low density for the substitution or to be used in conjunction with NiCr for enhancing the fireside corrosion and erosion of the materials. Another alternative is the use of titanium boride as a coating for chemical stability required for long-term service and high erosion resistance over the state-of-the-art, high fracture toughness (K_{1C} ~12 $MPam^{1/2}$) and excellent corrosion resistance (k_p~1.9X10^{-11} $g^2/cm^4/s$ at 800^oC in air).

Southern Illinois University in collaboration with Gas Technology Institute conducted a four-year program to verify the suitability of the novel use of TiC and TiB_2 powders produced by a low temperature patented process and coated on high creep strength materials by a proven HVOF process, to support commercial adoption in AUSC coal fired power plants. The coatings showed the potential of answering technical challenges posed by the high temperatures and corrosive environment resulting from sulfur species in the gas stream and in the ash and from the failure of the oxide scale in the repeated heating–cooling treatment and cycling of oxidizing-reducing conditions. The overarching aim of the research endeavor was to synthesize oxidation, corrosion and wear resistant TiC and TiB_2 coatings on existing boiler materials for applications at high temperatures (500 -750 ^oC) using the HVOF process and demonstrated the feasibility of these coating to be used in AUSC boilers and turbines.

Accomplishments

Air oxidation, Steam and air corrosion, Simulated ash and Simulated flue gas corrosion studies were performed on coated coupons to optimize the range of conditions for the coating process. The project was largely successful in demonstrating the ability of Ti based coatings to provide corrosion protection in AUSC boiler conditions and be considered an alternate to the expensive, thick weld overlay of NiCr coatings. The main bottleneck is the identification of optimized HVOF coating parameters for dense uniform coatings.

Achievements:

a) Facile synthesis of TiC and TiB_2 nanosized powders with narrow size distribution.
b) HVOF thermal spray coating of these powders on 304 H, 430 and P91 substrates.
c) Corrosion characterization of the coated substrates that increased the longevity of the substrate subjected to fireside corrosion and steam side oxidation in AUSC boiler tubes.

Contents

EXECUTIVE SUMMARY

Supercritical Rankine cycles facilitate the attainment of higher efficiencies and lowered emissions. The high temperatures and enhanced reactivity of supercritical water still pose significant risk of degradation and fatigue from oxidizing, corroding and eroding environment. In addition, ash particulates and unburnt carbon and pyritic sulfur can cause erosion of the surface and thus loss of material. Unburnt carbon and pyritic sulfur may also cause localized reduction sites TiC and TiB_2 are suitable coating alternatives on account of the material features such as the high hardness, the high melting point, the high strength, low density and chemical stability required for long-term service. The report summarizes the findings of the research endeavors to characterize the corrosion resistance performance and characteristics of TiC and TiB_2 coatings on an austenitic (304H) and a high Cr ferritic (430) and a low Cr ferritic (P91) steels. The non oxide ceramics of titanium were produced by a patented carbothermal process that reduces the cost of production by nearly 50 % as compared to current commercial processes. The coatings were applied by HVOF thermal spray coating method. The materials may have applications as boiler materials exposed to high temperatures (500 -750 ^oC) and high pressures (~350 bars) expected in in AUSC boilers and turbines.

The specific objectives of the proposed project are a) synthesis of nanoparticles of TiC by a patented process, b) extension of the process to synthesize nanosized TiB_2 powder, c) optimization of HVOF spray coating of the TiC and TiB_2 on select ferritic, austenitic and nickel alloy samples generally used for waterwall tubing, high temperature boiler sections, turbine blades and USC tubing applications, d) laboratory evaluation of the corrosion resistance of the coatings employing simulated flue gas and simulated ash, e) selection of optimum alloy protection system in different temperature/chemical regimes and f) field evaluation of fabricated probes of select coating in actual boiler/turbine environment.

Corrosion studies conducted under this project includes air oxidation studies, steam and air oxidation studies to simulate both steam side and air side corrosion and ash corrosion studies and flue gas corrosion studies to simulate the fireside corrosion conditions. The samples were exposed to the relevant environments for 180, 360 and 800 hrs (approx. over 1 week, two weeks and 1 month) and the pre and post exposure samples were analyzed for mass change, phase changes on the surface, morphological changes, oxygen and sulfur content on the surface and diffusion into the substrate as a function of depth. The impact of coating and exposure to the various alloying materials were also analyzed.

The TiC, TiB_2 and the Ti metals were successful in retarding the deterioration of the substrate due to the corrosive environment they were exposed to during these tests. The most corrosive environment was that of the simulated ash using a mixture of alkali chlorides and sulfates which are known to be molten in the temperature range of interest (600 – 750 ^oC) followed by the simulated flue gas conditions. The flue gas composition mimicked the flue gas obtained from a PC boiler combusting Illinois coal. Of the three coating choices, TiB_2 provided the least protection although the difference was not significantly low. The TiC and the Ti metal coatings performed equally well although the commercially obtained Ti metal coated the substrate more uniformly. Since Ti metal is more than 10 fold more expensive than the synthesized TiC nanoparticles, TiC synthesized from 32 % or 33 % C coated TiO_2 and carburized for two hours at 140 or 1500 ^oC is recommended as the coating for these materials.

The coatings limited the penetration of oxygen into the substrates ranged from negligible to a few micrometers even after 800 hrs of exposure while oxygen penetration into the uncoated substrates, especially the ferritic steels, were several micrometers after 180 hrs of exposure. In the coated substrate, the oxygen penetration was largely due to the non-uniform coating applied and thus the HVOF coating process needs to be further tuned. Currently, an oxidant fuel mixture comprising of oxygen and hydrogen with a flame temperature of 2500 ^{o}C is optimal. In addition to the coating powder composition, coating time, distance of the substrate, and carrier gas flow rates affect the coating quality. Nonetheless, in most of these cases (even the low Cr steel), the oxygen penetration progress was retarded by the diffusion of chromium towards the surface and forming a protective chromium oxide layer. The presence of the titanium based coating on the surface prevented the evaporation of the chromium and thus acting not only as a barrier to the oxygen from attacking the substrate but providing a second line of defense by not allowing the protective chromium to be lost. As a result, little or no difference in the oxidation between the 180 hr and 800 hr exposures was observed in many cases. The presence of both steam and oxygen was found to be more corrosive. However, the TiC coated materials showed little deterioration in terms of surface roughening, coarsening, spalling, and oxygen penetration, when compared to the bare substrates or with the ones coated with Ti metal or TiB_2.

In general, it was found that coated surface contained titanium oxides (TiO_2 and Ti_3O_5) in addition to the original precursor. This is probably due to the high temperature and presence of oxygen during the coating. There is an increase in the oxygen content in the coating after exposure although TiC is also identified as a phase in the post exposure coats when TiC was used as the coating material. Based on the several tests, it is hypothesized that the coating itself is oxidized initially but the oxide layer is non-porous and does not allow further penetration of the oxygen.

In the case of sulfur attack, whether due to the sulfates in the ash or the SO_2 in the flue gas, it was found that the sulfur tends to associate with the iron where it is not exposed to the oxygen. In coated substrates with bare surfaces, it was found that the sulfur was associated with the iron on the surface but that the sulfur was concentrated to the edges of the coated section bonded with the iron. Thus, a uniform dense coating should prevent corrosion due to sulfur based components. The most exciting finding was that coatings performed extremely well against the attack by the sulfates, chlorides, sulfates and trisulfates of alkali metals. The bare substrates formed micro cracks in the early stages of the attack and completely disintegrated by 800 hrs, the TiC coated substrates were not deteriorated.

In summary, dense, uniform TiC coatings may offer an inexpensive but robust alternative to NiCr weld overlays. The 48 month project gained several insights into the corrosion of the substrates and corrosion prevention mechanisms by which the coatings afford protection under severe conditions. In addition, the TiC powder synthesis was also characterized due to the needs that arose during this process. Thus broadly, we have been able to achieve the following.

a) Facile synthesis of TiC and TiB_2 nanosized powders with narrow size distribution.
b) HVOF thermal spray coating of these powders on 304 H, 430 and P91 substrates.
c) Corrosion characterization of the coated substrates that increased the longevity of the substrate subjected to fireside corrosion and steam side oxidation in AUSC boiler tubes.

INTRODUCTION

In order to sustain the global growth experienced currently, the appetite for energy is going to continually increase. To meet this demand, it is projected that coal based power plants will continue to play a major role. Coupled with this demand for energy is an increase in the public awareness regarding the need to maintain clean water and air leading to the development of the ISO 50001 protocol that calls for sustainable energy management. Therefore, to maintain coal as an integral part of the sustainable energy solution, it is necessary to enhance the efficiency of these power plants (to reduce resource depletion and emissions) and to find low cost environmental compliance solutions. Figure 1 shows the improvements in both efficiency and CO_2 emission obtained by the use of advance cycles over the conventional subcritical cycles.

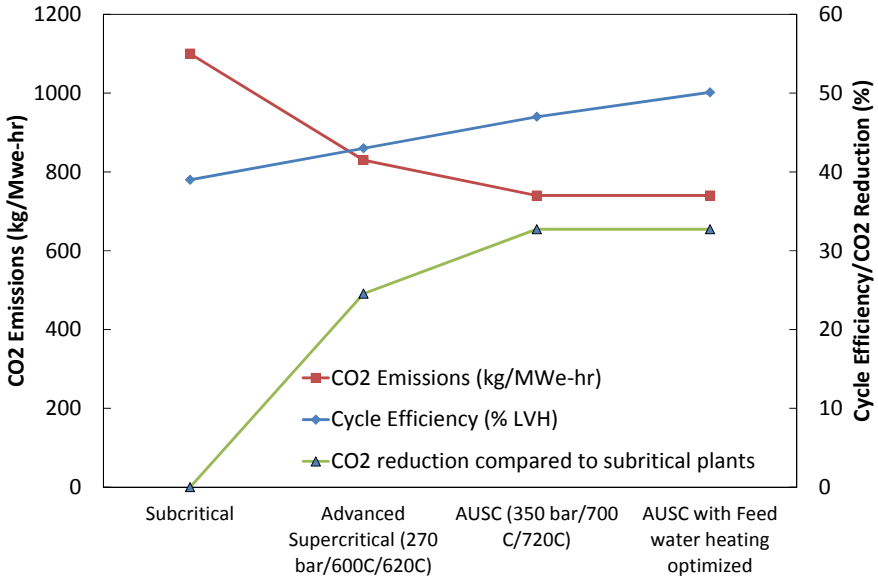

Figure 1. Efficiency improvements and CO_2 reduction.

The report presents the finding of the research on the development of materials for one such technology solution – namely the Advanced UltraSupercritcal (AUSC) cycle. It has been estimated that an increase in the efficiency of these AUSC systems by 10 % can result in over 20 % reduction in emissions when compared to the conventional subcritical steam power plants. Worldwide, more than a dozen plants are operating at steam conditions close to 593°C (1100°F)/27 MPa (4000 psi and plant operation at 620°C (1150°F) and may be viewed as a near-term possibility. The AUSC power plants are expected to operate at around 760 °C and 350 bars. While these power plants are feasible to operate, one of the bottlenecks are the materials needed for safe design at these conditions. The material issues critical to safe operations are mechanical properties such as creep rupture strength, resistance to steam-side oxidation and fireside corrosion, good thermal conductivity, low coefficient of expansion, and manufacturing process issues such as

weldability and fabricability. Past studies[1,2,3,4,5,6,7,8,9] funded by US DOE under the Vision 21 plan had made significant headway in the development of such materials for use under high pressures and temperatures especially in terms of the creep strength. Ferritic alloys were found to be suitable for the heavy boiler sections experiencing low temperatures and water wall tubings, austenitic alloys were found to be suitable for tubular applications and nickel alloys were found to be suitable for heavy boiler sections experiencing high temperatures and for tubular sections in general. Ferritics and some of the austenitics are commercially available while some of the austenitics such as Sanicro 25 have been validated but not yet codified. On the other hand, most of the nickel alloys for supercritical applications are still being validated. Figure 2 shows the creep rupture strength vs. temperature of some of the suitable components.

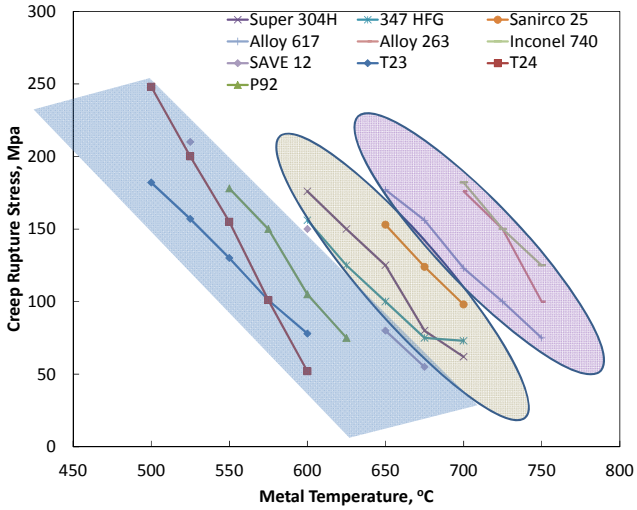

Figure 2. Creep rupture test vs temperature for the ferritic, austenitic and super alloys.

[1] R. Viswanathan, "U.S. Program on Materials Technology for USC Power Plants", Proceedings from the Fourth International Conference on Advances in Materials Technology for Fossil Power Plants, October 2004

[2] J.L. Blough, G. J. Stanko, M. T. Krawchuk, "Superheater Corrosion in Ultra-Supercritical Power Plants, Long-Term Field Exposure at TVA's Gallatin Station," Palo Alto, CA: Electric Power Research Institute, February 1999. TR-111239

[3] J. L. Blough, M. Krawchuk, G. J. Stanko, W. Wolowodiuk, "Superheater Corrosion: Field Test Results," Palo Alto, CA: Electric Power Research Institute, November 1993. TR-103438

[4] W. Wolowodiuk, S. Kihara, and K. Nakagawa, "Laboratory Coal Ash Corrosion Tests," Palo Alto, CA: Electric Power Research Institute, July 1989. GS-6449

[5] J. L. Blough, W. W. Seitz, A. Girshik, "Fireside Corrosion Testing of Candidate Superheater Tube Alloys, Coatings, and Claddings – Phase II Field testing," Oak Ridge, TN: Oak Ridge National Laboratory, June 1998. ORNL/Sub/93-SM401/02

[6] H. Hack, G. S. Stanko, "Fireside Corrosion Resistance of Advanced Materials for Ultra-Supercritical Coal-Fired Plants," 22nd Annual International Pittsburgh Coal Conference, September 2005

[7] H. Hack, G. S. Stanko, "Update on Fireside Corrosion Resistance of Advanced Materials for Ultra-Supercritical Coal-Fired Power Plants," The 31st International Technical Conference on Coal Utilization & Fuel Systems, May 21-25, 2006, Clearwater, Florida, USA

[8] H. Hack, G. S. Stanko, "Experimental Results for Fireside Corrosion Resistance of Advanced Materials in Ultra-Supercritical Coal-Fired Power Plants", The 32nd International Technical Conference on Coal Utilization & Fuel Systems, June 10 – 15, 2007, Clearwater, Florida, USAY

[9] R. Vishwanathan, W. Bakkar, Materials for Ultrasupercritical Coal Power Plants—Boiler Materials: Part 1, Journal of Materials Engineering and Performance, Volume 10, No. 1, 81-95, 2001

The high temperatures of operations still pose significant risk of degradation and fatigue from oxidizing, corroding and eroding environment. In addition to unused O_2, water from combustion and SO_x from the coal sulfur oxidation that result in highly corrosive environment, acid gases such as HCl and other sulfur compounds may also be present. These gases create a corrosive environment that is further accentuated due to the elevated temperatures. In addition, ash particulates and unburnt carbon and pyritic sulfur can cause erosion of the surface and, thus, loss of material. Unburnt carbon and pyritic sulfur may also cause localized reduction sites. As a result, fireside corrosion protection and steam oxidation protection alternatives to currently used, expensive Ni-Cr overlays need to be identified and evaluated.

It has been well established that materials provide a bottleneck for long term applicability of AUSC technology. A US DOE funded consortium consisting of EPRI, Energy Industries of Ohio, Alstom Power, Babcock and Wilcox, Foster Wheeler Development Corporation, ORNL and Riley Power[1, 9, 10] conducted a comprehensive study of materials that would be suitable for various components in SC and USC technologies. The studies were focused extensively and primarily on mechanical properties. As for the material degradation issues, it was reported that the Inconel-622, -52, and -72 weld overlays and laser clad 50/50 performed better in terms of corrosion resistance when compared to the wrought alloys while the best performance was obtained from the chromed coating followed by SiCr and AlCr coating. The study focused on improving the corrosion resistance by increasing the chromium content. The team identified the temperature range of 600 – 750^oC to exhibit the worst corrosion in all the materials. They correctly attributed this observation to the existence of liquid trisulfates. At lower temperatures, the trisulfates are solid and at higher temperatures, they vaporize. Thus, this temperature range would be critical for evaluation of fireside corrosion.

Mandated NO_x emission reduction requirements have led to the introduction of staged combustion which in turn resulted in the use of sub-stoichiometric air to fuel ratio with additional air being supplied in the overfire burner ports. This in particular have led to (documented) severe corrosion in the waterwall tubing in the existing subcritical boilers and this problem is only expected to be accentuated in AUSC boilers. It appears that the problem is the dual effect of H_2S and CO mixing with air in the overfire ports and the presence of pyritic ash resulting in alternating oxidizing and reducing conditions. Thus, there is a need for an inexpensive coating technology for alleviating the issue of corrosion. Therefore, other than careful boiler design, selection of materials used is also critical.

Research with regard to improving high temperature corrosion and erosion resistance of materials has been conducted, and various attempts were reported. Methods for improving high temperature corrosion resistance mainly fall into two categories: (1) addition of beneficial elements to the substrate, such as Ni, Cr, and Al to act as diffusion barriers, to form a continuous oxidation layer to improve adherence of the oxidation layer[11, 12, 13, 14], and (2) application of protective coating onto the substrate, such as Zr, Si, Al, and Ti based coatings. For addition of beneficial elements, it has

[10] R.Viswanathan, R.Purgert, S.Goodstine, J.Tanzosh, G.Stanko, J.P. Shingledecker, B.Vitalis, U.S. Program on Materials Technology for Ultrasupercritical Coal-Fired Boilers, Advances in Materials Technology for Fossil Power Plants: Proceedings of the 5th International Conference, 2008

[11] S. Chevalier, P. Juzon, G. Borchardt, A. Galerie, K. Przybylski, and J. P. Larpin, Oxidation of Metals, 2010, vol.73, pp.43-64

[12] Z. G. Zhang, F. Gesmundo, P. Y. Hou, and Y. Niu, Corrosion Science, 2006, vol.48, pp.741

[13] B. A. Pint, Oxidation of Metals, 1996, vol.45, pp.1-37

[14] W. J. Quadakkers and L. Singheiser, Materials Science Forum, 2001, vol.77, pp.369–372.

been reported that alloy steels with low amount of Cr addition (less than 3% Cr) can improve oxidation resistance of the steels at temperature below 580^0C. However, spallation was observed at longer operation time[15],[16]. Increasing Cr content in austenitic stainless steels significantly improved oxidation resistance of steels, as an uniform thin Cr_2O_3 protective layer was formed directly on the surface of the steel, and greatly reduced oxidation rate of the substrate[17],[18], . Improvement of corrosion resistance by means of applying protective coating using coating methods such as CVD, PVD, Sol-Gel, weld overly, laser cladding, and HVOF was also widely reported[1920212223242526]. Al_2O_3/ZrO_2 coating was reported to have reduced oxidation rate of Ti-Al based alloy by restricting oxygen diffusion at the surface of the alloy. The coating also eliminated cracks and spallation of oxidation layer formed on the alloy[27]. Inconel 625 cladding was also proven to help corrosion resistance of steels at temperature below 400 ^oC[28], but the corrosion resistance ability decreases at higher temperature. However, cost is another issue with Inconel 625 cladding. Other than cladding, weld overlay and HVOF were also common method of applying corrosion resistance coating on substrates. While weld overlay can be used under severe corrosion environment, repeated overlay process may lead to embrittlement of the coating.

One of the causes for continuous corrosion of metal at corrosive environment is the spallation of oxidation scales or protective coatings. For example, magnetite formed on surface of steels are usually porous, and vacant space tend to occur at the interface of magnetite and substrate, which leads to exfoliation of the magnetite[29] . Spallation of oxide layer of γ-TiAl alloy was also observed during 1000^0C cyclic oxidation test. It was reported that the spallation of oxide layer caused increase of oxidation rate of the γ-TiAl alloy[19].

Titanium carbide (TiC) has been investigated as a suitable alternative on account of the material features such as the high hardness, the high melting point, the high strength and the low density for the substitution or to be used in conjunction with NiCr for enhancing the fireside corrosion and erosion of the materials. Another alternative is the use of titanium boride as a coating for chemical stability required for long-term service and high erosion resistance over the state-of-the-art, high

[15] R. Viswanathan, J. Sarver, and J.M. Tanzosh, ASM International, 2006, vol.15, pp. 255-274
[16] P. Mayer and A.V. Manolescu, High Temperature Corrosion, R.A. Rapp, Ed., NACE, 1983, pp.368-379
[17] N. Otsuka and H. Fujikawa, Corrosion, 1991, vol.47, issue 4, pp.240-248
[18] Izumi K, Murakami M, Deguchi T l, J Am Ceram Soc, vol.72, pp.1246-1248
[19] E. N'Dah, S. Tsipas, F. J. Bolıvar, M. P. Hierro, and F. J. Pe´rez, Oxidation of Metals, 2008, vol.69, pp.77-94
[20] M. Guglielmi, D. Festa, P.C. Innocenzi, P. Colombo and M. Gobbin, Non-Cryst Solids, 1992, vol. 147-148, pp.474-477
[21] M. Guglielmi, D. Festa, P. Innocenzi, L. Mancinelli Degli, Esposti, N. Maliavski and E. Tchekounova, Cer Acta, 1995, vol.7, pp.31
[22] Z. Li, W. Gao, M. Yoshihara, Y. He: Materials Science and Engineering A, 2003, vol.347, pp. 243-252
[23] W. Gao, Z. Li, "Nano-Structured Alloy and Composite Coatings for High Temperature Applications", Materials Research, VOl 4, No. 1, 175-182, 2004
[24] K. Mo, G. Lovicu, H. M. Tung, X. Chen, and J. F. Stubbins: Journal of Engineering for Gas Turbines and Power, 2011, Vol.133, 052908-9
[25] T.S. Sidhu, S. Prakash, and R.D. Agrawal: ASM International, 2006, vol.15, pp.811-816
[26] N. Espallargas, J. Berget, J. M. Guilemany, A. V. Benedetti, P. H. Suegama: Surface & Coatings Technology, 2008, vol.202, pp.1405-1417
[27] X. J. Zhang, Q. Li, S. Y. Zhao, C. X. Gao and Z. G. Zhang, Journal of Sol-Gel Science and Technology, 2008, vol.47, pp.107-114
[28] W. Spiegel, CheMin GmbH, Augsburg, Germany, 2002
[29] Maria Oksa, Erja Turunen, Tomi Suhonen, Tommi Varis and Simo-Pekka Hannula, coatings, 2011, vol.1, 17-52

fracture toughness (K_{1C} ~12 $Mpam^{1/2}$) and excellent corrosion resistance (k_p~1.9X10^{-11} $g^2/cm^4/s$ at 800^{o}C in air).

Among the previously mentioned coating materials, TiC and TiB_2 are also suitable coating alternatives on account of the material features such as the high hardness, the high melting point, the high strength, low density and chemical stability required for long-term service. TiC and TiB_2 were proven to have good corrosion resistance. Voitocich[30] [had found that no significant weight gain was observed for TiC up to 800^{0}C, and only slight oxidation was observed. Berger et al.[31] [also found that TiC is among one of the most oxidation resistance carbide from the result of their research.

	Melting Temp	Density	Hardness	Young's
	°C	g/cm^3	GPa	GPa
TiC	3070	4.65	28	456
TiB_2	2900	4.5	34	570
B_4C	2500	2.52	38	450

HVOF (High velocity oxy-fuel) thermal spray method is known for formation of dense, low porosity, homogeneous and low microstructure coating with high adhesiveness. In HVOF thermal spray method, coating is formed by combusting coating material powder with fuel and oxygen in a combustion chamber, which generates a supersonic flow of melted or half-melted coating powder particles through the nozzle of the HVOF system to destination substrate. As previously mentioned, spallation of scale is one of the main corrosion issues for either alloys and corrosion resistance coatings, HVOF has thus become a highly desired coating method for oxidation resistance layer. The dense coating formed by HVOF thermal spray is also desired for restricting access of chlorine from salt containing environment, and thus improved salt corrosion resistance.

Gao and Li[23, 32] reported that Ti-Al/Ti-C coatings provided excellent spallation resistance at these temperatures. Bankiewizc et al[33] evaluated three commercially available steels, namely low-alloy steel (10CrMo9-10), austenitic stainless steel (AISI347), and high nickel austenitic stainless steel (S28) for molten salt induced corrosion in the presence of synthetic ash comprised of $ZnCL_2$-KCl-K_2SO_4 at temperatures in the range of 300 -600 ^{o}C. They reported that the corrosion rates were accelerated with an increase in the chloride content in the melts. Chang[34] studied the isothermal and cyclic oxidation behavior of Ti-Al alloys and reported than the microstructure of the oxide scale was an outer scale of fast-growing TiO_2 and an internal scale of Al_2O_3. However, Al_2O_3 did not form a continuous barrier. The formation of TiO_2 and discontinuity in the Al_2O_3 scales would make a coating of this material rather corrosion prone and would not be a suitable coating material for fireside corrosion protection or for corrosion protection in the waterwall tubing. Zhang et al reported the improvement of oxidation resistance of Ti-Al alloys by a coating of alumina –zirconia. Chevalier et al[11] studied the high temperature oxidation behavior of Fe_3Al and Fe_3Al-Zr intermetallic compounds and showed that the presence of Zr improved the adherence of α-Al_2O_3

[30] R. F. Voitovich and É. A. Pugach, Soviet Powder Metallurgy and Metal Ceramics, 1972, vol.11, issue 2, pp.132-136

[31] Berger, L. M., P. Vuoristo, T. Mantyla, and W. Gruner, ASM International, 1998, pp.75-82

[32] W. Gao, Z. Li, "Nano-Structured Alloy and Composite Coatings for High Temperature Applications"International Symposium on High Temperature Corrosion in Energy Related Systems, Angra dos Reis - RJ, September 2002

[33] D. Bankiewicz, P. Yrjas, and M. Hupa, High-Temperature Corrosion of Superheater Tube Materials Exposed to Zinc Salts, *Energy & Fuels 23,* 3469–3474, 2009

[34] S.Y. Chang, The Isothermal and Cyclic Oxidation Behavior of a Titanium Aluminide Alloy at Elevated Temperature, Journal of Materials Engineering and Performance, 16, 508-514, 2007

scale. D'Nah et al[35] studied the oxidation resistance of Al-Mn coating on P92 ferritic steel. They found that while good resistance was provided by the coating, the processing method was critical to the obtained resistance of the coating. A brittle coating would cause it to crack under thermal cycling and become prone to corrosion. Mo et al[24] studied the corrosion resistance of Alloys 230 and 617 and found that both alloys suffered from internal oxidation during high temperature corrosion in air studies. Mobin and Hasan[36] conducted in depth studies on the corrosion reaction between metal oxide (Al_2O_3 and Cr_2O_3) and molten salts (sodium sulfate).

Fukuda et al[37] reported that NiCrSiB alloy HVOF coatings and Inconel 625 plasma sprayed coatings have been used successfully on waterwall tubes in waste incinerators while TiO_2-Al_2O_3/Inconel 625 cement HVOF coatings were applied on superheater tubes for long term durability. Past studies have also shown that high velocity oxy-fuel (HVOF) thermal spray coatings with good wear resistance can be produced from Ni(Cr)-TiC powders manufactured by self-propagating high temperature synthesis (SHS) reactions. We plan to use the process patented by Koc[10-12] for the production of the powders and subsequently use HVOF spray coating technique.

Chun et al[38] studied the erosion and corrosion resistance of titanium diboride cermets and found that the corrosion rates in the temperature range of concern was nearly of the order of magnitude observed for Ni-Cr coating (particularly within the range where protection is provided Cr_2O_3 growth. However, the corrosion studies were conducted to simulate fluid catalytic cracking conditions and not USC conditions. The TiB_2 itself has corrosion rates that are an order higher to those of Ni-Cr.

Based on the above discussion, it is quite clear that there is a need for enhanced corrosion protection at higher temperatures especially from coal ash corrosion. Current measures include overlays of NiCr alloys, diffusion coating of M-Cr alloys and laser cladding to increase the chromium content. However, carburization due to CO disproportionation or unburnt carbon will adversely affect chromium protection. Amongst the alternate high temperature materials discussed, titanium diboride has shown to provide reasonable protection under FCC conditions.

OBJECTIVES

The overall goal of this project was to evaluate the suitability of TiC and TiB_2 coatings for providing corrosion protection under AUSC boiler conditions.

[35] E. N'Dah, S. Tsipas, F. J. Bolı´var, M. P. Hierro, F. J. Pe´rez, Improvement of 9% Ferritic Steel Against Cyclic Oxidation by CVD-FBR Al–Mn Coating, Oxid Met . 69, 77–94, 2008

[36] M. Mobin, S. K. Hasan. Studies on high temperature corrosion reactions involving metal oxides and sodium sulfate, Anti-Corrosion Methods and Materials, Vol. 55 · No 3 123–129, 2008

[37] Fukuda, K. Kawahara, and T. Hosoda, Application of High Velocity Flame Sprayings for Superheater Tubes in Waste Incinerators, Corrosion p 00264.1-00264.14, 2000

[38] C M Chun, N-R V. Bangaru, N. Thirumalai, Erosion–Corrosion-Resistant Titanium Diboride Cermets for High-Temperature Process Applications, Int. J. Appl. Ceram. Technol., Vol 5 No. 6, 597–609, 2008

EXPERIMENTAL

Figure 3 shows the approach adopted for this research.

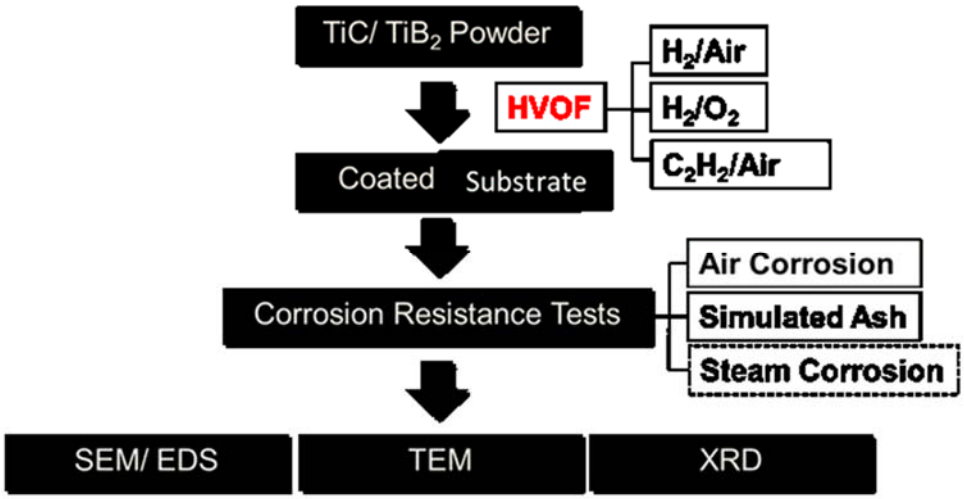

Figure 3. Experimental Approach

Synthesis of TiC and TiB_2:

Synthesis of TiC and TiB_2 was conducted using a patented process described by Koc et al[39][40][41]and shown in Figure 4. Type P-25 Degussa titania nanoparticles were used as starting powder for the carbothermal process. Figure 5 is the XRD of the acquired titania. The powders were then reacted with propylene (C_3H_6, purity of 99.5%) in a split furnace (Carbolite, Watertown, WI) consisting of 10cm ID x 35cm long stainless steel vessel (Figure 6) at 600^{o}C to form carbon coated titania powders. Pyrolysis of propylene (cracking) occurs at 500^{0}C, and the cracked propylene served as source of carbon for the coating process of titania. The carbon content of the coated titania was controlled by numbers of reaction cycles in the split surface. Final composition of the coated titania was controlled at 32-33 wt.%. The carbon coated titania then served as precursor for both the synthesis of TiC and TiB_2.

For the synthesis of TiC, the carbon coated titania was then carburized in a high temperature box furnace (CM Furnace Bloomberg, NJ). The coated titania powders were heat treated at 1300 to 1500^{0}C for 1 to 2 hours under flowing argon gas to form TiC with different morphology. For TiB_2 synthesis, carbon coated precursor was mixed with stoichiometric amounts of B_4C (H.C. Starck Grade HS) and mechanically milled for about 20 minutes in a miller (SPEX 8000 Mixer/Mill). Thorough mixing was insured by addition of polymer balls.

[39] G. Glatzmaier and R. Koc: US Patent, 1994, no. 532.494
[40] R. Koc and G. Glatzmaier: US Patent, 1995, no.5417.952
[41] R. Koc, G. Glatzmaier, and J. Sibold: Journal of Materials Science, 2001, vol.36, pp.995-999

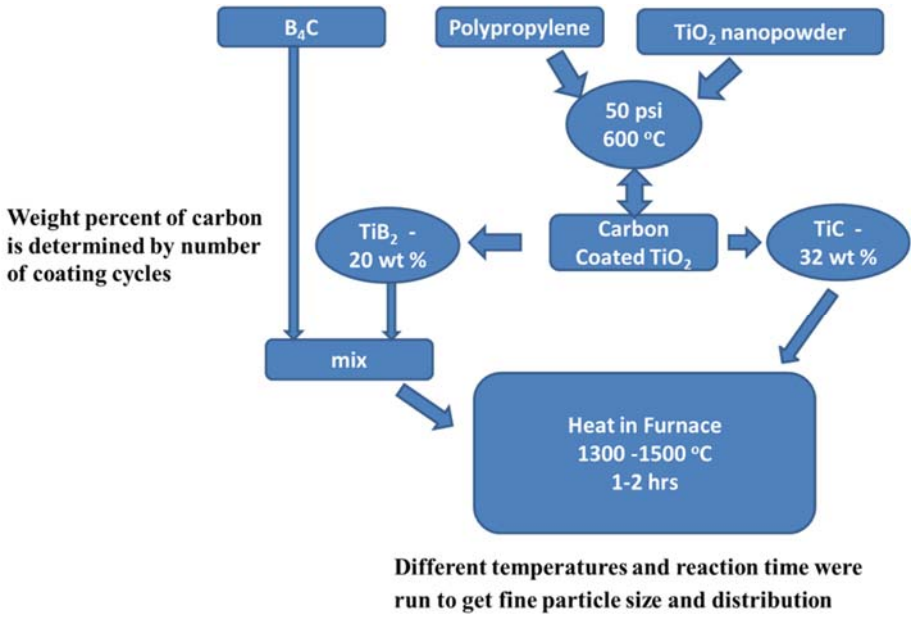

Figure 4. TiC or TiB2 Synthesis Procedure

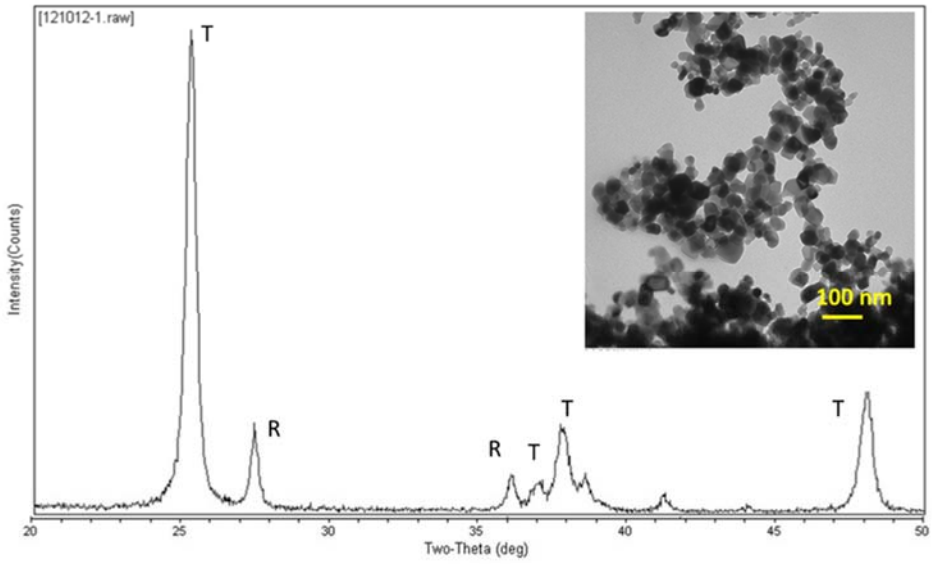

Figure 5. XRD of the as received nano sized titania

Figure 6. Carbon coating furnace

Material Selection

Table 2 contains the substrates of interest. Of the listed ones, an austenitic, ferritic and a super alloy was planned to be tested. However, after evaluating the austenitic steel 304 H, it was decided to test two ferritic steels, namely 430 and P 91. The compositions of the steels are provided below the Table 2.

Table 2 Substrate Choice and selection

	Substrate Material	Class	Applicable Component
1	Super 304H	Austenitic	SH/RH tubes
2	347HFG	Austenitic	SH/RH tubes
3	Sarnico 25	Austenitic	SH/RH tubes
4	HR3C	Austenitic	SH/RH tubes
5	STD617/CCA 617	Nickel Alloy	Tubing, HP turbine-casing, piping, rotor - 700 °C
6	Haynes 230	Nickel Alloy	SH tubes, HP turbine rotor – 700°C
7	Inconel 740	Nickel Alloy	SH tubes, HP turbine - casing, piping, rotor- 760 °C
8	Haynes 263	Nickel Alloy	HP turbine casing – 700 °C
9	P91/P92	Ferritic	Low Temp SH/RH
10	T91/T92	Ferritic	Low Temp SH/RH, HP turbine piping – 620°C
11	Save 12	Ferritic	HP turbine casing, rotor, blades – 620 °C
12	T23/T24	Ferritic	Furnace Tubes

Steel	C	Si	Mn	P	S	Ni	Cr	Al	Mo	V	N	Fe
304 H	0.04-0.1	0.750	2.000	0.045	0.030	8.0-10.5	18.0-20.0					bal.
430	0.070	0.300	0.900	0.028	0.001	0.080	15.970	0.140				bal.
P91	0.08-0.12	0.20-0.50	0.30-0.60	0.02 Max	0.010 Max	0.40 Max	8.0-9.5	0.040 Max	0.85-1.05	0.18-0.25	0.030-0.070	bal.

HVOF Coating:

The as-prepared TiC and TiB_2 powders were then coated to stainless steel substrates using HVOF thermal spray method at a facility at Gas Technology Institute, Des Plaines, IL. Figure 7 shows the general process of HVOF thermal coating process as well as the design of the gun. Detailed HVOF parameters are as shown in the relevant sections. Surface of the steel substrates was roughened by water honing before HVOF coating for better powder adhesiveness (Figure 8). The as-prepared TiC/ TiB_2 powders were then reacted with various combination of fuel and oxidant, such as: H_2/Air, H_2/O_2 and C_2H_2/Air in the reaction chamber of HVOF system, then coated onto the substrates. Figure 9 shows the HVOF coating process in action and the resulting partially coated samples.

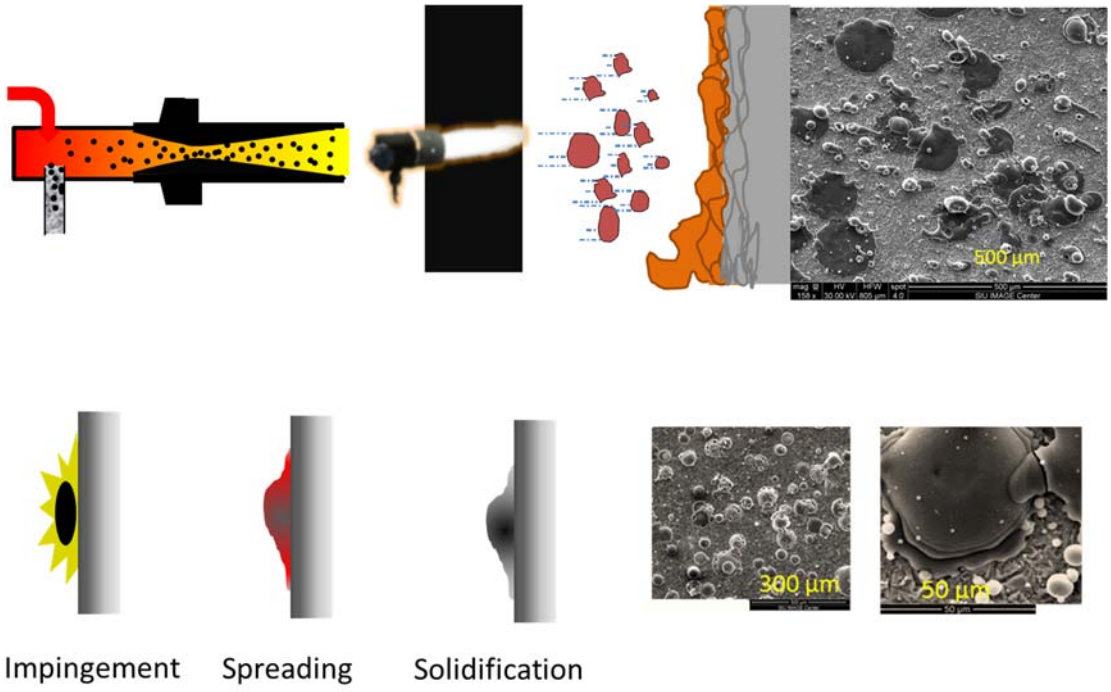

Figure 7. HVOF Process schematic and SEM images of coated substrate.

Figure 8. Water Honing.

Figure 9. HVOF coating at GTI

Corrosion Studies:

High temperature air, flue gas, steam-oxygen and salt corrosion resistance tests were performed for the TiC/ TiB_2 coated stainless steel substrates, and uncoated stainless steels for comparison. Air corrosion test (Figure 10) was conducted in a box furnace. Coated and uncoated stainless steel substrates were placed on alumina crucibles inside the furnace and were heat treated at 750^{0}C with 5^{0}C/min temperature gradient for 800 hours. Simulated ash corrosion test was also conducted in the same furnace at same temperature and duration. A salt mixture of NaCl, Na_2SO_4, KCl and K_2SO_4 in the ratio of 1:1:1:1 was layered on top of the substrates to simulate ash particulates in the boiler. The substrates were heat treated at 750^{0}C with 5^{0}C/min temperature gradient for 800 hours. Simulated flue gas and steam-oxygen corrosion was also conducted in a tube furnace. The coupons were placed in the tube furnace and exposed to the simulated flue gas (Composition in Table 4) for 180 and 800 hrs. The samples before and after the corrosion studies were subjected to non-destructive testing discussed next. A typical pulverized coal USC boiler flue gas composition from combustion of high BTU bituminous coal was used. Unfortunately, no HCl was introduced since we were not able to acquire a dilute HCl in Nitrogen gas.

Table 4 Simulated Flue Gas Composition

O_2	N_2	CO_2	H_2O	SO_2
2.99	74.21	14.06	8.52	0.021

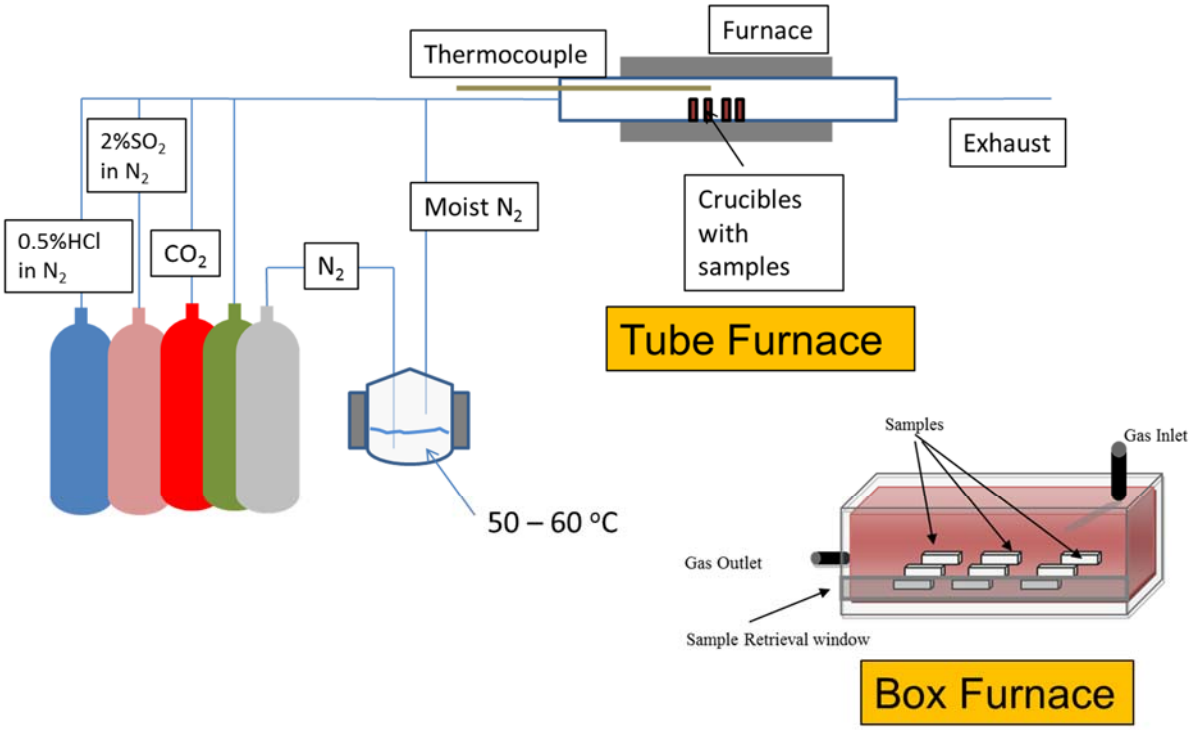

Figure 10. High temperature corrosion setup.

Characterization:

Crystallinity of the substrates before and after air corrosion and simulated ash corrosion tests were analyzed by X-ray diffraction (XRD, Rigaku, Tokyo, Japan). Surface morphology of the as prepared powders, surface of the coated and uncoated substrate, and cross-sectional examination of the substrates were characterized with scanning electron microscope (SEM, FEI QuantaTM 450 FEG, Oregon, USA, with a field emission electron gun). Elemental distribution and material composition were analyzed with EDS coupled with SEM. Transmission electron microscope (TEM, Hitachi H7650, Tokyo, Japan, with LaB_6 filament) was also utilized for analysis of TiC/ TiB_2 particles.

Improved sample preparation of stainless steel samples for SEM and EDS analysis

In order to obtain sharper SEM/EDS results and avoid contamination on the cross section of the substrates caused during sample cutting, the post-testing Ti coated stainless steel samples were sanded (#800 sand paper) on cross sectional area. Low temperature sanding on the cross sectional area of the sample was expected to improve analysis results by eliminating residuals and slight deformation caused by cutting bulk stainless steel plates into smaller pieces (1 inch square) for SEM analysis. Figure 11 shows cross sectional (a) SEM image and (b) EDS analysis result of Ti coated stainless steel before sanding process. The SEM image and EDS results of the same sample after sanding process is as shown in Figure 12.

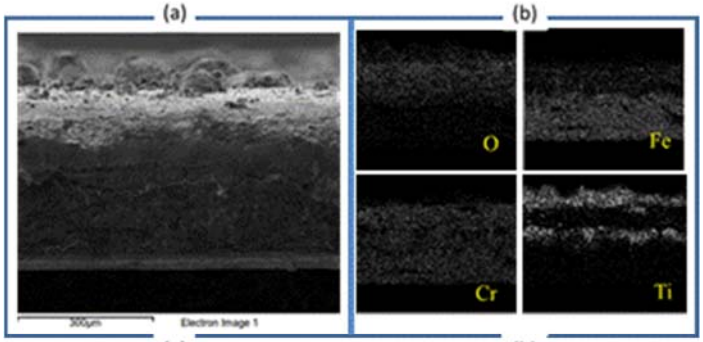

Figure 11. Cross sectional (a) SEM image and (b) EDS analysis result of Ti coated stainless steel after 800 hours of air corrosion test at 750°C before sanding process.

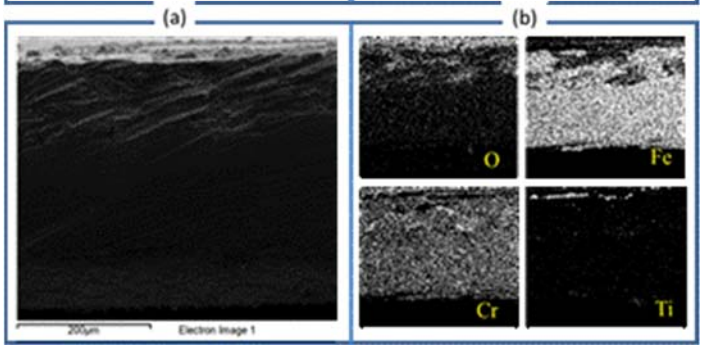

Figure 12. Cross sectional (a) SEM image and (b) EDS analysis result of Ti coated stainless steel after 800 hours of air corrosion test at 750°C after sanding process.

EDS results from substrate after sanding process showed higher contrast of signal of element detected. Also, finer details of the elemental distribution can be observed. The second layer of Ti observed, probably separated from the surface while cutting, as shown in Figure 11(b) was eliminated after the sanding process, and only surface Ti coating was observed after sanding.

Improvement was also observed from the back-scattering image of the Ti coated substrates, as shown in Figure 13. BSED image of the substrate before and after sanding are as shown in Figure. 13(a) and (b). A clearer image of the cross-sectional area with better phase separation can be observed from the BSED image of sanded substrate compared to that before sanding process. However, traces of sanding were observed from the BSED image of the sanded substrate. Therefore, finer sanding medium should have been utilized for better results.

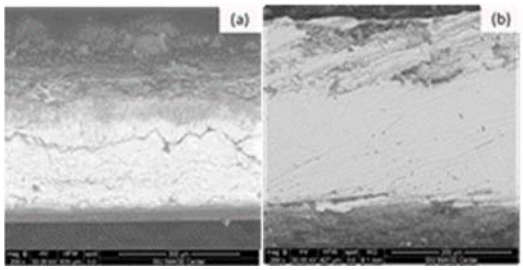

Figure 13. . Back-scattered SEM image of Ti coated sample (a) before and (b) after sanding process

In order for the samples to fit in the SEM, coated and uncoated stainless steel substrates were shear cut into smaller pieces. However, certain degree of roughness was introduced, as well as slight amount of undesired deformation was formed. In order to obtain optimum analysis results, such uneven surface was smoothed by polishing. Cross section of steel samples was polished using sand papers following the order: #400, #800, #1200, #2000 grade. SEM images of steel sample before and after polishing are as shown in Figure 14(a). Much smoother cross section of the sample can be observed. Interface between Ti coating and stainless steel substrate was also more easily observed from SEM images from the polished samples. EDS results of the steel sample before and after polishing are as shown in Figure 14(b). Compared between the elemental distribution maps, it can be seen that additional traces of titanium appeared in the lower cross section of the sample. This may have been caused by the shear forces applied on the sample during cutting, bringing titanium coating to the side of the substrate. Much smoother distribution of elements was observed for sample being polished. Note that the samples illustrated were Ti coated on both sides, thus the Ti distribution of both side of the Ti elemental map.

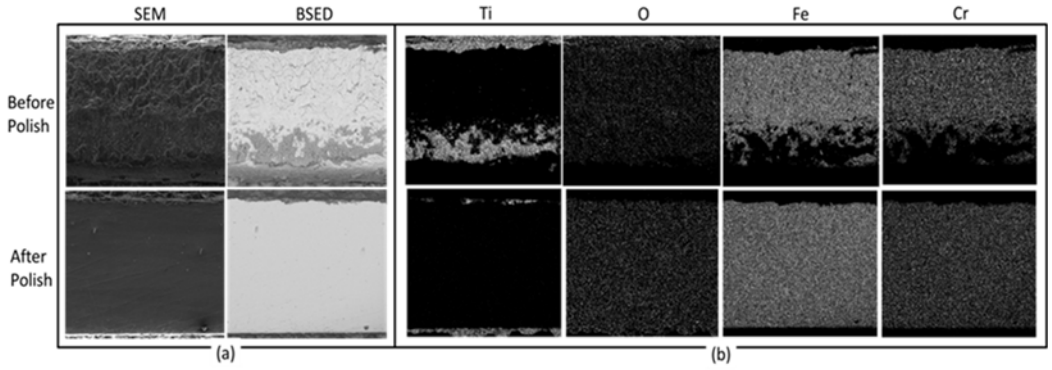

Figure 14. a) SEM secondary, back-scattering electron images and (b) EDS maps of cross section of coated steel sample before and after polishing.

RESULTS AND DISCUSSION

The results section is divided into five parts. The first part describes the effect of synthesis parameters on the physical and compositional effects of the resulting powders. To improve the HVOF coating conditions, a narrow size distribution was required spurring the evaluation of process parameters on the powder properties. Essentially, the carburizing time and the duration for conversion of C coated precursor to TiC or TiB_2 was evaluated. In addition, two different C loadings were considered for TiC (32 and 33%) and for TiB_2 (14 and 20 %). The HVOF parameters that were altered were the oxidant fuel choice (that affects the velocity as well as the temperature of the flame) and flow rate, the distance of the gun from the substrate and the duration of coating. It must be noted here that the variation of the parameters was a learning based optimization than a pre-planned slew of tests in that the results from the prior coating tests were considered for the next set of tests. The austenitic steels were coated first followed by ferritic steel 430. Both these steels were coated on one side. Even though it was apparent from the first set of coatings that both sides need to be coated to evaluate mass change more accurately, the coupons that could be obtained were relatively thin and thus difficult to coat both sides (Note that the 430 steel was thicker than the 304H but not sufficient.). The ferritic steel P91 was much significantly thicker and both sides were coated with different coating parameters. Finally, the corrosion tests on these coupons were conducted. Initially it was planned to conduct only air and salt corrosion studies. However, we continued to evaluate the corrosion of these samples in simulated flue gas (based on IL coal combustion) and with steam and oxygen for tube side corrosion. The data from 304 H corrosion and from the corrosion studies on 430 steel, it was decided to conduct observe the corrosion protection afforded by these coating to a low Cr steel rather than a high Ni alloy. Thus, instead of the choice of a super alloy, P91 was selected. During the evaluation of the corroded samples, TiO_2 was identified on the surface even though the coatings afforded good corrosion resistance. Thus in the latter stages of the project, we evaluated the impact of Ti metal coating for two reasons. The first is that for comparison of performance with the ceramic powders and the second is to evaluate the ease and uniformity of the coating, since the HVOF processes parameter optimization was not complete to obtain complete coverage of the coated surface.

The results show in the following section will show that the size distribution of the powders can be controlled by altering the synthesis conditions. As mentioned earlier, the HVOF coatings process needs to be still optimized. However, the corrosion tests provided sufficient information to evaluate the impact of the coating of these non-oxide ceramics of titanium. It was originally planned that the post corrosion characterization would involve analysis of mass change and surface morphology as well as the distribution of the corrosion products on the surface. However, evaluating the performance based on mass change was a challenge for the following reasons: a) non –uniform coating thickness and incomplete surface coverage introduced significant variability in the mass change data, b) the one sided coatings posed a problem in that the uncoated side was also exposed to the corrosive environment, and c) oxidation of the surface resulted in mass increase while spallation and detachment of the corroded surface resulted in mass loss and since insufficient number of time intervals were considered, the overall data was not reliable. A better measure was the cross sectional analysis yielding the depth of oxygen and sulfur penetration combined with surface distribution of the same.

Powder Synthesis

Initially, approximately 60 g of TiC powders were synthesized at 1500ºC and 2 hrs of treatment to the carbon coated TiO_2 powders and sent to GTI. Figure 15 contains two SEM images at different magnifications from the first batch of TiC samples prepared by the carbothermal process. While the particle sizes are observed to be less than 100 nm range, the particles also appear to agglomerate to form larger particulates. Figure 16 is the XRD of the produced TiC powders.

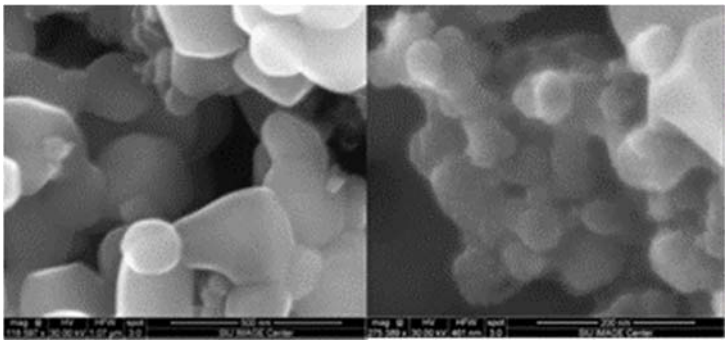

Figure 15. SEM images of as prepared TiC. These powders were synthesized by the carbothermal process at 1500 °C.

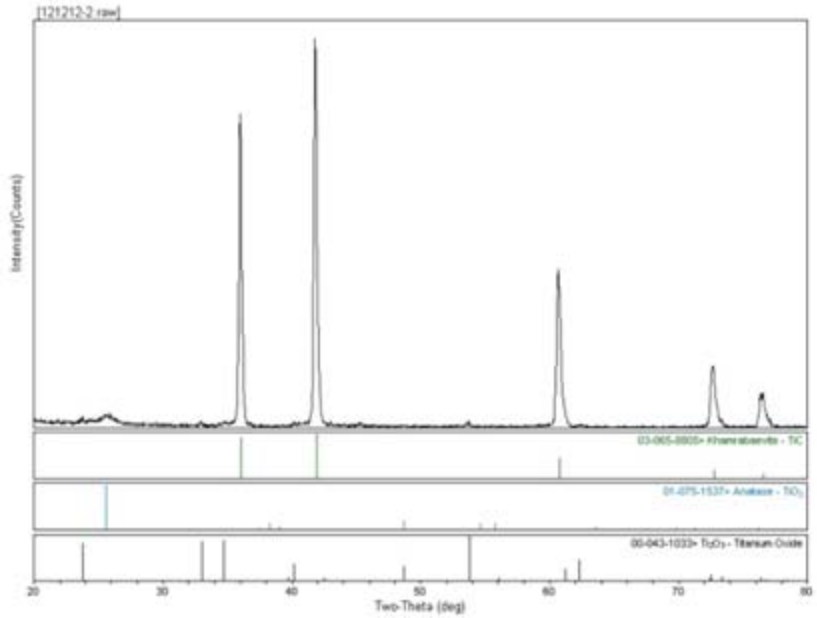

Figure 16. XRD spectra of as prepared TiC. These powders were synthesized by the carbothermal process at 1500 °C.

Personnel at GTI conducted several tests to spray coat these powders on to 304H steel substrates. The primary issue of these powders was difficulty in dispersing them evenly. It was recommended that the particle size should be further lowered and the distribution narrowed to enable more even coating. It was thus decided to reduce the temperature and the processing time. The TiC synthesis process parameters were altered to obtain finer (20-30 nm) particles. It is observed from Figure 17 that reducing the processing temperature resulted in a narrower particle size range. However,

the XRD spectra (Figure 18) show the presence of TiO_2 which indicate that not all of the TiO_2 converted to carbides. Thus a set of experiments altering the processing time and/or temperature was conducted to obtain desired narrow range of pure TiC particles.

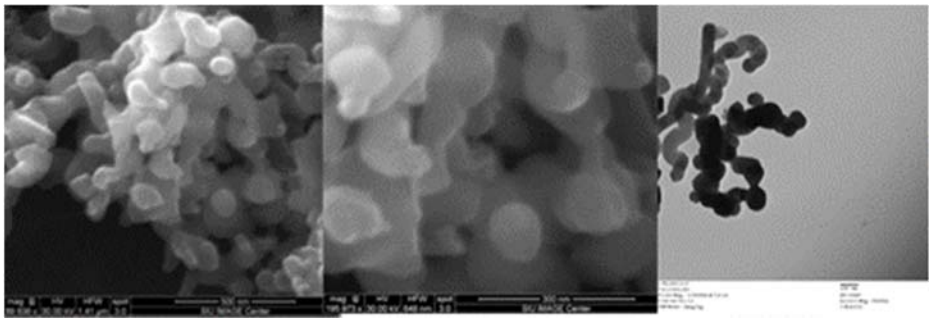

Figure 17. SEM and TEM images of as prepared TiC. These powders were synthesized by the carbothermal process at 1300 °C.

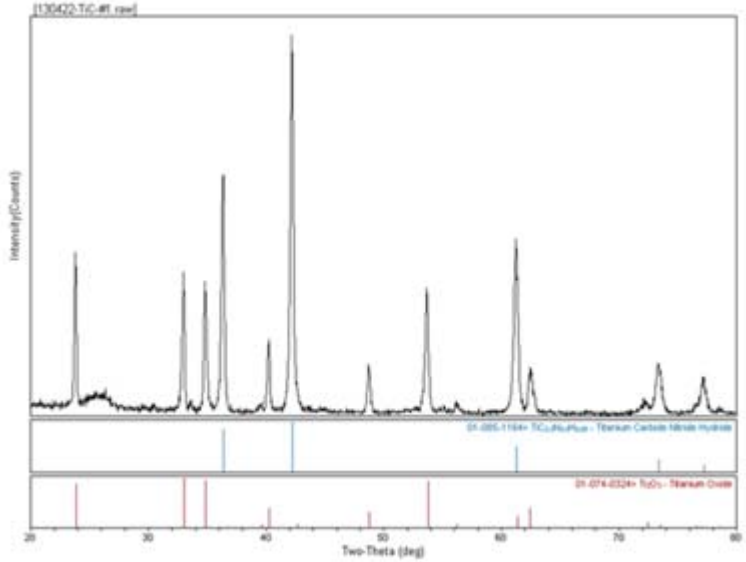

Figure 18. XRD spectra of as prepared TiC. These powders were synthesized by the carbothermal process at 1300 °C.

Figure 19 are the SEM images of the samples prepared at different carburization temperatures and synthesis times. We observe that the morphology of the particles changes with an increase in temperature. Figure 20 shows the TEM of the powders along with the particle size distribution. Two more synthesis experiments were conducted at 1300 and 1400 °C for 2 hrs of synthesis. In general, the powders are finer than 200 nm in diameter. We see that finer particle sizes are obtained at lower temperatures. Figure 21 compares the XRD diffractograms obtained at the three temperatures. We observe that the crystallinity of the material increases with temperature. Some unconverted TiO_2 is still found in the samples. In order to remove any trace of TiO_2 from the produced powders (or in other words, complete conversion to TiC) two additional samples were synthesized at 1400 °C and 1500°C with 33 % C coated TiO_2 for two hours. Figure 22 are the TEM images of the samples prepared at 1400 and 1500 °C for a synthesis time of 2 hrs and the

particle size distribution is provided in Figure 23. We see that finer particle sizes are obtained at lower temperatures. Figure 24 is the comparison of the XRD diffractograms obtained at the two temperatures. Complete conversion is obtained for both temperatures.

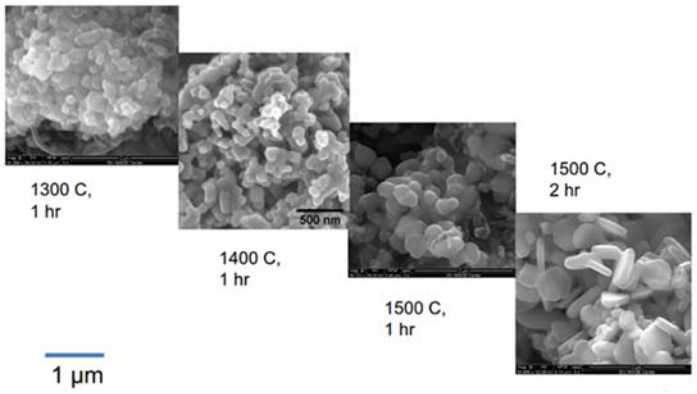

Figure 19. SEM images of TiC prepared at three different temperatures.

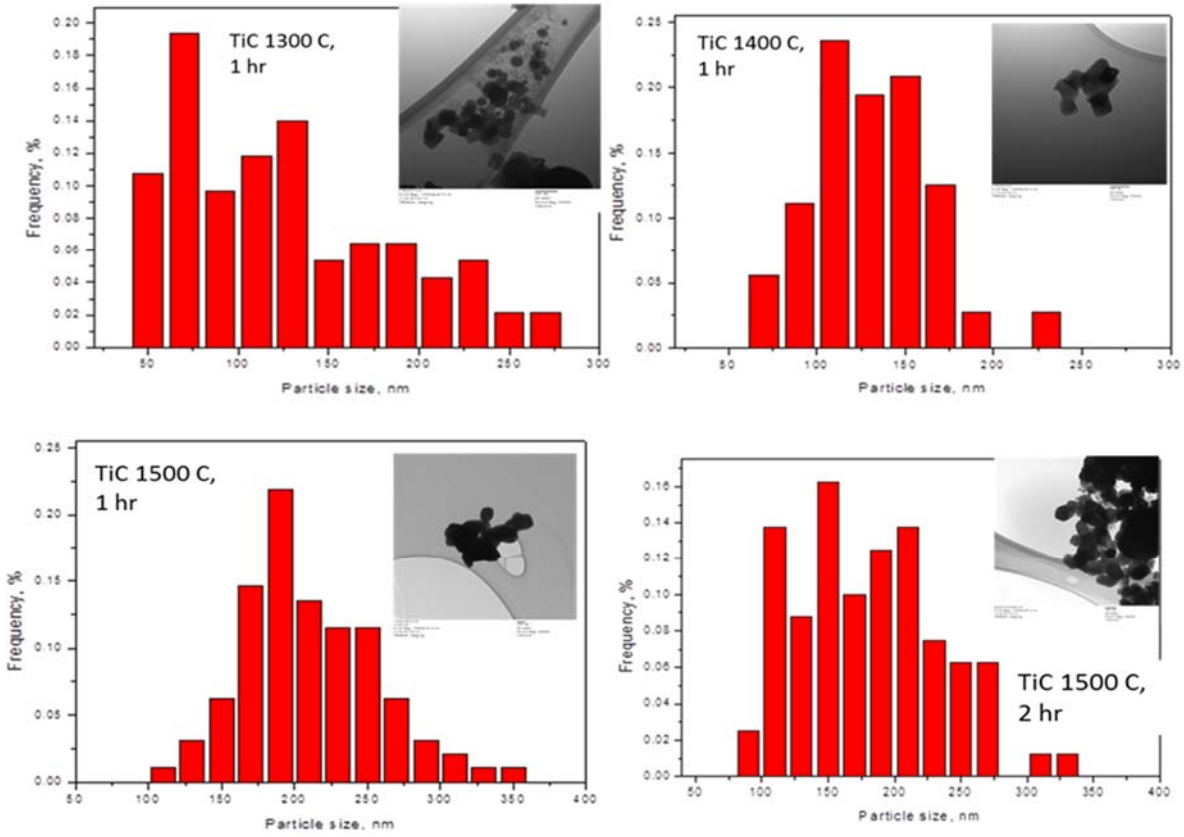

Figure 20. Particle size distribution of the TiC powders prepared under different conditions.

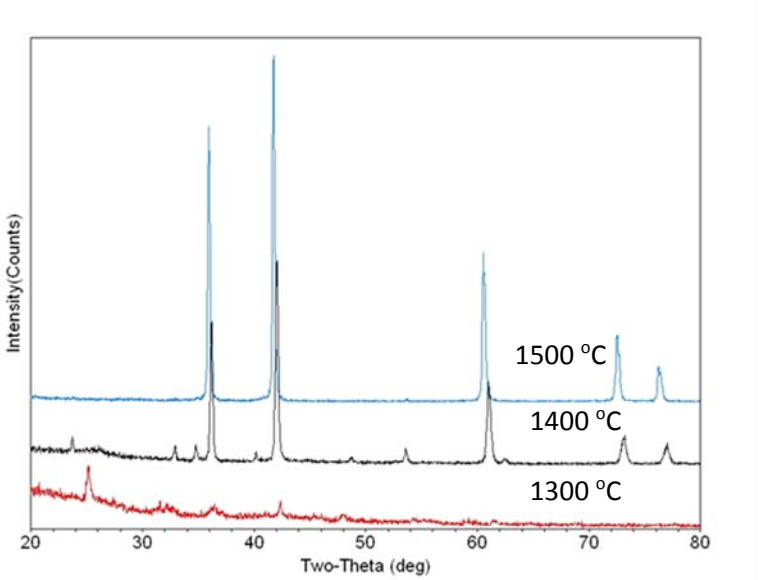

Figure 21. XRD Diffractograms of TiC powders prepared at three different temperatures.

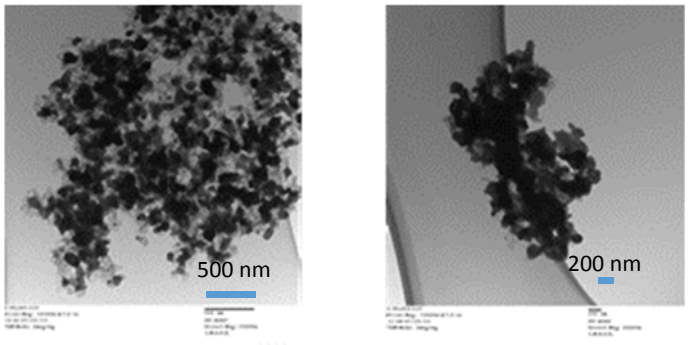

Figure 22. TEM images of the TiC powders prepared at 1400°C (left) and 1500 °C (right).

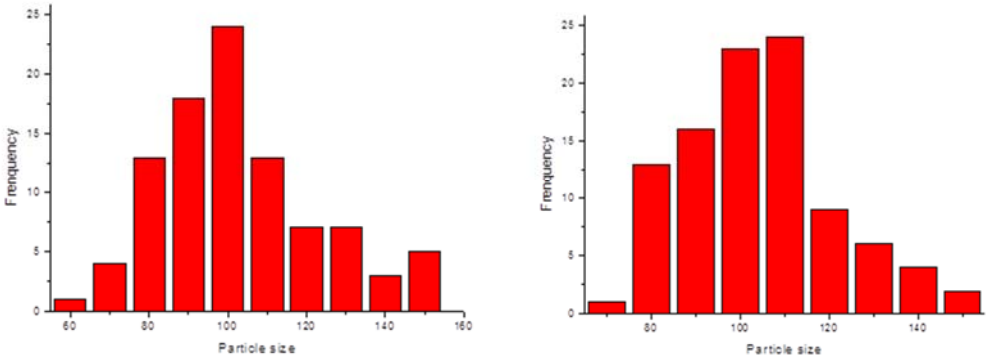

Figure 23. Particle size distribution of TiC powders prepared at 1400°C (left) and 1500 °C (right).

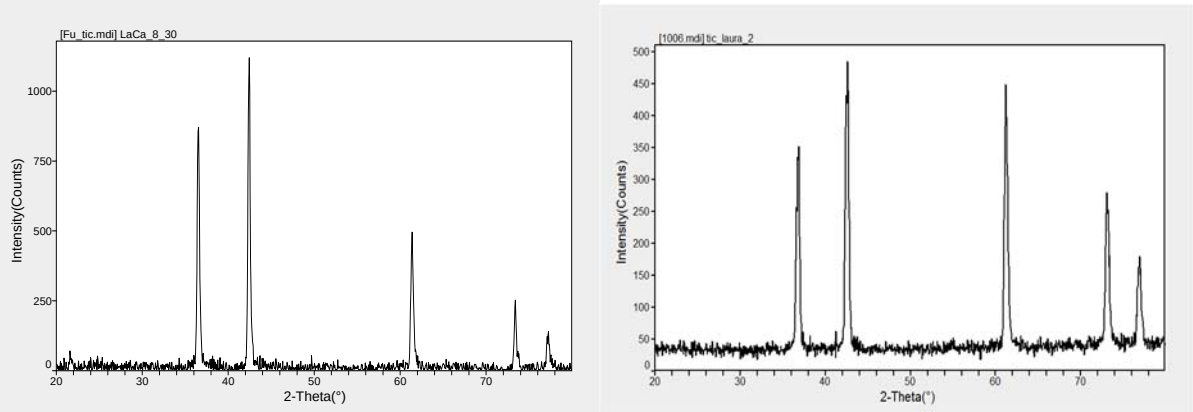

Figure 24. XRD Diffractogram of the TiC powder prepared at (left) 1400°C and (right) 1500 °C and 2 hrs. (The intermediate step contained 33 % C).

For the TiB_2 synthesis, two samples were prepared one with 20 % C in the carbon coated TiO_2 and the other with 14 % C in the carbon coated TiO_2. The TiB_2 was then prepared by adding B_4C and heating at 1500 °C for 2 hrs. Figure 25 shows the particle size distribution along with the TEM image (inset) for the powder produced with the latter condition. The TiB_2 powder appears to be significantly coarser than the TiC powders. Figure 26 compares the XRD diffractogram of the two samples. Under these synthesis conditions, some unconverted TiO_2 is still observed. Higher purity sample was obtained at 20 % C intermediate than the 14 % C intermediate.

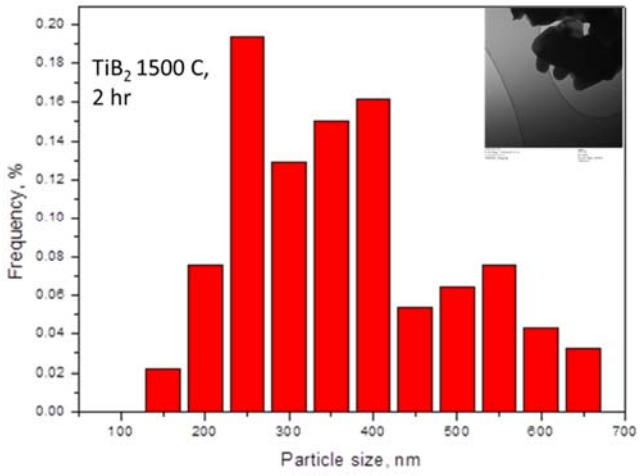

Figure 25. Particle size distribution of the TiB_2 powders prepared from a precursor with 14 % C coated TiO_2 (inset (TEM image)

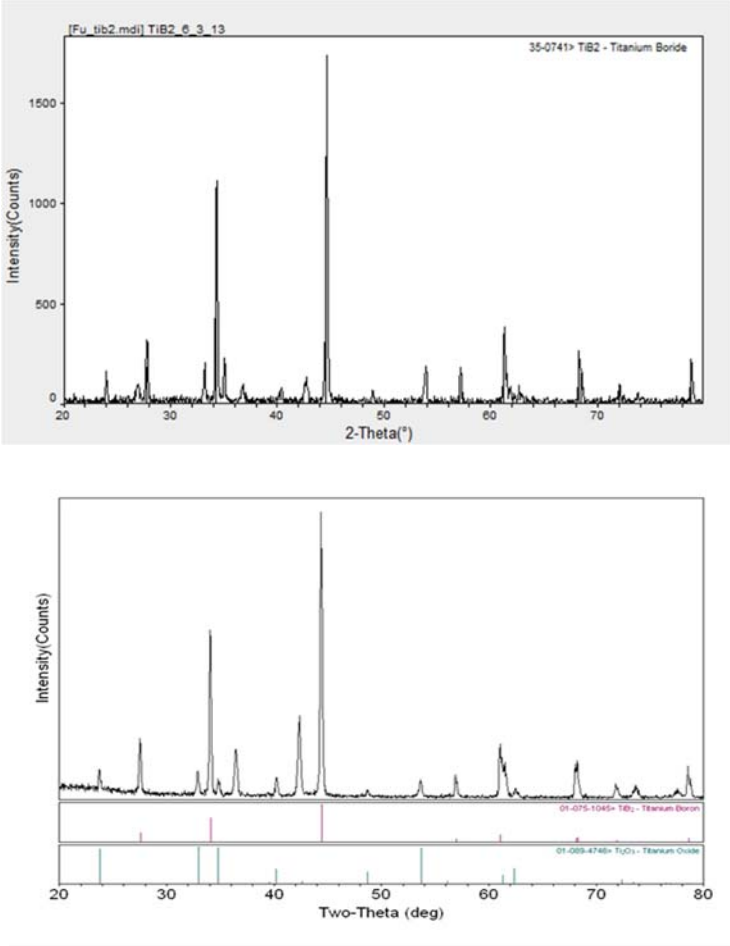

Figure 26. XRD diffractogram of TiB_2 prepared from a precursor with (top) with 20 % C coated TiO_2 (bottom)14 % C coated TiO_2.

Summary

In summary, 1400 ºC with 33% C coated TiO_2 carburized for 2 hrs provides the best results in times of finer sizes and narrower size distribution of the TiC powder. For TiB_2, higher %C coated TiO_2 provides more complete conversion to the product.

HVOF Thermal Spray Coating

304 H

The first set of steel samples that were coated were that of 304H austenitic steels. Figure27 and 28 contains the SEM images of the first batch of coatings under different conditions and the original SS304H surface for comparison. Figure 29 are the plots obtained from (EDS) that shows the elemental composition of the two coating.

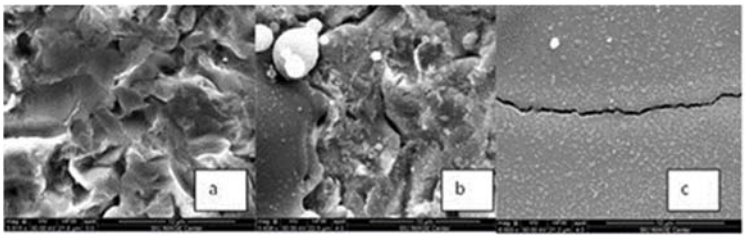

Figure 27. SEM images of a) uncoated substrate, b) thermal spray coated substrate S_TiC#1, and c) thermal spray coated substrate S_TiC#2.

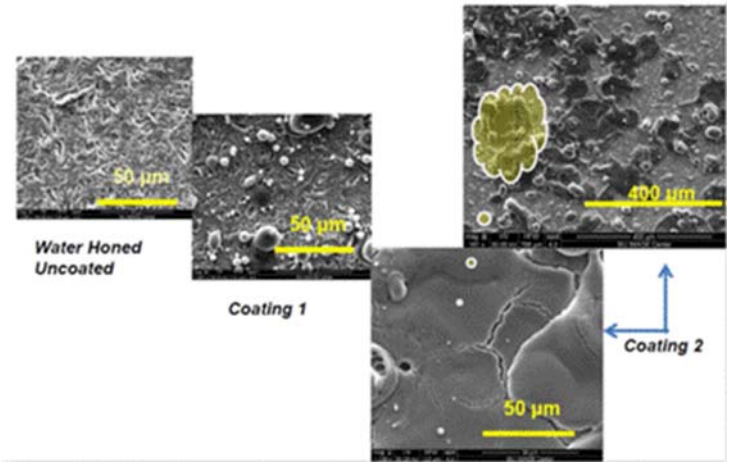

Figure 28. SEM images of the HVOF TiC coated and uncoated samples obtained from GTI.

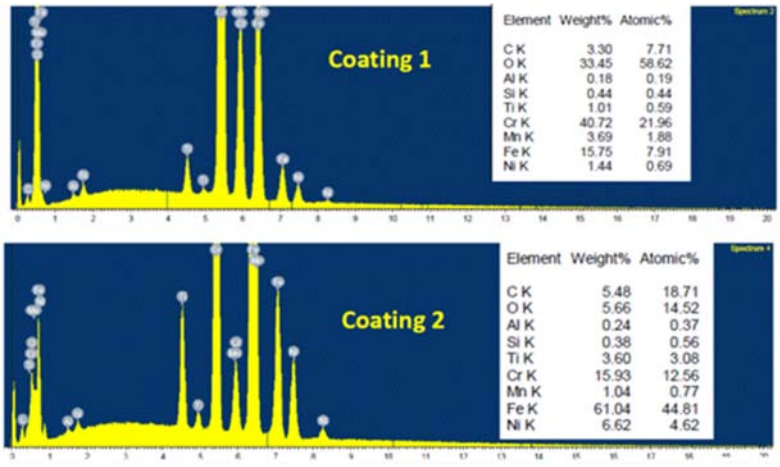

Figure 29. EDS spectra of the HVOF TiC coated SS304H (Coating 1 and 2) obtained from GTI.

After the initial air corrosion and salt corrosion tests, coatings were modified to analyze the effect of flame temperature due to oxidant/fuel combinations on the coatings. Table 5 contains the data on HVOF coating conditions. Figure 30 is the SEM image of the cross section of the uncoated sample 3 (left) and the backscatter image on the right. Figure 31 compares the SEM images of cross-section of samples obtained when the HVOF flame was based on different gases namely hydrogen and air (left) hydrogen and oxygen (middle) and acetylene and air (right). Figure 32 compares the different coating samples using the same gases (acetylene and air). Figure 33 is a sample SEM image of the top surface of an as received coating (Sample 10) produced using acetylene/air flame.

Table 5. Coating Set 2 for 304H steels. Effect of oxidant-fuel choice and time of coating

S#	Atmosphere	Conditions					
3	Control	H_2 L/m	O_2 L/m	Air L/m	C_2H_2 L/m	T °C	D cm
4	H_2/Air	46		9		3200	25
5	H_2/O_2	46	12			3200	25
6	C_2H_2/Air			9	24	2500	25
7	H_2/O_2	46	12			3200	25
8	H_2/O_2	46	12			3200	25
9	C_2H_2/Air			9	24	2500	25
10	C_2H_2/Air			9	24	2500	25
11	C_2H_2/Air			9	24	2500	25
12	C_2H_2/Air			9	24	2500	25

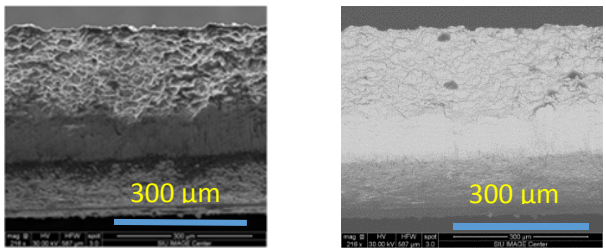

Figure 30. SEM (left) and backscatter image (right) of the control substrate SS 304H.

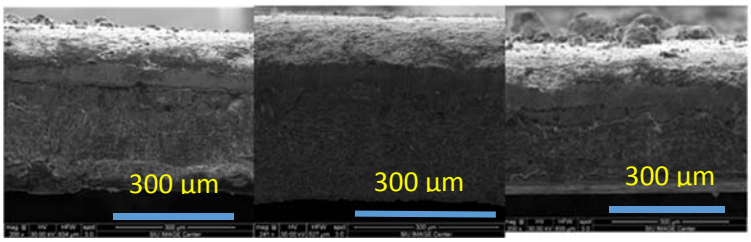

Figure 31. SEM images of the cross section of the coatings obtained in hydrogen and air (left), hydrogen and oxygen (middle) and acetylene and air (right).

Figure 32. SEM images of the cross section of the two coatings obtained in acetylene and air.

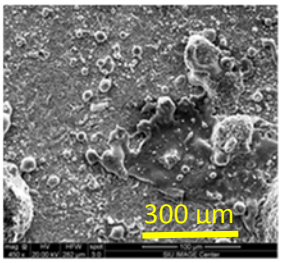

Figure 33. SEM image of the coated surface. Coating conducted in acetylene –air flame.

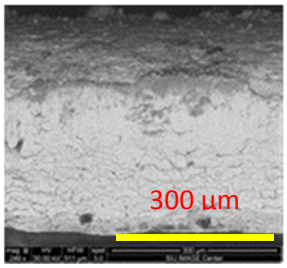

Figure 34. Sample back scatter image of the cross section. Coating conducted in acetylene air flame.

Figure 34 is the sample backscatter image and Figure 35 contains the information on elemental distribution in cross section of the samples.

Figure 35. Elemental mapping of the cross section of the as-received sample 11. Coating obtained in acetylene - air flame.

A third iteration of coating was conducted on the 304 H samples. Table 6 shows the HVOF coating parameters for this iteration. Ti metal as well as TiB_2 and TiC containing different percentage of carbon sintered at various temperature were used as coating material. The flow rate of each spraying atmosphere and spraying distance were kept the same for all 9 samples, while coating time was altered for better coating results.

Table 6. HVOF coating parameter and coating materials for 304 H stainless steel substrates

Spray Parameters	
H2 Flowrate	76 LPM
O2 Flowrate	13 LPM
N2 Flowrate	1.8LPM
Spraying Distance: 27cm	

Samples	Coating Time (min)	Coating Powder
1	1	Ti Metal
2	3	Ti Metal
3	5	Ti Metal
4	3	TiC 32%C 1400C 1 hr
5	10	TiC 32%C 1400C 1 hr
6	10	Ti Metal
7	8	TiB2
8	6.5	TiC 33% 1500C 2hrs
9	10	TiC 33% 1500C 2hrs

Figure 36 shows the photographs of the as-received coated substrates with different coating parameter. Thicker coating can be observed from samples coated with Ti metal (sample #2, 3, 6). For samples coated with TiC with 32% carbon sintered at 1400^{0}C for one hour as source material, slightly thicker coating can be observed (sample #4, #5) for higher coating time. However, opposite result was observed for samples coated with TiC with 33% carbon sintered at 1400^{0}C for one hour as source material.

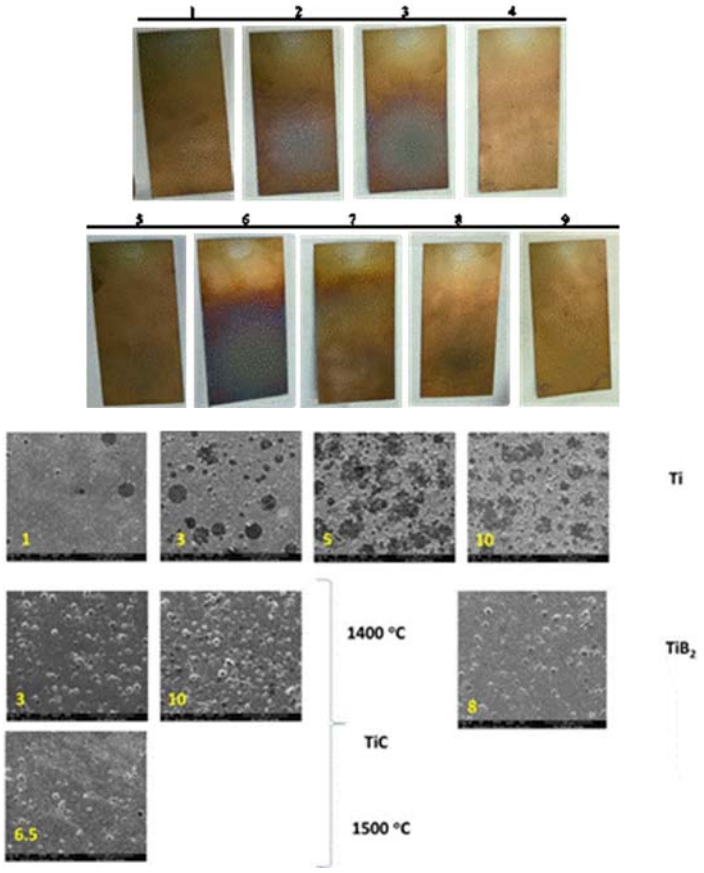

Figure 36. Photos and SEM images of coated stainless steel substrates with different coating parameters and source materials.

SEM images of Ti coated samples coated by HVOF using Ti metal as source material for 1, 3, 5, and 10 minutes (sample #1, 2, 3, 6) are as shown in Figure 37 (a) through (d). With time increase of time of coating, density of Ti coating on the surface increased, as well as thickness of the coating. Sample coated for 5 minutes had significant increased amount of Ti coating compared to sample coated for 1 and 3 minutes. However, increase of Ti coating on the surface of sample was not as profound for sample coated for 10 minutes compared with sample coated for 5 minutes. Overlapping of Ti coating can also be observed on sample #2, #3 and #6. At higher magnification, Ti coating for 1 minute was found mostly composed of single layer structure as shown in Figure 38(a). For samples coated with longer coating duration, overlapping of Ti coatings can be observed. Figure 38 (b) and (c) show the coating morphology of 3 and 5 minute coating. On the other hand, coating composed of small grains was also observed for sample coated with Ti with longer coating duration.

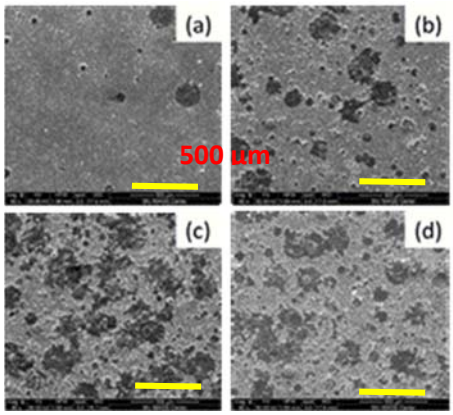

Figure 37. SEM images of Ti coated samples coated by HVOF using Ti metal as source material with coating duration of (a)1, (b)3, (c) 5, and (d)10 minutes.

Figure 38. SEM images of Ti coated samples coated by HVOF using Ti metal as source material with coating duration of (a) 1, (b) 3, and (c) 5 minutes at higher magnification

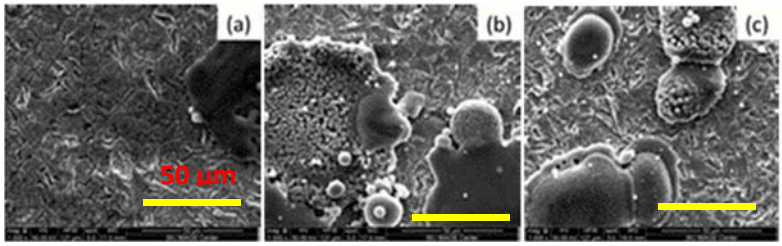

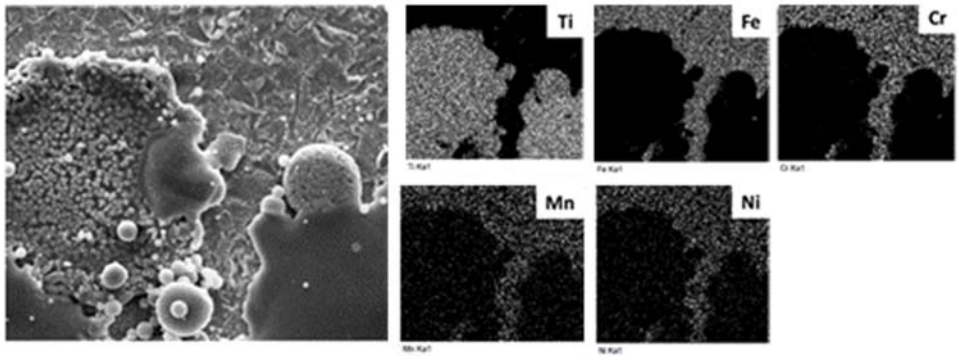

Figure 39. EDS mapping result with regards to Ti, Fe, Cr, Mn, and Ni for Ti coated sample coated with Ti metal by HVOF method for 3 minutes (33%C based TiC).

EDS mapping result for 3 minute coating sample (Figure 38 (b)) is shown in Figure 39. From the EDS result, iron and chromium from the stainless steel substrate are covered entirely by titanium where the coating was observed. On the contrary, slight amount of Mn and Ni were found at the Ti coating site. SEM images of the surface of sample #4 and #5 (source of TiC from 32% C coated TiO_2 carburized at 1400 ^oC for 1 hr) are shown in Figure 40 (a) and (b). Similar to the results observed from samples coated with Ti metal as source material, coating overlapping was observed for sample #5 which was coated for 10 minutes compared to that of sample #4, which was coated for 3 minutes by HVOF. Area covered by TiC coating was also found to have significantly increased with longer coating time. Compared to samples coated with Ti metal, the TiC coating appeared to be more concentrated on smaller area. This localized coating morphology may be a result of small particles used as source coating materials. At higher magnifications, as shown in Figure 40(c), coatings were also found to be porous in parts of the coated area, which was not observed from coatings from Ti metals.

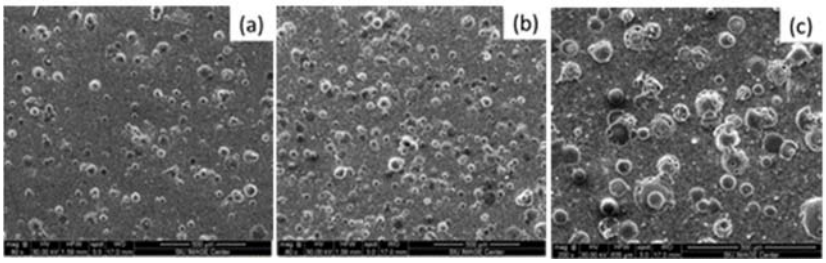

Figure 40. SEM images of Ti coated samples coated by HVOF using TiC powders synthesized from carbon coated TiO_2 with 32% carbon content sintered at 1400^oC for 1 hour as source material with coating duration of (a)3, (b)10 minutes, and (c) Figure 40(b) at higher magnification.

304H stainless steel samples were also coated using TiC synthesized at different condition. Sample #8 and #9 were coated using TiC powder synthesized from carbon coated TiO_2 powder containing 33% of carbon sintered at 1500^{0}C for 2 hours, with HVOF coating duration of 6.5 minutes and 10 minutes respectively. SEM images of the surfaces of sample #8 and #9 are as shown in Figure 41 (a) and (b). Ti coating composed of grain-like structure can be observed from the SEM images. Unlike the surface morphology of samples coated with Ti metal, which the grains were mixed with dense Ti coating layer, the TiC coating on sample #8 and #9 are composed of mostly small grains. On the other hand, existence of small particles irregular in shape was found on stainless steel surface of sample #8. Result from SEM back-scattering image as shown in Figure 41(c) shows that the small particles did not vary in phase compared to the stainless steel substrate. Further EDS analysis was therefore carried out in order to identify the elemental composition of the small particles, and the result is shown in Figure 42. The elemental analysis of the small particles on the surface of sample #8 (6.5 min coating with TiC prepared from 33 % C coated TiO_2 can carburized at 1500 ^oC for 2 hrs) shows that at Point 1 where only the stainless steel substrate is presented, the elemental composition is mainly iron (Fe, 71.16 at%), chromium (Cr, 20.49 at%), and nickel (Ni, 7.57 at%); Whereas at point two, where the small particles irregular in shape is presented, the main elemental composition is iron (Fe, 54.5 at%), oxygen (O, 22.06 at%), chromium (Cr, 15.85 at%), nickel (Ni, 7.57 at%), and very small amount of titanium (Ti, 1.91 at%). The significant increase in oxygen percentage indicated that the small particles should be certain form of oxide.

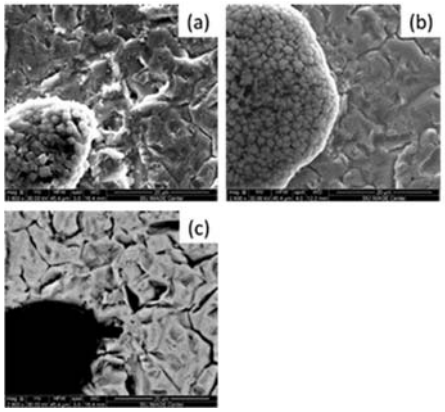

Figure 41. SEM images of Ti coated samples coated by HVOF using TiC powders synthesized from carbon coated TiO_2 with 33% carbon content sintered at 1500 ℃ for 2 hours as source material with coating duration of (a)6.5, (b)10 minutes, and (c) Back-scattering SEM image of area shown in Figure 41(a).

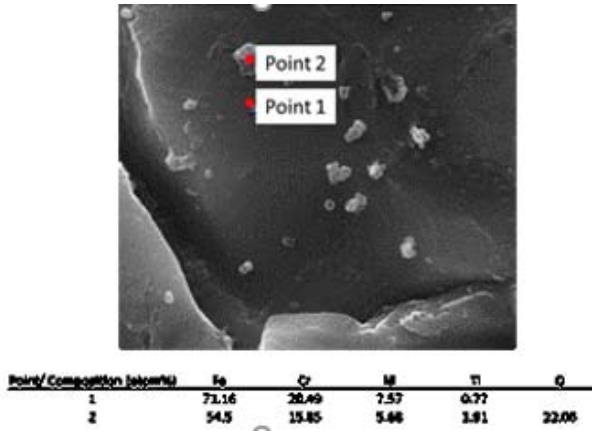

Point/ Composition (atomic)	Fe	Cr	Ni	Ti	O
1	71.16	20.49	7.57	0.77	
2	54.5	15.85	5.66	1.91	22.06

Figure 42. EDS point elemental analysis result of sample #8 at (Point 1) 304H surface, and (Point 2) small particles on 304H surface

Other than TiC, TiB_2 was also used as coating source material for the 304H stainless steel substrate. SEM images of the Ti coated samples are as shown in Figure 43 (a), and (b). As shown in Figure 43(a), similar to the surface morphology of samples coated with TiC powders, the Ti coatings appeared to be more localized. Porous Ti coatings were also observed from the SEM image. At higher magnification, as shown in Figure 43 (b), however, coating area composed of spheres can be observed, other than Ti coatings composed of grain-like structures, as observed from Ti coating with TiC as source material

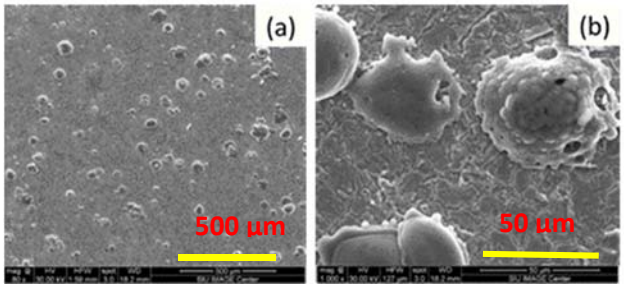

Figure 43. SEM images of Ti coated samples coated by HVOF using TiB2 powders as source material with coating duration of 8 minutes, (a) overall view, and (b) image at higher magnification.

430 Ferritic Steel

We continued and used identical conditions as reported in Table 6 to conduct the first set of coating for 430 ferritic steels. Then, 430 ferritic steel coupons were coated with TiC and TiB_2 using the

HVOF thermal spray method. The coating conditions and the source of Ti are provided in Table 7. In order to prevent corrosion on the uncoated sides, these samples were Ti coated on both sides of the substrates. Based on previous experiments, H_2/O_2 mixtures were used. Figure 44 shows the pictures of front and back side of Ti coated samples received. Samples coated with TiC synthesized at 1400^0C, 1500^0C, and samples coated with TiB_2 are shown in Figure 44 (a), (b), and (c). Between the two TiC coated substrates, a thicker layer of coatings was observed for substrate coated with TiC synthesized at 1400^0C. Coatings on substrate coated with TiB_2 powders also appeared to be higher in density compared to samples coated with TiC synthesized at 1500^0C.

Table 7. HVOF coating parameter and coating materials for the 430 ferritic steel substrates

	Source Material		
Spray Parameters	TiC 1400 °C, 1hr, 32%C	TiC 1500 °C, 2 hr, 32%C	TiB_2 20 % C
H_2 Flowrate (LPM)	76	76	76
O_2 Flowrate (LPM)	13	13	13
N_2 Flowrate (LPM)	4.3	1.4	1.4
Spraying Distance (cm)	27	28	28
Time (min./side)	5	12	20

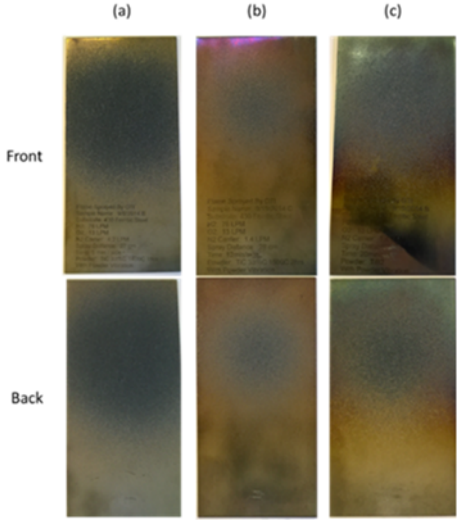

Figure 44. Front and back picture of 430 ferritic steels coated with (a) TiC synthesized at 1400^oC, (b) TiC synthesized at 1500^oC, and (c) TiB_2.

Figure 45 are the SEM images and corresponding Ti maps from EDS results of the Ti coated 430 steel substrates. Between substrates coated with TiC synthesized at 1400^0C (Fig. 45(a)), and 1500^0C (Fig. 45(b)), coatings composed of particles with smaller diameter variation can be observed the coating with TiC produced at the lower temperature. In addition, from the Ti maps according to the EDS result, higher percentage of steel surface was covered with Ti coatings for substrate coated with TiC powders synthesized at 1400^0C. For substrates coated with TiB_2, additional porous structures were observed by Ti coatings, as shown in Fig. 45 (c). The porous structures were identified as composed of Ti from EDS results.

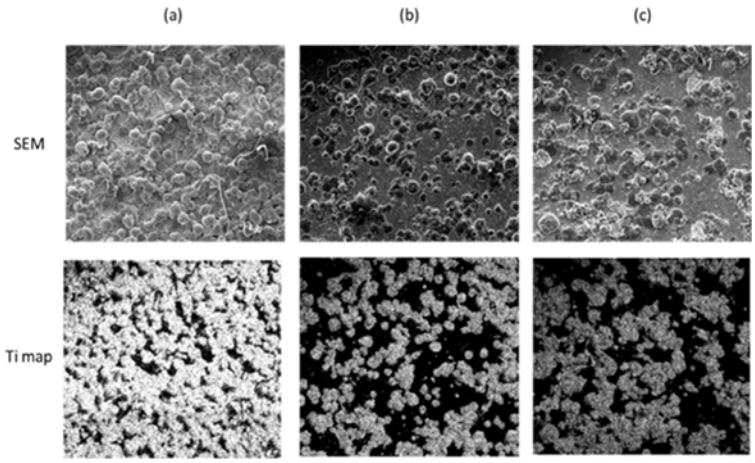

Figure 45. SEM images and corresponding Ti maps for 430 ferritic steels coated with (a) TiC synthesized at 1400°C, (b) TiC synthesized at 1500°C, and (c) TiB_2

P91 Ferritic Steel

P91 ferritic steel coupons were coated with TiC and Ti metals using the HVOF thermal spray method. The coating conditions and the source of Ti are provided in Table 8 and the coated sample pictures are in Figure 46. N_2 carrier flow rate and coating times were varied. In addition, one sample was glass blasted to smoothen the surface prior to water honing. In order to prevent corrosion on the uncoated sides, these samples were Ti coated on both sides of the substrates. Based on previous experiments, H_2/O_2 mixtures were used.

Table 8. HVOF coating parameters for the P91 coated substrates for the P91 coated substrates

HVOF Spray coating	
Spray Parameters	
H_2 Flow rate	76 LPM
O_2 Flow rate	13 LPM
N_2 Flow rate	1.8 LPM (Low Flow)/ 3.6 LPM (High Flow)
Spray Distance	27cm

Samples		Coating Time (min)	Coating Powder	Coating Conditions
A		0	Control, no coating	Glass blasted, then surface ground
B	Side A	12	TiC 32%C 1500C 2hr	Low N_2 carrier flow
	Side B	3	TiC 32%C 1500C 2hr	High N_2 carrier flow
C	Side A	12	Ti Metal	Low N_2 carrier flow
	Side B	3	Ti Metal	High N_2 carrier flow
D	Side A	12	TiC 32%C 1500C 2hr	High N_2 carrier flow
	Side B	12+12	TiC 32%C 1500C 2hr	High N_2 carrier flow
E		0	Glass Blasted Control	
F	Side A	12	TiC 32%C 1500C 2hr	Glass blasted, Low N_2 carrier flow
	Side B	12	TiC 32%C 1500C 2hr	Glass blasted, High N_2 carrier flow

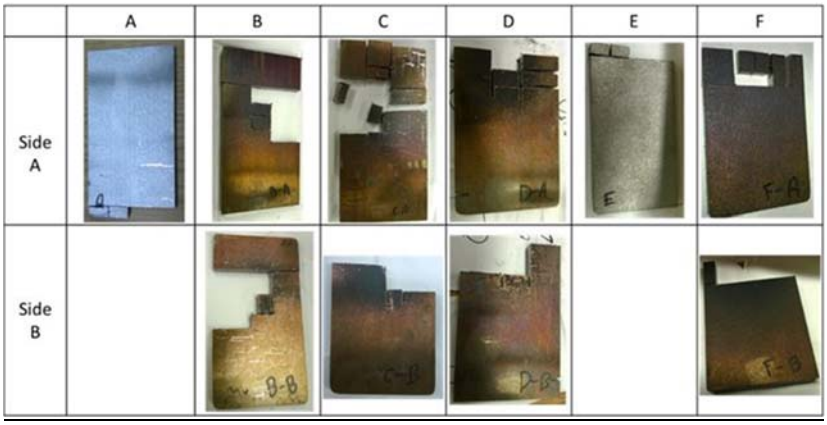

Figure 46. Photos of as-received P91 substrates.

As-received substrate A

Substrate A was glass blasted then surface ground, as a control for coated substrates B, C, and D. SEM Secondary Electron (SE) and Backscattering Electron (BSE) images of substrate A at 80X and 500X magnification were shown in Figure 47 (a) and (b). A striped texture can be observed from the surface of substrate. Backscattering electron images showed uniform composition of the substrate throughout the observed area.

As-received substrate B

Figure48. shows the SEM (a)Secondary electron and (b)Backscattering electron images of the two sides of substrate B (B-A and B-B). The difference between the two coatings was flow rate of the N_2 carrier. Side A (B-A) was coated with lower N_2 carrier flow for 12 minutes, and side B (B-B) was coated with higher carrier flow for 3 minutes. It can be observed that substrate B-B was covered more uniformly with TiC, from both SE and BSE images. At 500X magnification of the coated area, more overlap between coating splashes of coating materials were observed on side B.

As-received substrate C

Substrate C was coated with Ti metal as source on both sides. SEM secondary images for both sides of substrate C are shown in Figure 49 at (a)80X magnification, and (b)500X magnification. Side A (C-A) was coated with low N_2 carrier flow for 12 minutes, and side B (C-B) was coated with high N_2 carrier flow for 12 minutes. Similar to what was observed from substrate B, surface coated with high N_2 carrier flow for 3 minutes (C-B) had better coating coverage compared to surface coated with low N_2 carrier flow for 12 minutes (C-A). A more uniform coverage of P91 surface by the Ti material can also be observed at higher magnification (Figure 49 (b)). The coatings formed by Ti metal exhibited a more plate-like morphology.

As-received substrate D

Both sides of substrate D were coated with high N_2 carrier flow. Side A of substrate D (D-A) was coated for 12 minutes, and side B of the same substrate was coated for 12+12 minutes. From the SEM SE and BSE images, as shown in Figure 50, dense coating can be observed for both sides of

the substrates at the coated area. However, areas not being coated with the coating particles can still be observed. At 500X magnification, a more 3 dimensional coating can be observed on side B of substrate D. Coating materials in spherical form were also presented on side B of the substrate, whereas coating composed of lesser layers of coating overlaps was observed on side A.

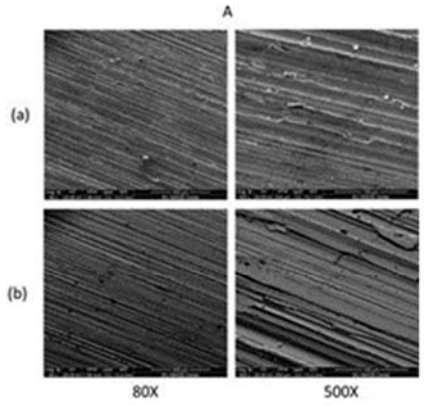

Figure 47. SEM (a)Secondary electron and (b)Backscattering electron images of as-received substrate A at 80X and 500X magnification.

Figure 48 SEM (a)Secondary electron and (b)Backscattering electron images of both sides of as-received substrate B (B-A and B-B) at 80X and 500X magnification

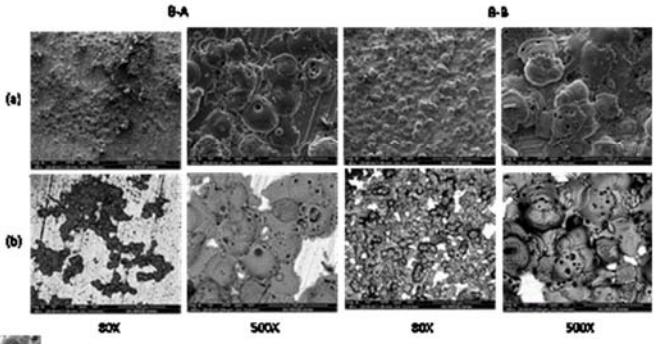

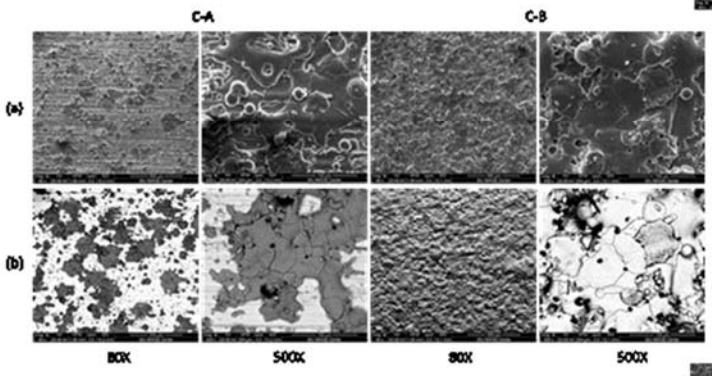

Figure 49. SEM (a)Secondary electron and (b)Backscattering electron images of both sides of as-received substrate C (C-A and C-B) at 80X and 500X magnification

Figure 50. SEM (a)Secondary electron and (b)Backscattering electron images of both sides of as-received substrate D (D-A and D-B) at 80X and 500X magnification.

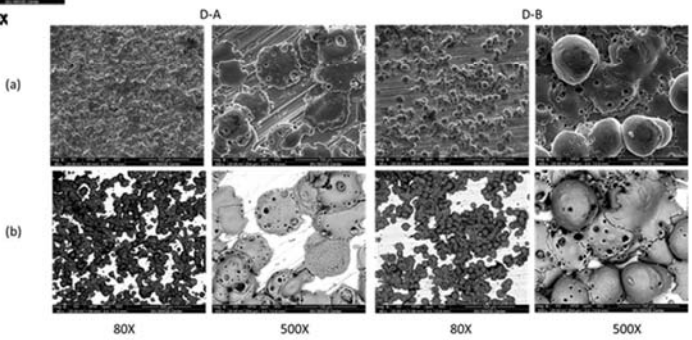

As-received substrate E

Substrate E was glass blasted substrate without coating, and served as control substrate for substrate F. SEM Secondary Electron (SE) and Backscattering Electron (BSE) images of substrate E at 80X and 500X magnification were shown in Figure 51 (a) and (b). Compared to substrates A through D, the surface on substrate E consisted of flake-like surface. Pores and cracks were also observed on the surface of substrate E.

As-received substrate F

Glass blasted substrate was utilized as matrix for substrate F. Both sides of the substrate were coated with TiC powders as source, but with low N_2 carrier flow for side A, and high carrier flow for side B, both coated for 12 minutes. SEM images of the substrates are shown in Figure 52: (a)Secondary electron, and (b) back scattering electron images for both sides of substrate F. An undulated surface coated with coating particles can be observed. On side B, which higher N_2 carrier flow was carried, a more concentrated coating was presented. Higher degree of surface coverage by the coating was observed on side B of the substrate as well as higher amount of coating material overlaps.

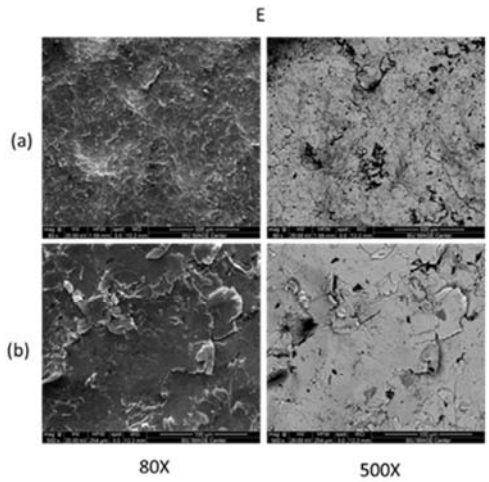

Figure 51. SEM (a)Secondary electron and (b)Backscattering electron images of as-received substrate E at 80X and 500X magnification.

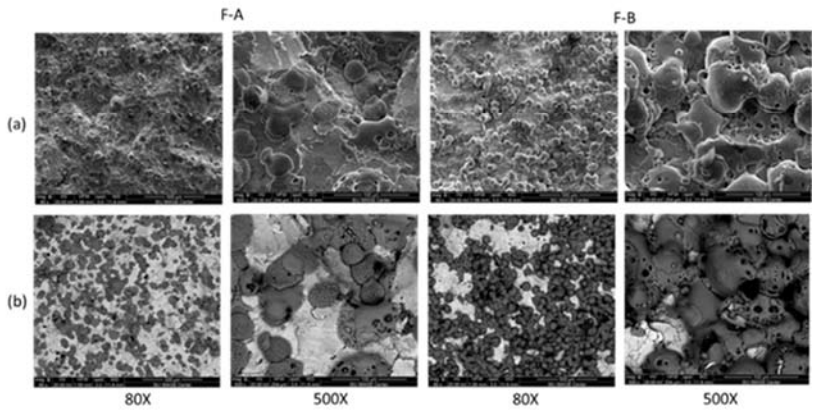

Figure 52. SEM (a)Secondary electron and (b)Backscattering electron images of both sides of as-received substrate F (F-A and F-B) at 80X and 500X magnification.

EDS mapping results for as-received substrate A

EDS mapping results for as-received substrate A are shown in Figure 53. Uniform distribution of elements analyzed can be observed from each maps. Detailed quantitative elemental analysis results for this substrate are also shown in Table 9, showing similar trend of elemental composition compared to the chemical composition of commercial P91 steel.

EDS mapping results for as-received substrates B, C, D, and F

EDS mapping results for iron and titanium for both sides of the as-received coated substrates are shown in Figure 54. Titanium coating condition and distribution of Ti and Fe on the surface of the substrates can be observed from the elemental maps. For all coated substrates, a clear interface between Ti and Fe was presented, indicating Ti coating covering the matrix of substrate.

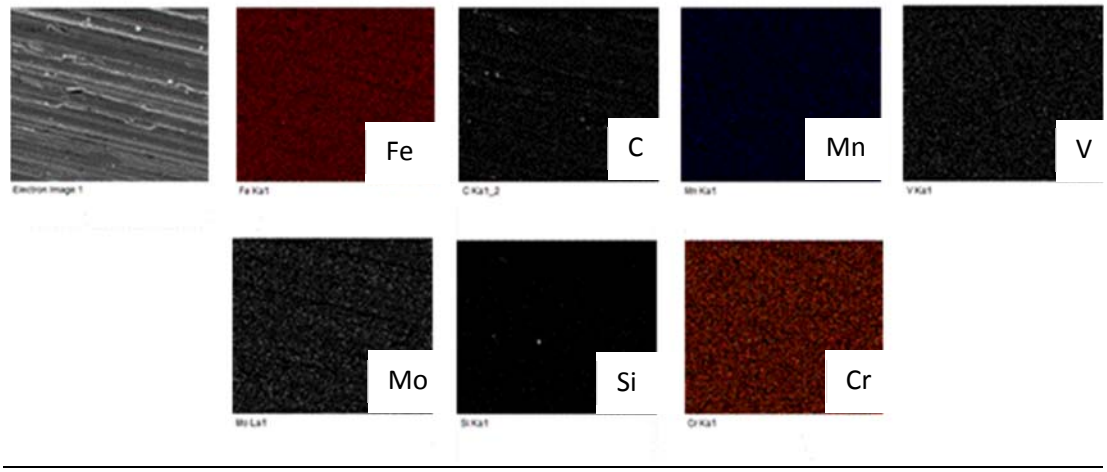

Figure 53. SEM image and corresponding EDS mapping results for as-received substrate A.

Table 9. Quantitative elemental analysis result of as-received substrate A.

Element	Weight%	Atomic%
O K	8.12	23.43
Si K	0.48	0.79
V K	0.21	0.19
Cr K	8.51	7.56
Mn K	0.49	0.41
Fe K	81.31	67.20
Mo L	0.87	0.42
Totals	100.00	

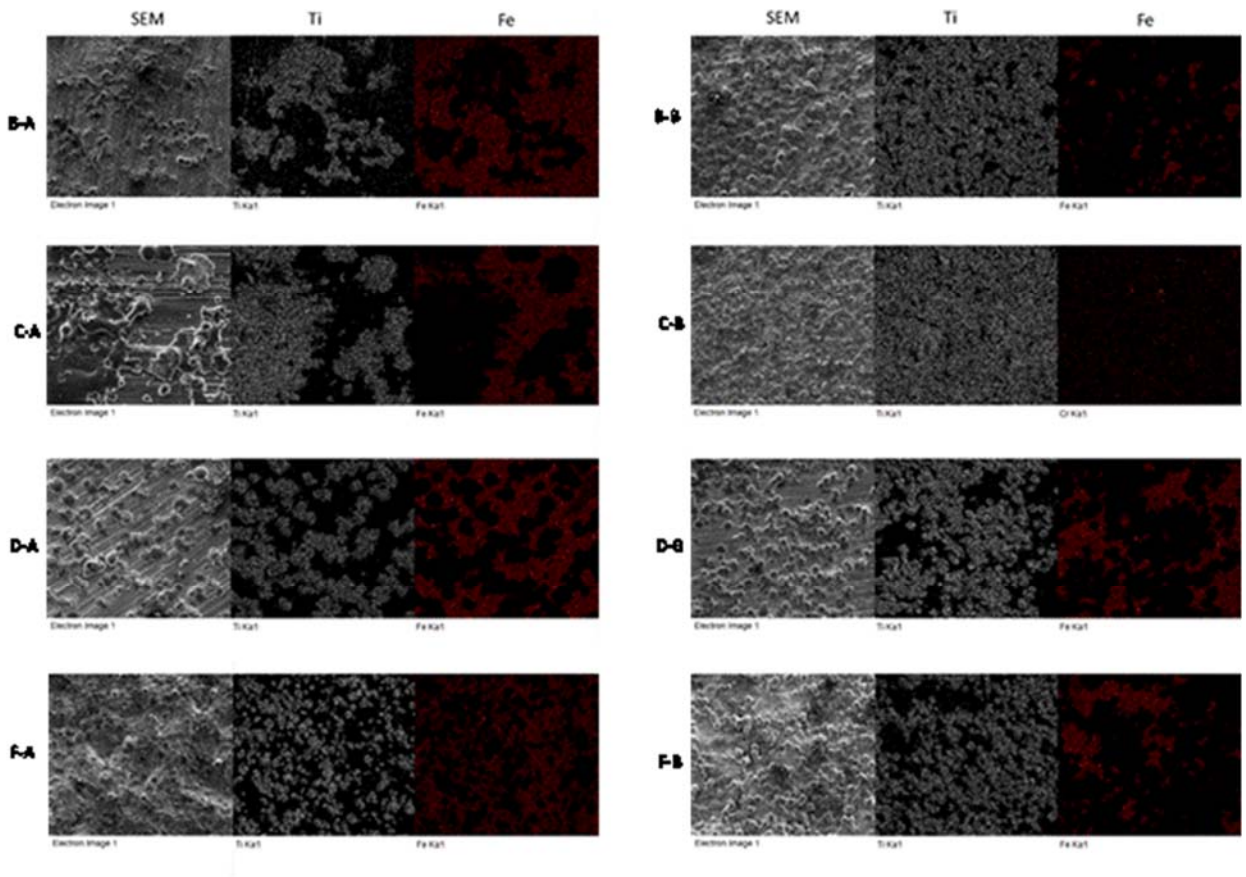

Figure 54. SEM images and corresponding EDS mapping results for Ti and Fe for both sides of as-received Ti coated substrate B, C, D, and F.

CORROSION STUDIES

304 H

Summary of Findings

In general, the use of TiC improved the corrosion resistance of the 304H substrate. Figure 55 is shows two surfaces (top and bottom of the same coupon) – one coated and the other uncoated exposed to air for 800 hrs at 750 °C. While the coated surface shows relatively no visible signs of degradation, the uncoated side turned black due to the formation of magnetite and chromium oxide (Figure 56). Additionally, it is observed in Figure 57 that the oxygen penetration is limited to the surface on the coated side and progresses from the bottom (uncoated) primarily.

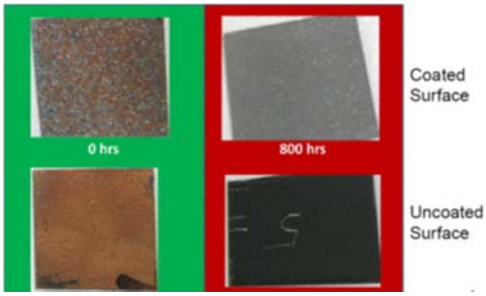

Figure 55. Optimal images of the coated and uncoated sides of HVOF TiC coated sample (Coating 2) before and after 800 hrs of air oxidation tests at 750 °C.

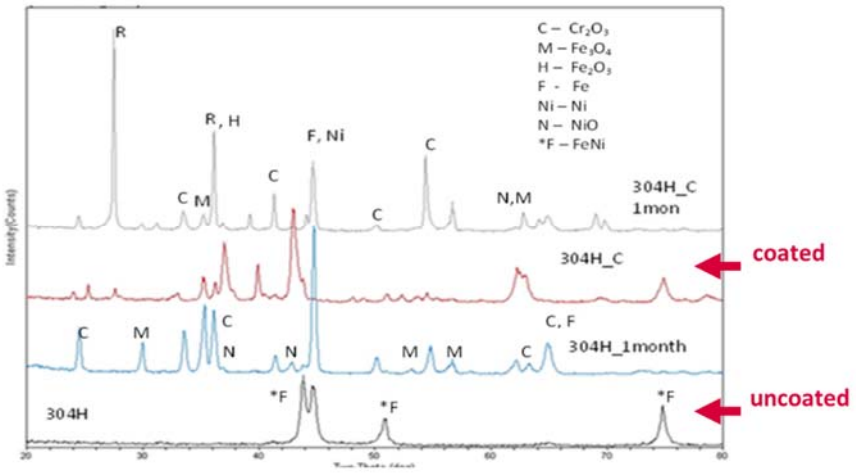

Figure 56. X-ray diffractograms of the uncoated and HVOF TiC coated (Coating 2) SS 304 H before and after exposure to air at 750 °C for 800 hrs.

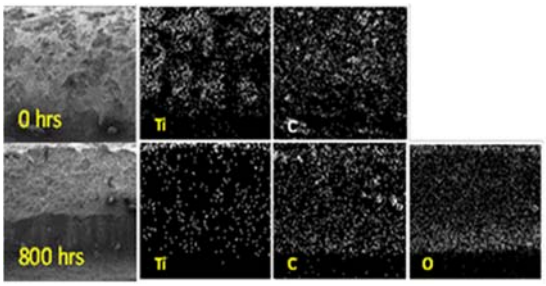

Figure 57. Elemental distribution of Ti, C and O along the cross section of the HVOF TiC coated sample-Coating 2- before and after exposure to air at 750 °C for 800 hrs.

EDS line scan analysis was utilized as new analysis method for the stainless steels substrates. The EDS line scan result of a TiC coated 304H substrate after 800 hours of air corrosion test is shown in Figure 58. Elemental composition of 5 spots along the cross section of the substrate were analyzed, with spectrum 13 at the surface where the Ti coating was applied, and spectrum 2 close to the center of the substrate. According to the analysis result, significant amount of titanium was found on the surface, along with oxygen, iron, chromium, relatively smaller amount of nickel, and manganese. With increase of distance from the point of analysis to the surface of the substrate, increase amount of iron, oxygen, chromium, and nickel was observed. Amount of oxygen was found to decrease with increased distance from the surface. Increase of iron, chromium and nickel indicates that the titanium based coating can serve as barrier coating, restricting access of oxygen and outward diffusion of iron.

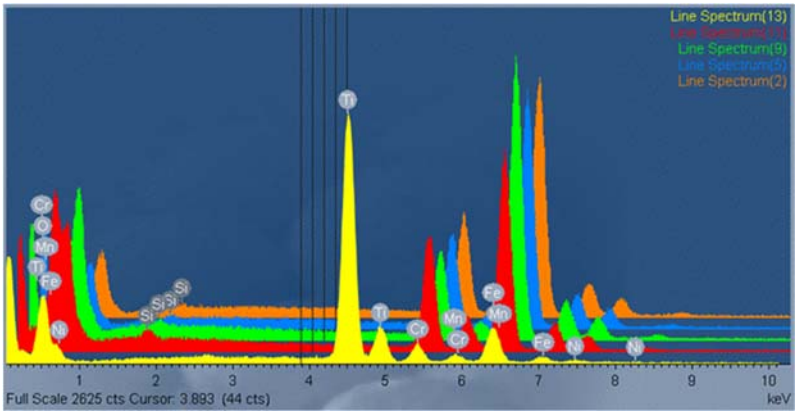

Figure 58. EDS line scan result of Ti coated 304H substrate after 800 hours of air corrosion test at 750^{o}C

The HVOF coating process was further tuned and the effect of the type of oxidant fuel combination was evaluated. The coated samples showed significant improvement in corrosion resistance as compared to the uncoated samples. Figure 59 and Figure 60 compares the uncoated samples exposed to 750 ^{o}C air for 800 hrs as compared to the TiC coated sample using the air-acetylene based coating process. Traces of oxidation was found deep into the uncoated substrate after 800 hrs of testing (Figure 59). The amount of chromium was found to increase after 800 hrs of heat treatment for the uncoated substrate. For the coated sample (Figure 60) the amount of chromium was found to slightly increase with time of heat treatment. No significant increase of oxygen was observed after 180 hrs of testing, and slight amount of oxygen was found after 800 hrs of testing.

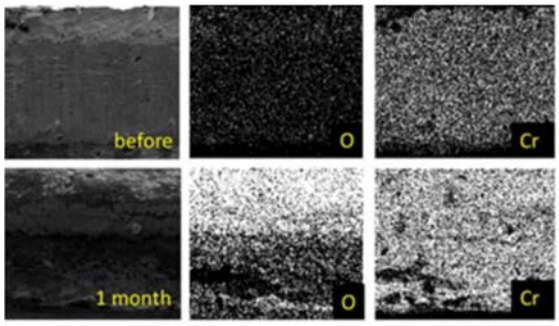

Figure 59. EDS result of cross sectional area of uncoated stainless steel substrate for Chromium and Oxygen.

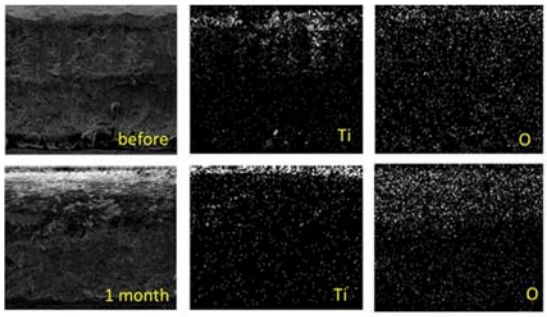

Figure 60. EDS result of cross sectional area of coated stainless steel substrate (obtained from acetylene/ air flame)

As mentioned earlier, it was determined that coating with H_2/O_2 based flame provided the best coating (based on XRD data shown later). The final set of experiments were conducted to evaluate the effect of titanium metal, and TiC obtained from 32 % C coated TiO_2 and 33 % C coated TiO_2 prepared was 1500 ^oC for 2 hrs. Figure 61 shows EDS results of elemental maps for samples coated with (a) Ti metal (5 min coating), (b) TiC powder sintered at 1400^0C (32 % C coated TiO_2 precursor), (c)TiB_2, and (d)TiC sintered at 1500^0C (33 % C coated TiO_2 precursor) with regards to Ti, Fe, Cr, and O. From the oxygen distribution maps, higher concentration of oxygen can be observed at the surface of the all substrates, and considerably lower amount of oxygen was observed at regions away from the surface, indicating low oxygen penetration from the surface during air corrosion test at 750^0C for 800 hrs. From the depth profiles, it is clearly seen that relatively low amount of iron occurs in the same region as the high oxygen. For the sample with TiC prepared at lower temperature and 3 min of coating and the TiB_2 sample, come chromium appears to have diffused to the high oxygen region (partially due to the incomplete coating). This is not observed for the other two samples. Thus, both Ti metal and TiC sintered at 1500^0C (33 % C coated TiO_2 precursor) and coated for 10 minutes appears to provide substantial oxidation protection to 304 H.

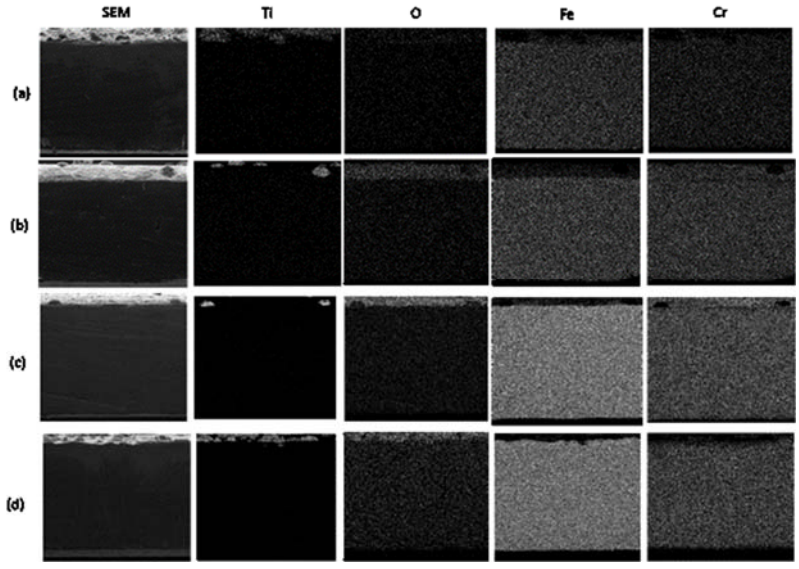

Figure 61. SEM images and EDS results of then cross section of(a) Ti metal (5 min coating), (b) TiC powder sintered at 1400 ^oC (32 % C coated TiO_2 precursor, 3 min), (c)TiB_2 (8 min coating), and (d)TiC sintered at 1500 ^oC (33 % C coated TiO_2 precursor, 10 minute coating) coupons tested for 800 hr in air at 750 ^oC

When resistance to the sulfates and chlorides was tested at 750 ^oC for 800 hrs, the uncoated sample failed (simply disintegrated). As for the coated sample, it is clear from the optical image (Figure 62), that the coated surface was substantially protected and the any corrosion that occurred propagated from the uncoated side as the salts melted and encapsulated the sample. Figure 63

shows the SEM images and elemental profile of the 180 hr test where it is observed that in over a weeks' time, micro cracks are formed on the uncoated substrate that led to the destruction by 800 hrs. These cracks were absent in the coated sample.

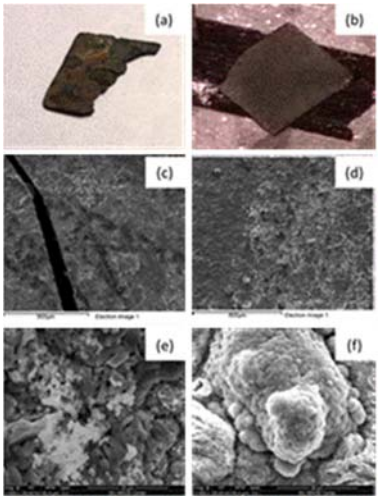

Figure 62. Photo of (a) uncoated 304H, (b) Ti coated 304H, SEM images of (b, e) uncoated 304H, and (d, f) Ti coated 304H after 800 hours of salt corrosion test at 750°C

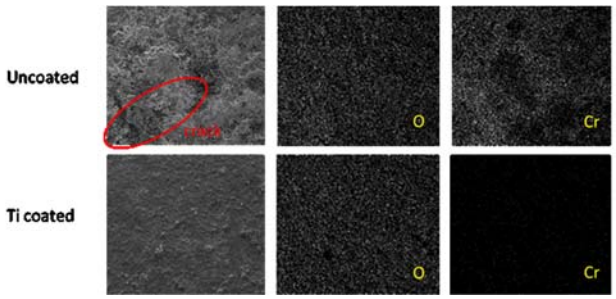

Figure 63. SEM images and EDS results of uncoated and coated substrate before and after 180 hr ash corrosion test.

Simulated flue gas experiments were conducted at 500, 600, 650, and 700 °C. Significant change in surface morphology including large cracks and increased amount of small iron oxide particles was observed for the uncoated steel after 180 hrs. Large oxidation and sulfurization grains were obviously seen in the SEM images, accompanied with corrosion pits and spallation of oxidation scales. Moreover, fine porous structures (less than 1um in diameter) were found on localized surface area on the steels, which were not found before the corrosion test. For the Ti metal coated samples, SEM shows increased roughness and cracks while the EDS results showed that higher amount of sulfur was presented at the rougher areas found on the samples, as shown in higher amount of sulfur was observed around the edges of Ti coating. Compared to Ti metal coated samples, surface of samples coated with TiC (32wt% Carbon coated TiO_2 precursor) and TiB_2 nanopowders are considerably smoother. No significant oxidation/ corrosion pattern or spallation of oxidation scales were observed on surface of these samples. Considerable amount of sulfurization and oxidation grains were observed on surface of sample samples coated with TiC (33wt% Carbon coated TiO_2 precursor). Corrosion islands were found on surface of coated with TiC (33wt% Carbon coated TiO_2 precursor) for 10 minutes, which seemed to be spalling off from the surface of the substrate. Note that sulfur and oxygen amount is significantly lower at Ti coating area. Figure 64 compares the surface morphology of the TiC and TiB_2 coated samples exposed to the simulated flue gas at 700 °C. Figure 65 compares the cross sectional elemental distribution for

samples coated with Ti metal (#6), both the TiCs (#5 and 9) and TiB_2 (#7) for 10 minutes that were exposed to simulated flue gas for 360 hrs. Signs of oxidation/ sulfurization was observed at surface of the stainless steel substrate of sample #6 at 700^{0}C corrosion test. However, Ti coating appeared to have stopped the oxidation and sulfurization from penetrating into the substrate, as no oxygen or sulfur was detected at deeper spots. The overall corrosion resistance impact by the type of coating and temerpature is summarized in Figure 66.

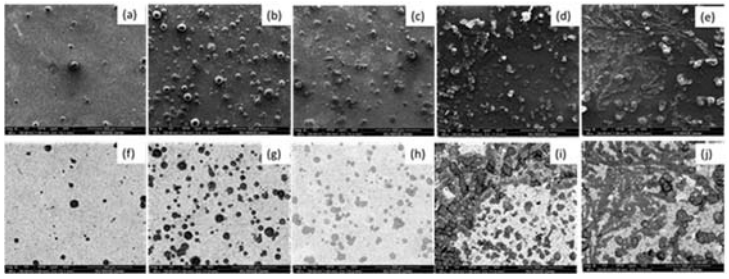

Figure 64. (a) to (e) SEM images of TiC (32wt% Carbon coated TiO_2 precursor) coating for (a) 3 min, (b) 10 min, (c) TiB2 coated and TiC (33wt% Carbon coated TiO_2 precursor) coating for (d) 6.5 min, (e) 10 min, and (f) to (j), backscattering images.

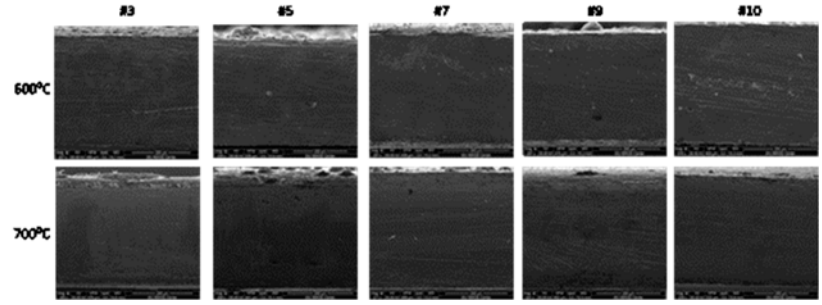

Figure 65. Cross sectional SEM images of sample #6, #5, #7, #9, and uncoated substrate after simulated flue gas corrosion test at 600^{o}C and 700^{o}C.

	500°C	600°C	650°C	700°C
Titanium	No noticeable oxidation or sulfurization on surface of sample	S – Less (coated) Less sulfur observed at coated area	Less sulfur and oxygen observed at coated area	Less oxygen observed at coated area
TiB_2		**S - Significantly** less (coated) sulfur and O -slightly less(coaated area	• Significantly less sulfur and oxygen at coated area • Concentrated sulfur and oxygen around coated area	Less oxygen observed at coated area
TiC		• Significantly less sulfur and oxygen at coated area • Concentrated sulfur and oxygen around coated area		Significantly less sulfur and slightly less oxygen at coated area

Figure 66. Effect of temperature and coating type on corrosion in simulated flue gas.

The following paragraphs provided further detailed analysis of the studies conducted on 304 H.

Air Corrosion Studies

The two coated samples and the uncoated sample sent as the first set was evaluated for air corrosion. Exposure to air for 180 and 800 hrs at 750 ^{o}C resulted in a loss of mass of 2.32 % and

6.53 %, respectively for the uncoated sample. For coating sample 1, mass loss of 2.13% and 4.21% were observed for the two time periods while for coating sample 2, there was a gain of 3.74 % and a loss of 0.73 % respectively. Figure 67 shows the SEM images of the SS304H in the as received condition, air oxidation tests for 180 hrs at 750 ^{o}C and for 800 hrs at 750 ^{o}C at two different magnifications. The changes in the surface due to high temperature air oxidation is evident from these figures.

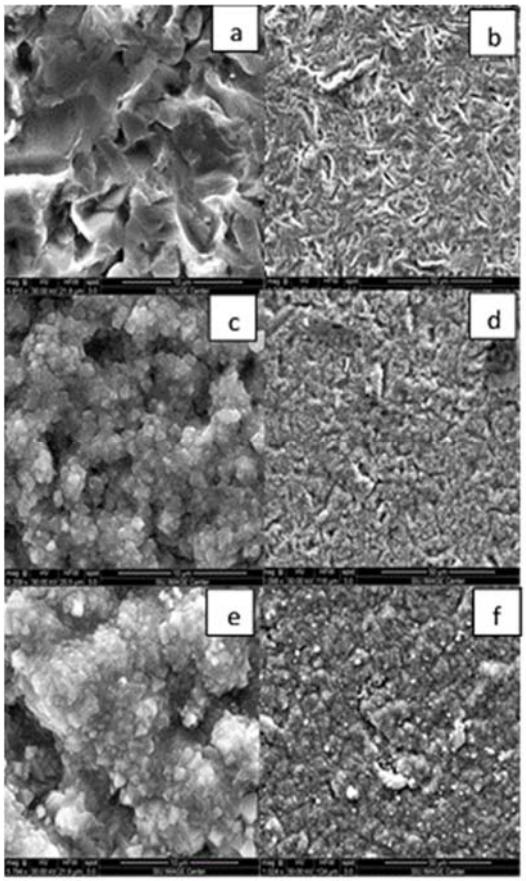

Figure 67. SEM images of surfaces of uncoated SS304H after air oxidation tests at 6k and 1k magnifications a&b) original sample, c&d) 750oC for 180 hrs and e&f) 750 ^{o}C for 800 hrs.

Figure 68 are the SEM images of Coating 1 and 2. The images on the left are those of the as received samples while those on the right are the samples after 800 hrs of air oxidation at 750 ^{o}C.

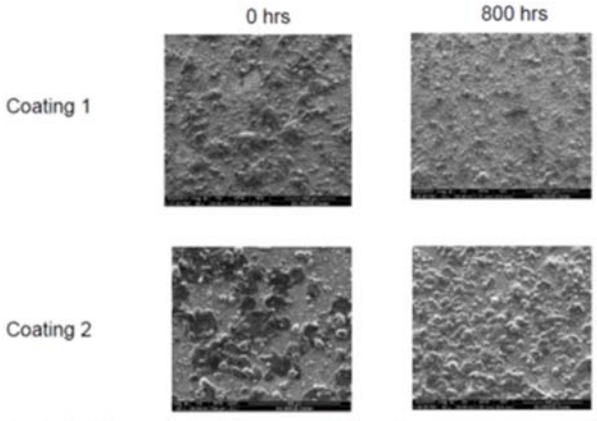

Figure 68. SEM images of HVOF TiC coated SS304H samples of as-received and air oxidized at 750 ^{o}C for 800 hrs

Of the two coated samples received, visual inspection showed that the Coating 2 was more uniform and thus the following discussion is on the results from Coating 2 although identical analyses was conducted on Coating 1. Figure 55 are optical images of Coating 2. It contains images from both the coated (top) and uncoated (bottom) sides of the sample. The images on the left are those of the as received sample while that on the right are those obtained after air oxidation experiments for 800 hrs at 750 ^{o}C. Figure 69 are the EDS spectra of the coated side before and after 800 hrs of air oxidation tests at 750 ^{o}C.

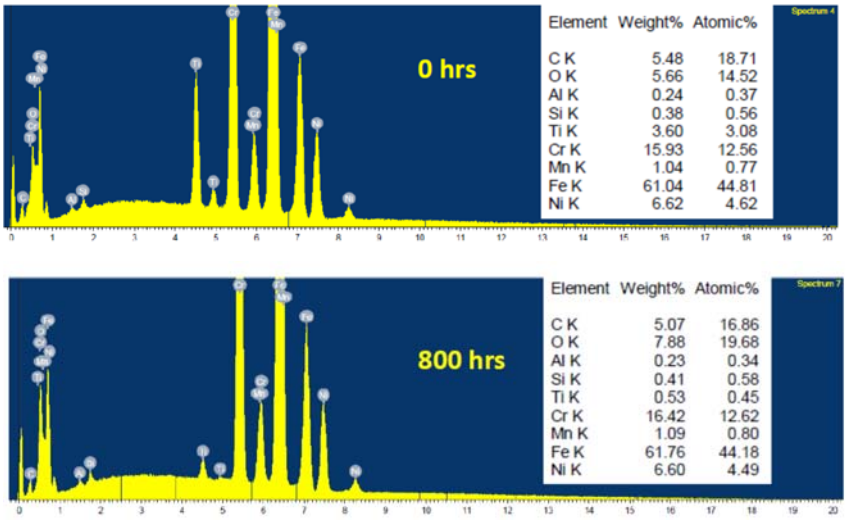

Figure 69. EDS spectra of the coated side before and after 800 hrs of air oxidation tests at 750 ^{o}C

We also conducted XRD analyses on the uncoated and Coating 2 samples and those spectra of the as received and the 800 hrs of air oxidized sample at 750 ^{o}C are shown in Figure 56. A distinct difference is observed in the two samples. However, the presence of iron and Ni show that the coating are not thick enough and not surprisingly some amount of magnetite and hematite are observed in coating 2 (304H_C) after 800 hrs of exposure to air at 750 ^{o}C. However, the oxidized states of iron cannot be deconvoluted enough to justify the claim that the surface is oxidized.

We have also conducted the electron microscopy under backscattering mode to observe the elemental distribution along the cross section (depth of the coating). Figures 70 and 57 are the images obtained from these tests. Figure 70 are the backscattering images of the coated (Coating 2) and uncoated samples. It is interesting to note the islands of C in the uncoated sample. Figure 57 shows the elemental distribution of the as received sample (top) and the sample obtained after exposure to air at750 ^{o}C for 800 hrs. We observed from the images on the bottom that while the coating has been oxidized to a certain degree, the SS304H substrate do not show oxygen and thus can be assumed to be protected from air oxidation for at least 800 hrs.

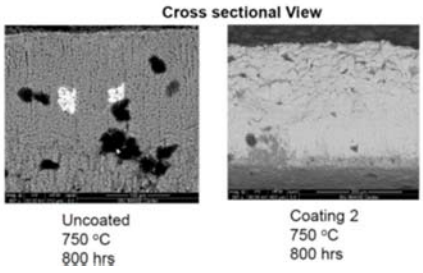

Figure 70. Electron microscopy images under backscattering mode of the cross section of the coated and uncoated samples after exposure to air for 800 hrs at 750 ^{o}C.

Detailed analysis of SEM and EDS results for the coated and uncoated stainless steel substrates were discussed in order to understand the corrosion resistance mechanism of the Ti coating. Figure 71 shows the SEM images of substrates before air corrosion test, and substrates exposed at 750^0C for 200, and 800 hours for uncoated 304H stainless steel (a, c, e) and Ti coated 304H (b, d, f). Significant change in surface morphology was observed for uncoated substrate. Formation of oxidant can be observed from the result after 200 hours of testing, as shown in Fig. 71(c). Also, severe cracking was found on the iron oxide due to thermal stress generated due to the high temperature. Oxygen can attack the 304H substrate from the cracks, and lead to continuous oxidation, and spallation of the oxidation layer. After 800 hours of testing, further spallation of the oxidation scale was observed, along with newly formed oxidation phase extruding the surface of the 304H, as shown in Fig. 71(e). Pores and voids created due to the presence of magnetite on the substrate were observed. The presented defects led to extensive oxidation of the substrate, as oxygen can access through the voids and react with iron under the oxidation layer, forming more spinel magnetite. Ti coated substrates on the other hand, did not suffer from severe corrosion due to oxidation. Fig. 71(b) shows titanium-rich particle coated on the substrate before oxidation test. Dense coating formed by HVOF thermal spray process was observed. In Fig. 71(d) and (f), distinct difference of surface morphology of the coated substrate can be observed compared to the uncoated 304H. No significant crack or spallation was observed for the dense titanium-rich coating after 200 hours of air corrosion test, as shown in Fig. 71(d). After 800 hours of testing, uniform continuous coating consisted of crystals mostly smaller than 200nm in diameter was observed. These crystals were determined as rutile TiO_2 crystals from XRD results. Increased grain size of the rutile crystals was observed after 800 hours of testing comparing to the crystals after 180 hours of testing. However, no spallation was observed after long exposure at 750^0C, and the rutile crystals appear to be densely and uniformly distributed on the surface of the 304H substrate, indicating good air corrosion resistance of the coating.

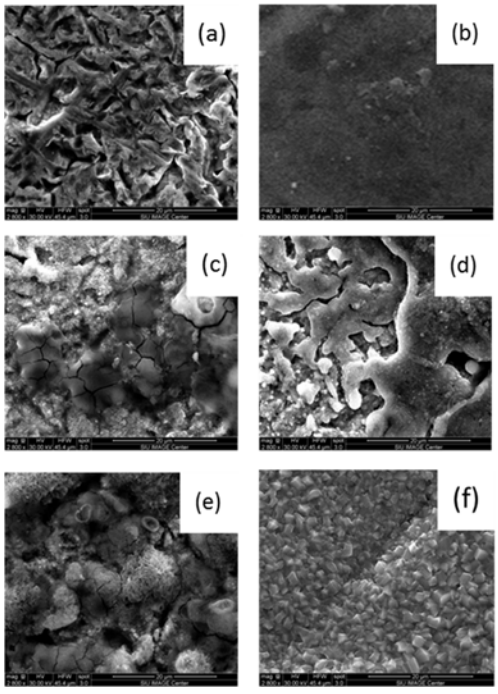

Figure 71 SEM images of substrates heat treated at 0, 180, and 800 hours of air corrosion test for uncoated 304H stainless steel (a-c) and Ti coated 304H (d-f).

Figure 72 shows the EDS result of uncoated 304H after 800 hours of air corrosion test at (a) the oxidation pattern formed on uncoated 304H and (b) surface not covered by the pattern. From the quantitative result, the oxidation pattern is determined to be dominant by iron oxide, and only small amount of chromium was observed on the pattern, whereas significantly higher amount of chromium was detected at uncoated area. This indicated that although protective Cr_2O_3 layer was formed on the surface of 304H, an extra layer of iron oxide was also formed on top of the Cr_2O_3 layer.

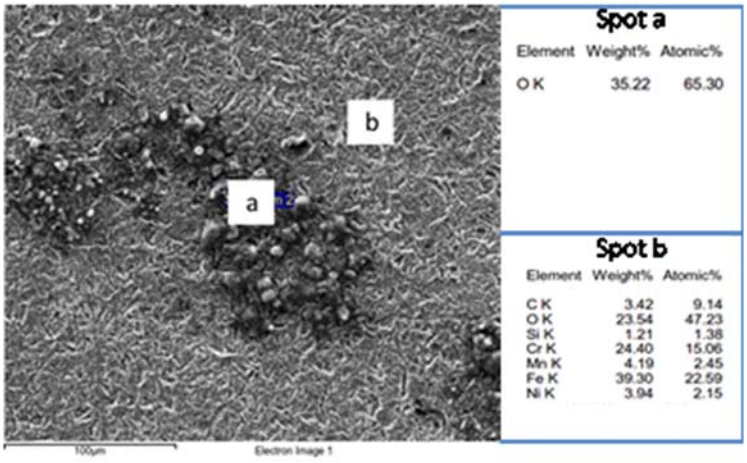

Figure 72. EDS analysis result of (a) oxidation pattern and (b) surface of uncoated 304H.

Table 10 contains the mass change data after air corrosion tests for 180 and 800 hrs for experimental set 2. This set contained 10 samples (including control) that were coated with using different oxidant fuel mixture for the thermal spray coating along with different coating duration. The TiC used was produced by using 33 % C coated TiO_2 carburized at 1400 ^oC for 2 hrs. It is observed in Table 10 that in spite of identical conditions, the air oxidation resulted in different weight change numbers which indicate problems associated with such a test. The results may also be correlated to the thickness of the coatings which in turn can be related to the time for coating. It is seen in the table that the corrosion extents are correlated well with the Ti at %. Figure 73 contains the elemental distribution on the surface of the sample 11 (C_2H_2 /Air) after it was exposed for 800 hrs to air at 750 ^oC. It can be seen that the chromium appears to get denser on the surface at the locations where Ti is not present.

800 hrs air corrosion test at 750^0C for both uncoated and TiC coated stainless steel substrates was also completed for samples 3-12. Characterization for the substrates was conducted. Surface morphology information of the substrates was obtained from SEM images, and elemental distribution of the substrates was further analyzed with EDS. Figure 74 shows the SEM images of surface of both as received and 800 hrs air corroded samples obtained under different thermal spray coating fuel/oxidant combinations. For uncoated substrate, it was observed that a new layer of structure was formed on the surface of the substrate after 800 hrs air corrosion test. From EDS result, the occurring patterns were composed of Iron oxide particles. EDS result of the oxidation pattern observed on uncoated substrate is as shown in Figure 75. It can be seen that the pattern is iron and iron/ oxygen- rich structure.

Table 10. Air corrosion experiments on the new coatings (750 °C)

Sample		180 hrs		800	
		After	Before	After	Before
3	Control	-2.56%	-6.39%	-4.98%	-6.63%
4	H_2/Air	15.80%	2.34%	32.14%	7.74%
5	H_2/O_2	42.74%	20.35%	45.02%	28.27%
6	C_2H_2/Air	4.49%	-6.17%	11.94%	-6.57%
7	H_2/O_2	-1.06%	-4.25%	-0.50%	-2.52%
8	H_2/O_2	-3.60%	-5.66%	-5.65%	-8.72%
9	C_2H_2/Air	-1.77%	-2.36%	-4.94%	-4.94%
10	C_2H_2/Air	0.00%	-2.64%	-4.43%	-9.96%
11	C_2H_2/Air	13.11%	-4.03%	12.58%	-6.82%
12	C_2H_2/Air	-7.55%	-10.46%	-10.67%	-14.22%

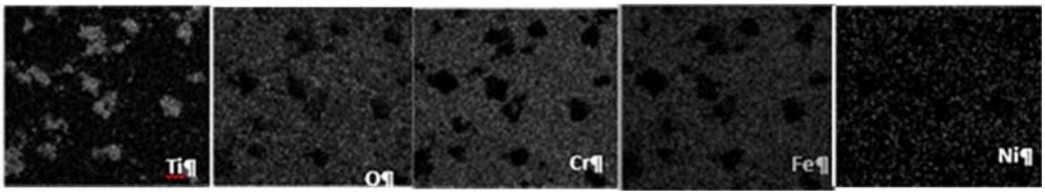

Figure 73. Elemental mapping of coated surface the air oxidized sample with coating obtained in hydrogen-oxygen flame.

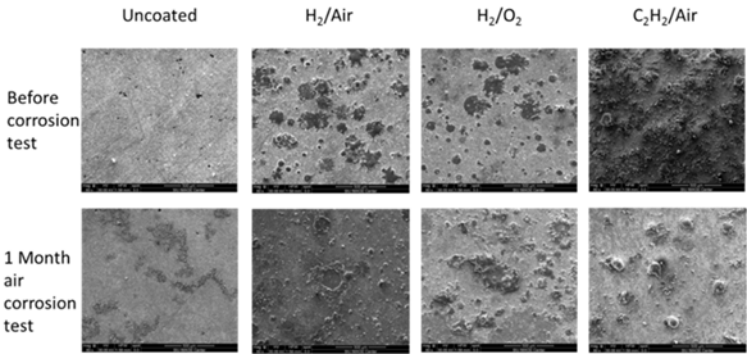

Figure 74. SEM images of uncoated substrate and coated substrates obtained from various types of flame before and after 800 hrs air corrosion test at 80X magnification.

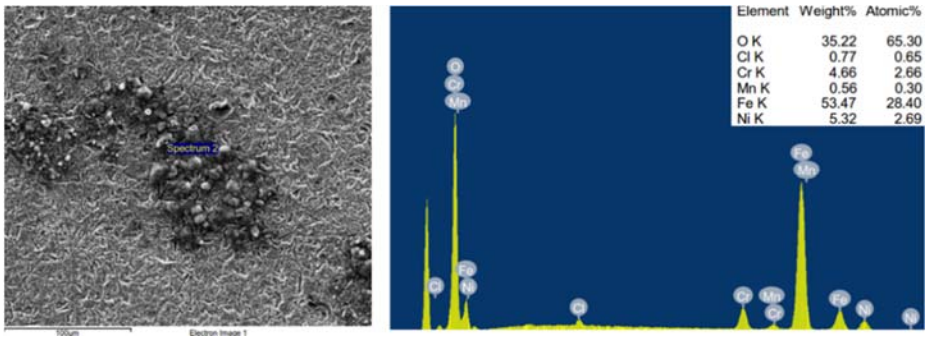

Figure 75. EDS result of oxidation pattern observed on uncoated substrate.

For TiC coated substrates obtained from Hydrogen/ oxygen flame, similar pattern was also found at area which Ti was not coated sufficiently, as shown in Figure 76. However, percentage of iron on the pattern found on coated substrate was significantly lower than that of uncoated substrate. Such oxidation pattern was not found at area with thicker TiC coating.

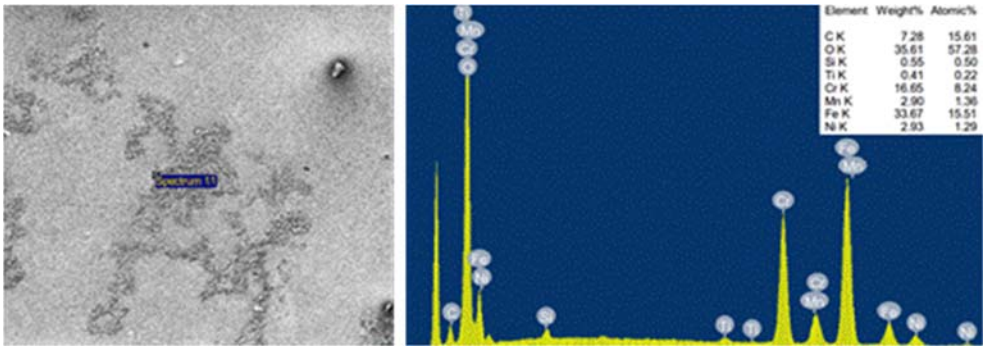

Figure 76. EDS result of oxidation pattern observed on Ti coated substrate obtained from Hydrogen/ Oxygen flame.

At higher magnification, as shown in Figure77, the oxidation pattern can be clearly seen that surface of the uncoated substrate. It can also be noticed that surface of the substrate was overall more rough after 800 hrs of air corrosion test. For TiC coated samples, it was observed that amount of smaller particles on the surface of substrate was found to decrease with time of heat treatment. The diminishing small particles were then confirmed to be composed of titanium-rich particles. Data from EDS study on the sample are shown in Figure 78 for the substrate obtained from acetylene/ air flame. Surface of larger coating particles were also found to be rougher after 800 hrs of corrosion test. No significant change in surface morphology was observed for surface areas lightly coated with TiC however.

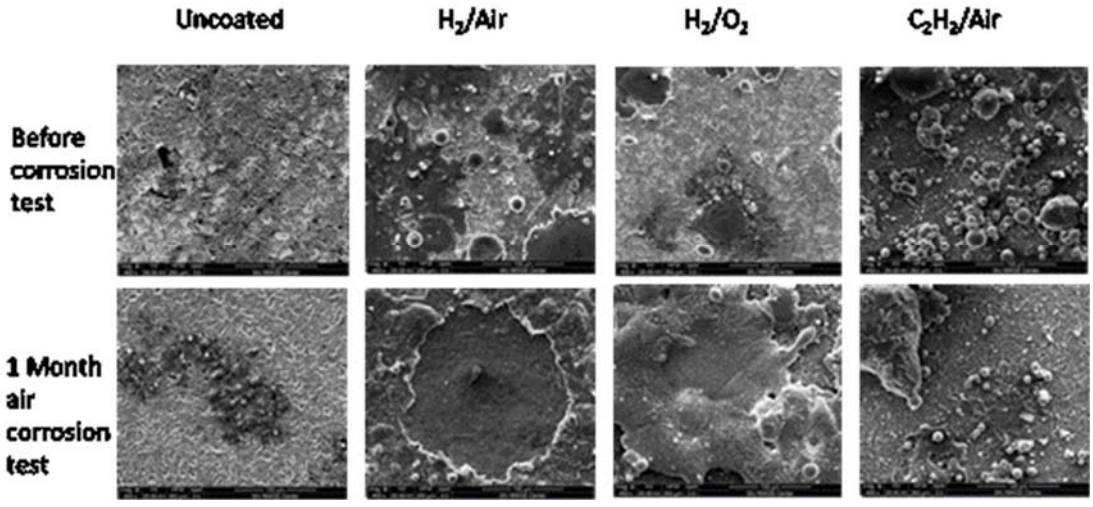

Figure 77. SEM images of uncoated and coated substrates obtained from various types of flame before and after 800 hrs air corrosion test at 450X magnification.

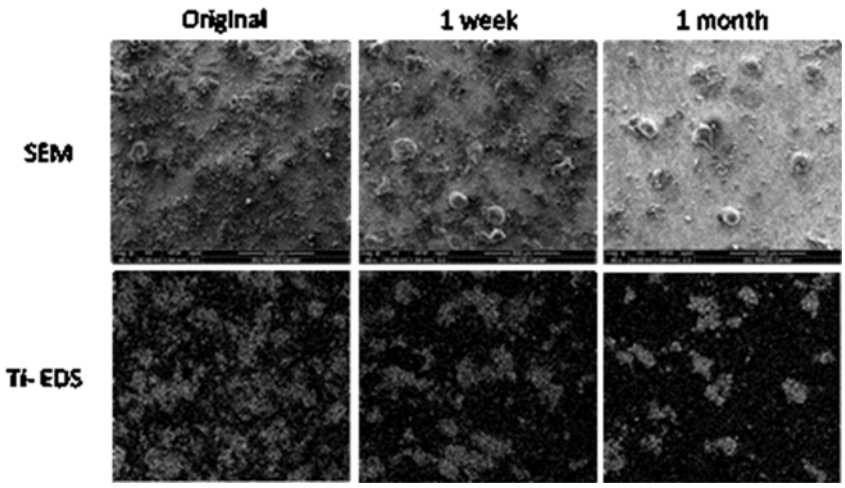

Figure 78. SEM images and Ti- EDS for substrate obtained from acetylene/ air flame before and after air corrosion test.

Change of oxygen percentage on the surface of coated substrate was further examined. From EDS data, the content of oxygen on coating particle was found to increase significantly from 200 hrs of air corrosion to 800 hrs. On the contrary, in areas coated with less TiC, the oxygen content decreased slightly within the same time frame. The result is shown in Figure 79. Oxidation due to air corrosion test of uncoated substrate was also observed from cross sectional EDS of the substrate, as shown in Figure 59. From the EDS data, significant amount of oxygen was found around the surface of substrate after 180 hrs of testing. Traces of oxidation was found deep into the substrate after 800 hrs of testing. Figure 60 shows EDS result of cross sectional area of coated sample obtained from acetylene/ air flame.

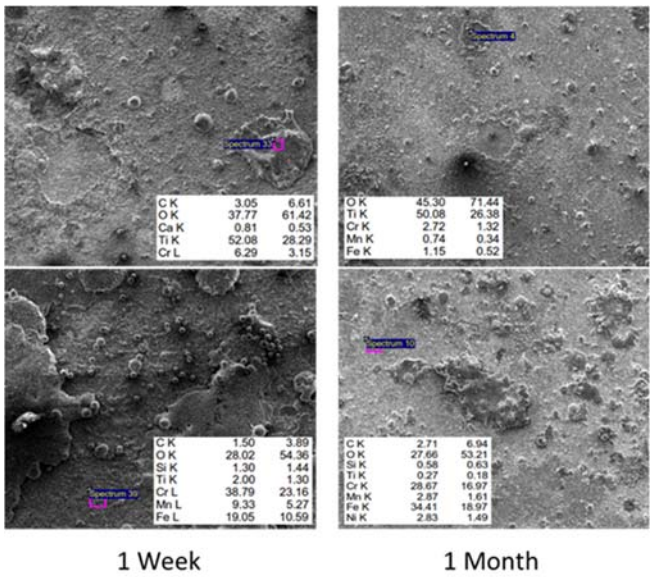

Figure 79. Comparison of oxygen percentage on coating particle and surface of Ti coated substrate at 180 hrs and 800 hrs of air corrosion test.

X-ray diffraction (Figure 80) was also conducted for both the uncoated and coated substrates after 800 hrs of air corrosion test. The $2\theta = 45^0$ peak in every pattern was identified as Fe(110) peak. TiC and peaks can be found on coated substrates, indicating TiC was successfully coated onto the stainless steel substrate with all three coating method based on different atmosphere.

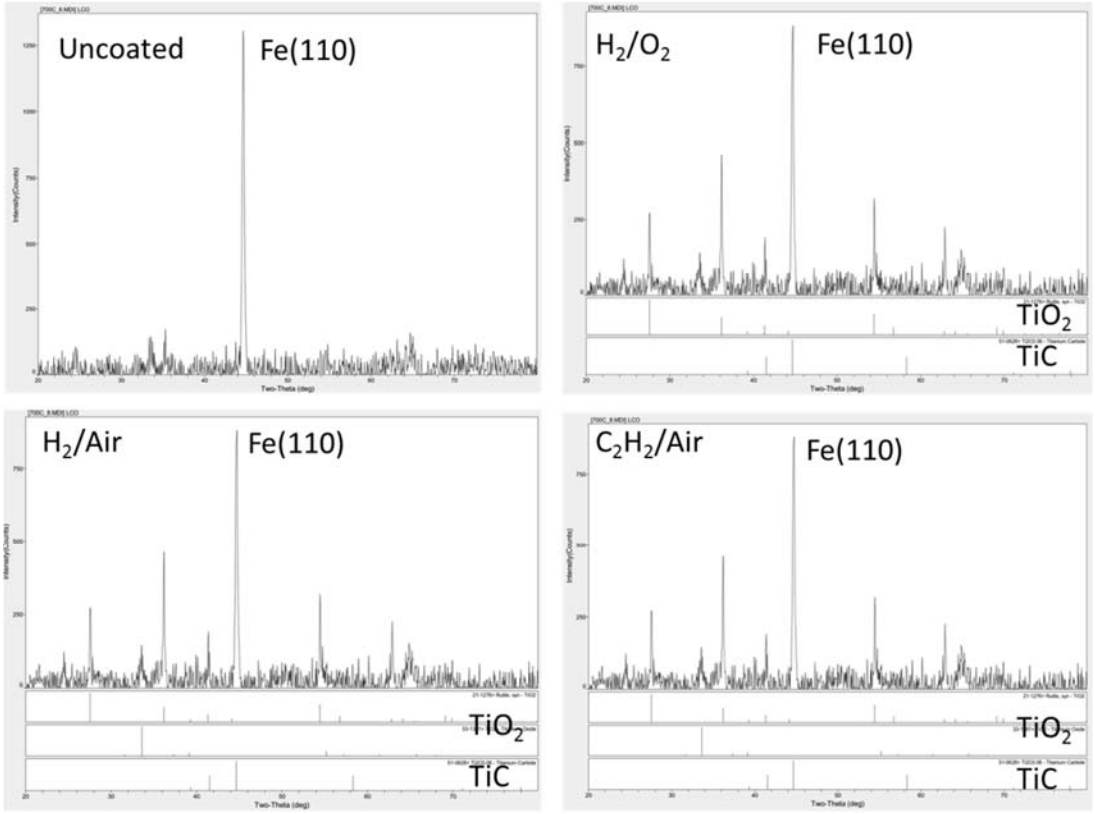

Figure 80. XRD pattern of uncoated substrate, and Ti coated substrate obtained from hydrogen-air flame, hydrogen-oxygen flame, and from acetylene flame.

It was determined that coating with H_2/O_2 based flame provided the best coating. The final set of experiments were conducted to evaluate the effect of titanium metal, and TiC obtained from 32 % C coated TiO_2 and 33 % C coated TiO_2 prepared wat 1500 ^oC for 2 hrs. SEM images and back-scattering images of samples coated with Ti metal (sample #1 to #3- 1 to 5 minute coating) are as shown in Figure 81 (a) to (c). From Figure 81(a), darker area around the Ti coating was observed in both images from secondary electrons and back-scattering electrons. The area was later identified with EDS as containing higher amount of oxygen, as shown in Figure 82 (a). Such oxidation area was not observed from images of sample #2 and #3 (3 and 5 minute coating of Ti metal), where the stainless steel surfaces were more evenly coated with titanium. However, flower like structure was observed on certain titanium coated area on sample #3, and was later identified as chromium and oxygen rich structures, as shown in Figure 82 (b).

SEM images and back-scattering images of stainless steels coated with TiC nanopowders (sample #4, 5, 8, 9) and with TiB_2 (sample #7) are shown in Figure 83 (a) to (d). Titanium based coatings are more localized for samples coated with nanopowders, possibly due to the structure of

nanopowders. Also, from the both secondary images and back-scattering images, no significant sign of oxidation of the stainless steel substrate was observed. However, for samples #4 and #5 (TiC from 32 % C coated TiO_2), flower-like structures were found by some Ti coated areas. The flower structures were later characterized by EDS as chromium and oxygen rich structures, as shown in Figure 84. For samples #8 and #9 (TiC from 33 % C coated TiO_2), higher amount of chromium was observed around some Ti coating concentrated areas, as shown in darker area by Ti coating in back-scattering images.

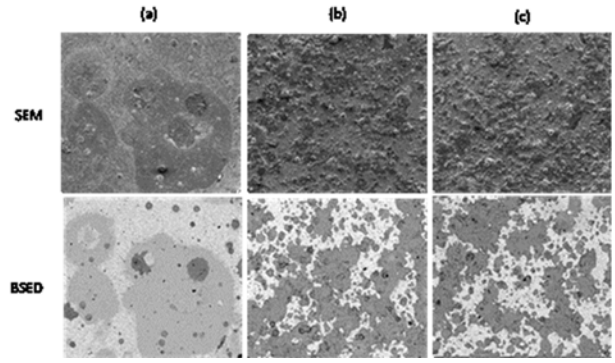

Figure 81SEM (secondary and back-scattering electron) images of Ti metal coated stainless steels (a) sample #1 (1 min coating) to (c) sample #3 (5 min coating) after 800 hrs of air corrosion test.

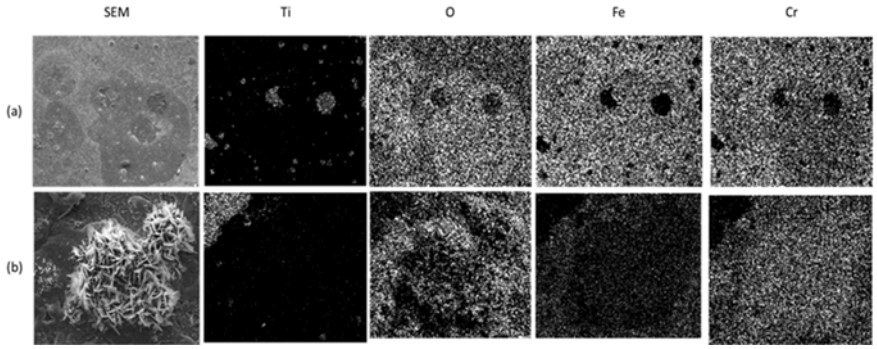

Figure 82 EDS result of (a) sample #1 (1 min coating), and (b) flower like structure on Ti coating of sample #3 (5 min coating) after 800 hrs of air corrosion test.

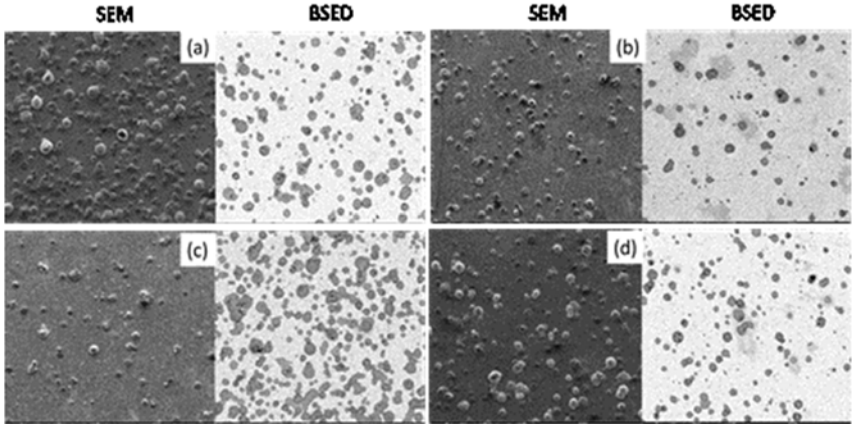

Figure 83 SEM (secondary electron and back-scattering electron) images of (a)sample #4 (3 min coating with TiC from 32 % C coated TiO_2, (b) sample #5 (10 min coating with TiC from 32 % C coated TiO_2, (c) sample #8 (6.5 min coating with TiC from 33 % C coated TiO_2)

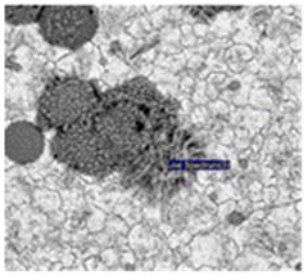

Element	Weight%	Atomic%
O K	41.28	70.09
Ti K	0.77	0.43
Cr K	35.47	18.53
Fe K	22.49	10.94

Figure 84. EDS result of flower structure on sample #4 (3 min coating with TiC from 32 % C coated TiO_2)

Cross sectional EDS analysis conducted for the Ti coated samples shows agreement with the surface SEM analysis for improved corrosion resistance of the substrates compared to the uncoated stainless steel substrates. Figure 61shows EDS results of elemental maps for samples coated with (a) Ti metal (5 min coating), (b) TiC powder sintered at 1400^0C (32 % C coated TiO_2 precursor), (c)TiB_2, and (d)TiC sintered at 1500^0C (33 % C coated TiO_2 precursor) with regards to Ti, Fe, Cr, and O. Considerably lower amount of oxygen was observed at the cross section of samples, indicating low oxygen penetration from the surface during air corrosion test at 750^0C for 800 hrs.

Simulated Ash Corrosion Tests

Coated and uncoated substrates were tested with simulated ash corrosion test. More in-depth discussion of the SEM and EDS results were studied. For these experiments we have layered the samples with a salt mixture of NaCl, Na_2SO_4, KCl and K_2SO_4 in the ratio of 1:1:1:1. We have used duplicates for all three samples. Table 11 contains the weight loss as a percentage of the initial weight after exposure to the salts for 800 hrs and 750 ^{o}C. It should be noted that visually, it was clear that the corrosion of the substrates that were coated with TiC were primarily corroded on the uncoated side and thus leading to weight loss. The samples were weighed immediately after removing from the high temperature zone (Before) and the samples were then air brushed and weighed again (After). From the SEM images as shown in Figure 63, cracks were found on samples without coating after 800 hrs of exposure. TiC coated samples does not seem to be affected structurally from the salt mixture. From extensive EDS analysis, amount of chromium on the surface of uncoated substrate is significantly higher than that of Ti coated substrate.

Table 12 contains the weight loss data on the various 304H substrates coated with TiC using different oxidant fuel combinations. Figure 62 show the visual condition of (a) uncoated and (b) TiC coated substrate and SEM images of (c) uncoated and (d) coated substrates after 800 hours of simulated ash corrosion test. The uncoated substrate suffered severe corrosion, which led to embrittlement and interlayer cracking. The cracking at the edge of the coated substrate is believed to be cause by molten salt flowing through the uncoated side of the substrate during corrosion test. Further investigation was conducted for both samples with SEM and EDS. Micro-cracks were observed on the uncoated substrates which were not found on the coated substrate. Small crystals along the crack were identified as iron rich structures. This may be evidence of outward diffusion of iron reacted with chloride forming iron chlorine. Also, iron oxide and iron chloride can be observed throughout the surface of the uncoated substrate. Further investigation was conducted with higher magnification of SEM image as shown in Fig. 62(e). It can be seen that the surface of the uncoated 304H is covered by iron oxide and iron chloride crystals with diverse grain size. Stacking of oxide particles with wide range of grain size resulted in large amount of pores,

loosening the strength of the oxide layer. In fact, the entire 304H substrate was embrittled and almost completely destroyed after the corrosion test. On the other hand, no significant crack or sign of corrosion was observed for the TiC coated substrate, as shown in Fig. 62(d). At higher magnification, SEM image of surface of the coated 304H revealed that the surface is covered by scale consist of dense clusters of iron-rich fine particles, as shown in Fig. 62(f). The dense scale may serve as barrier, preventing inward diffusion of reactive elements, restricting outward diffusion of the metal cations, and thus improved overall corrosion resistance.

Table 11 Results of Corrosion in Alkali Salt Environment at 750 °C and 800 hrs

Sample		Weight Loss (%)
SS 304H	uncoated	48.13
SS 304H	Coating 1	39.71
SS 304H	Coating 2	31.16

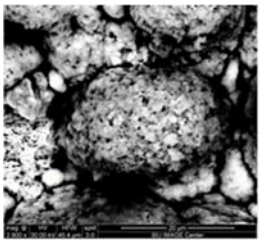

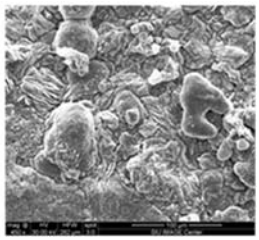

Figure 85 SEM image of surfaces after exposure to simulated ash environment after 800 hrs (left – uncoated, right - coated)

Table 12. Simulated ash corrosion tests for 200 hrs and 750 °C

	Spray Conditions							
Sample	H_2	O_2	Air	C_2H_2	T (°C)	d (cm)	Ti (at %)	Ash Corrosion (Wt Loss %)
Control							-	38.47
H_2/Air	46		9		3200	25	2.6	11.58
H_2/O_2	46	12			3200	25	10.93	1.44
C_2H_2/Air			9	24	2500	25	5.24	14.08
H_2/O_2	46	12			3200	25	1.91	18.26
H_2/O_2	46	12			3200	25	3.02	17.00
C_2H_2/Air			9	24	2500	25	1.29	24.63
C_2H_2/Air			9	24	2500	25	6.54	22.86
C_2H_2/Air			9	24	2500	25	8.86	12.05
C_2H_2/Air			9	24	2500	25	3.43	23.52

Improved parameters on SEM/ EDS analysis

Parameters with regard to distance between SEM pole piece and the sample, and voltage of the electron beam used during EDS analysis were optimized for better results. Figure 86 shows the EDS oxygen mapping result of the uncoated stainless steel substrate with (a) original parameter,

and (b)improved parameter. Higher contrast of oxygen signal can be seen from both substrates before air corrosion test(before), and after 800 hr air corrosion resistance test.

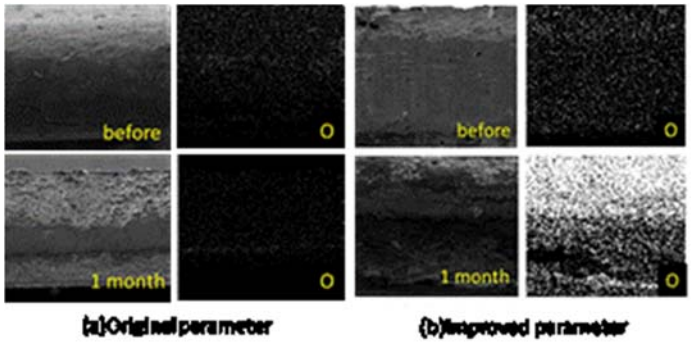

Figure 86 EDS results of uncoated stainless steel substrate recorded with (a)original parameter and (b)improved parameter with SEM

Simulated Flue Gas Corrosion

180 hrs of simulated flue gas corrosion test at 500 ^{0}C for Ti coated 304H steels

180 hrs of corrosion test in simulated flue gas condition at 500^{0}C was performed for the set three batch of Ti coated 304 stainless steels coated with parameters, and SEM/ EDS analysis was performed. Figure 87 shows the SEM images of uncoated 304 stainless steels (a) before corrosion test and (b) after 180 hrs of simulated flue gas test at 500^{0}C. This may be the result of severe oxidation/ sulfurization on the uncoated steels.

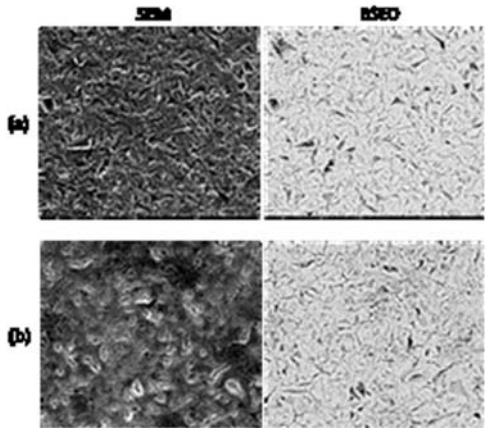

Figure 87. SEM (secondary and back-scattering electron) images of original 304 steel substrate (a) before, and (b) after 180 hrs simulated flue gas corrosion test at 500^{o}C.

For the Ti coated samples, after simulated flue gas corrosion test at 500^{0}C for one week, cracks as well as oxidation patterns were observed on samples coated with titanium metal. Such phenomenon was not observed for either Ti coated sample using TiC or TiB_2 as source of coating material. Figure 88 shows SEM image of selected Ti coated samples using (a), (b) titanium metal, (c) TiC, and (d) TiB_2 as source of coating. The granular structure observed on the Ti coating shown in Figure 88 (b) was later characterized as containing higher amount of oxygen, as shown in Figure 89.

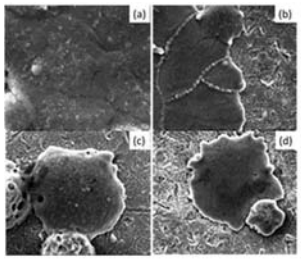

Figure 88. SEM images of surface of Ti coated samples (a) sample #2, (b) sample #3, (c) sample #4, (d) sample #7 after 180 hrs simulated flue gas corrosion test at 500°C

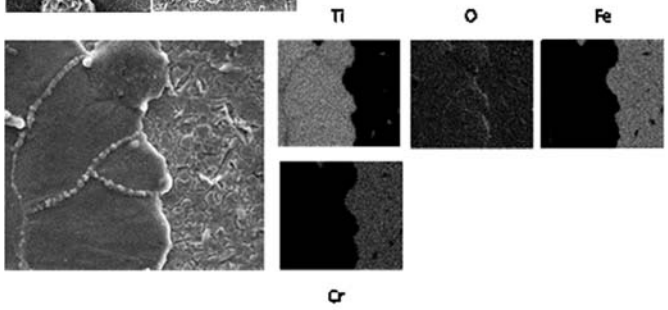

Figure 89. SEM image and EDS results of 304 stainless coated with Ti metal after 180 hrs simulated flue gas corrosion test at 500°C

360 hrs simulated flue gas corrosion test at 600 °C for Ti coated 304H stainless steels

Samples #1 to #3 and #6 are 304 steels coated with Ti metal as Titanium source under different coating time. SEM images of the surface of samples #1 (1 min coating) to #3 (5 min coating) and #6 (10 minute coating) are shown in Figure 90 (a) to (d). Rougher surface due to presence of newly formed oxidation grain and sulfurization structure compared to samples previously tested for air corrosion test was observed for sample #1 to #3. Larger Ti coating area was observed on sample #6 (10 min coating) compared to sample #1 to #3. This is due to longer coating time during HVOF coating process. It was observed that the larger Ti coating on sample #6 may have cracked during this corrosion test. SEM backscattering images of the samples are shown in Figure 90 (e) to (h). Presence of corrosion patterns were observed on area not coated with Ti as shown in the backscattering images.

EDS results showed that higher amount of sulfur was presented at the rougher areas found on the samples, as shown in Figure 91 (a) to (c). Higher amount of sulfur was observed around the edges of Ti coating on sample #6. Corrosion patterns on the stainless steel matrix of sample #1 shown in Figure 90(a) were identified as patterns consisted of higher amount of sulfur.

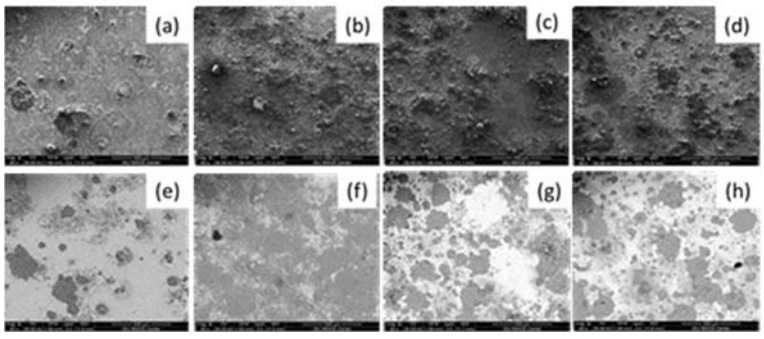

Figure 90. SEM images of sample (a)#1, (b)#2, (c)#3, and (d)#6 after 360 hrs simulated flue gas corrosion test at 600°C, and corresponding backscattering images (e) to (h).

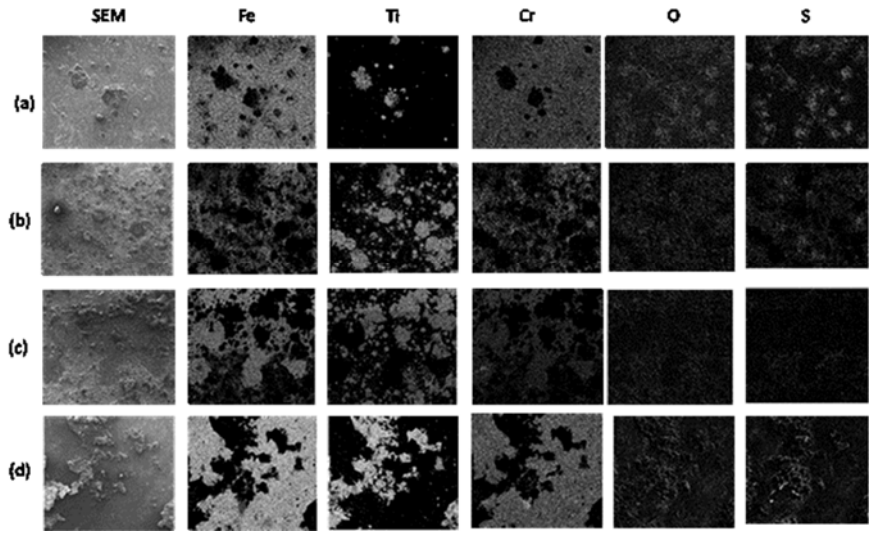

Figure 91. SEM and corresponding EDS results of sample (a)#1, (b)#2, (c)#3, and (d)#6 after 2 weeks simulated flue gas corrosion test at 600^{o}C

Samples #4, #5 are stainless steel substrates coated with TiC powders synthesized with 32 wt.% of carbon at 1400^{0}C and samples #8 and #9 are TiC powders synthesized with 33 wt.% of carbon at 1500^{0}C. Sample #7 was stainless steel coated with TiB_2 powders. SEM images of samples #4, #5, and #7 to #9 are shown in Figure 92 (a) to (e). Corresponding SEM backscattering images of the samples are shown in Figure 92 (f) to (j). EDS data on the samples are shown in Figure 93(a) to (e). No obvious sign of corrosion or crack of TiC coating was observed on the surface of sample #4 and #5. Surface of the stainless steel substrate did not show obvious sign of corrosion (oxidation or sulfurization) either. Note that the fibers observed on the surface sample #4 and #5 are from the support material in our test furnace, but not part of the coating/ stainless steel substrates. From EDS data it was determined that amount of sulfur present on the surface of substrate is less compared to samples coated with Ti metal. EDS data on sample #4 and #5 also confirmed that although presence of sulfur was found on the surface, no significant sign of oxidation or sulfurization was found on both the TiC coating, and the stainless steel substrate.

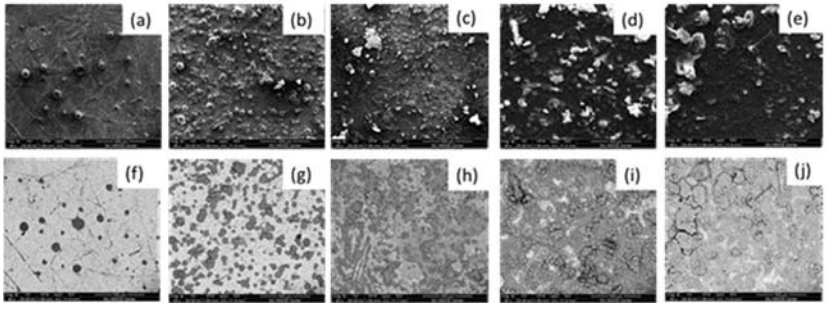

Figure 92 SEM images of sample (a)#4, (b)#5, (c)#7, (d)#8 and (d)#9 after 360 hrs simulated flue gas corrosion test at 600^{o}, and corresponding backscattering images (f) to (j).

Large area covered by sulfur as well as rectangular sulfur-rich particles were observed from EDS result of sample #7. Small flakes of iron oxide were also observed surrounding sulfur rich particles and TiB_2 coating particles. Increased amount of sulfur was also observed for sample #8 and #9. Sulfur-rich islands were found close to, and surrounded the TiC coatings. Higher amount of oxygen according to EDS results was also observed at area not coated with TiC.

SEM image of pristine 304 stainless steel is shown in Figure 94 (a). Corresponding backscattering image and EDS results are shown in Figure 94 (b) and (c), respectively. Surface of the uncoated substrate is covered by sulfur and oxygen rich particles and grains, with some grains larger than 100 μm in diameter. Intergranular corrosion can be observed leaving gaps between iron grains on the stainless steel matrix.

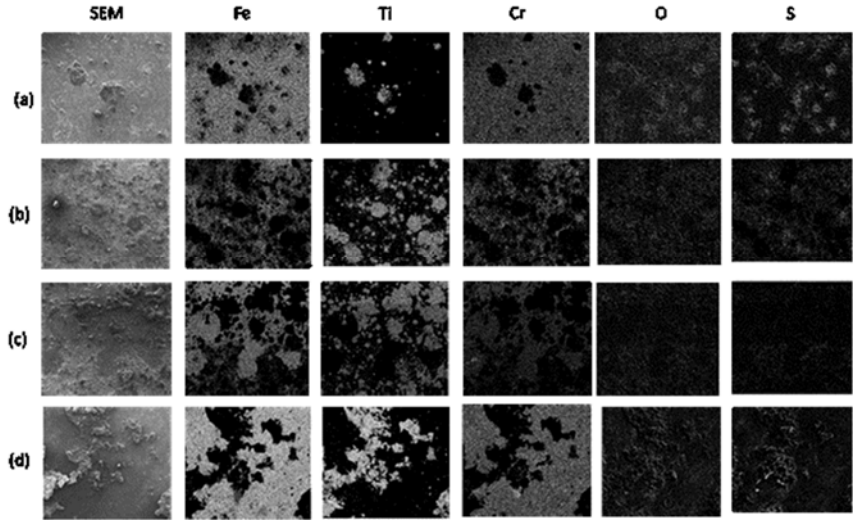

Figure 93. SEM and corresponding EDS results of sample (a)#4, (b)#5, (c)#7, (d)#8, and (e)#9 after 2 weeks simulated flue gas corrosion test at 600°C.

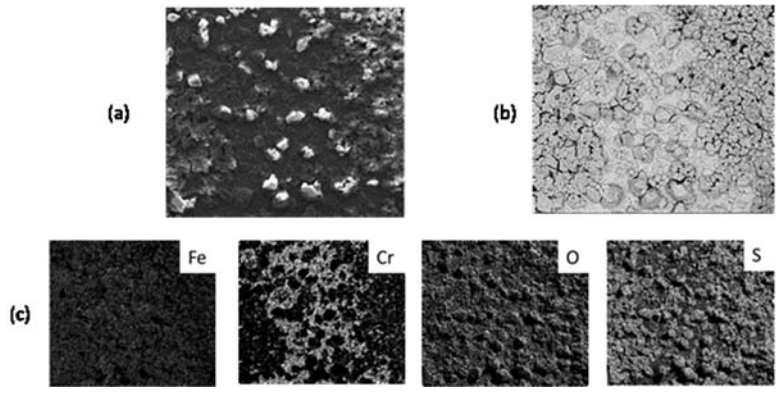

Figure 94(a)SEM (b)backscattering image and (c)EDS results of pristine 304 stainless steel after 360 hrs simulated flue gas corrosion test at 600°C.

180 hr simulated flue gas corrosion test at 650^{0}C for Ti coated 304 stainless steels

Ti coated 304 stainless steel samples as well as pristine 304 substrates were also tested under simulated flue gas condition at 650^{0}C for 180 hrs. SEM images of the surface of Ti coated samples using Ti metal as source, sample #1 to #3 and #6 are as shown in Figure 6 (a) to (d); corresponding backscattering images are shown in Figure 95 (e) to (h) Oxidation and sulfurization can be observed on the surface of the samples at areas not being coated with Ti. In addition, oxidation patterns on the Ti coatings were also found on these samples. EDS mapping results for sample #2 are shown in Figure 96. Most oxidation and sulfurization were observed at area with the absence of Ti. From the element maps, it can also be observed that distribution of oxygen and sulfur are similar to that of iron and chromium. This is indication that the stainless steel substrate is more prone to oxidation and sulfurization as compared to the Ti coating. Presence of chromium and

oxygen indicates the diffusion of chromium to the surface of substrates forming chromium oxide layer. Similar elemental distribution was observed for other Ti metal coated samples.

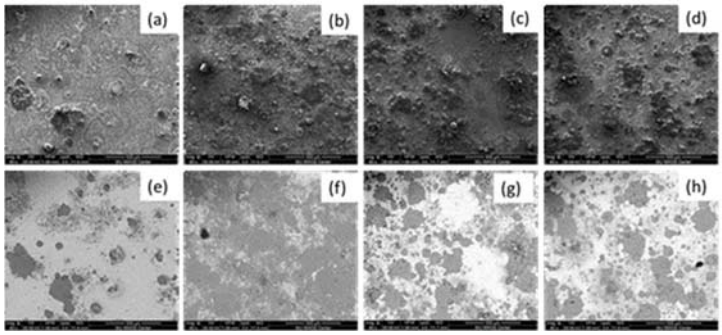

Figure 95 SEM images of sample (a)#1, (b)#2, (c)#3, and (d)#6 after 180 hrs simulated flue gas corrosion test at 650 ^{o}C, and corresponding backscattering images (e) to (h).

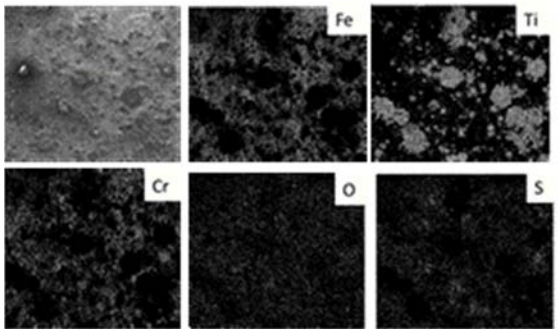

Figure 96 SEM and EDS mapping results of sample #2 after 180 hrs simulated flue gas corrosion test at 650^{o}C

SEM images of samples #4, #5, and #7 to #9 are shown in Figure 96 (a) to (e). Corresponding SEM backscattering images of the samples are shown in Figure 96 (f) to (j). For sample #4 and #5, where substrates were coated with TiC with 32wt% of carbon, sulfurization was localized on smaller areas compared to Ti coated samples. Areas with higher amount of sulfur can be seen as darker area around TiC coating in the backscattering images. Cracks of on the substrates due to intergranular corrosion were observed mostly around the edge of the TiC coating. No sign of oxidation or sulfurization was observed for the TiC coating. Similar surface morphology was observed on surface of sample #7, while sulfurization seemed to be slightly more concentrated around the TiB_2 coating areas. Localized sulfurization and oxidation around coating particles were also observed for substrates coated with TiC with 33wt% of carbon, sample #8 and #9. However, a more pronounced grain growth of the TiC coating was observed (Figure 97 (a) and (b)). Note that grain growth at the center of the coating seemed to be more pronounced as larger grains can be observed closer to the center of the coating.

Compared to the Ti coated substrate, extensive oxidation and sulfurization was observed on the pristine 304 stainless steel substrate after corrosion test. Figure 98 shows (a)SEM, (b)backscattering, and EDS mappings for the pristine 304 stainless steel substrate after corrosion test. Corrosion pits could be found throughout the surface of the uncoated substrate according to the SEM image of the sample shown in Figure 99(a). Other than that, backscattering image indicates that most of the surface of the sample is covered by sulfur, except small area surrounding sulfur islands. The small area mentioned appeared to be brighter in color in backscattering image, which indicated the areas should be iron from the substrate.

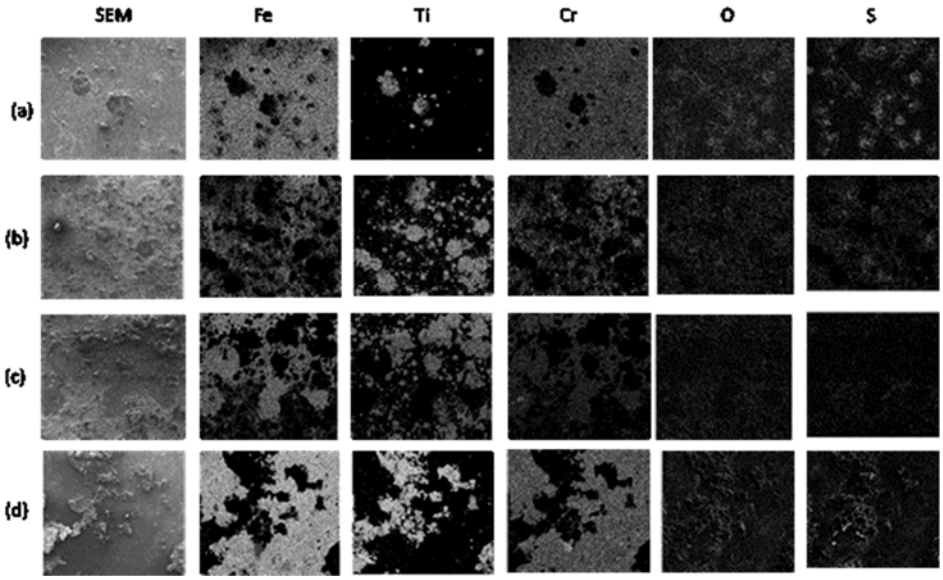

Figure 97 SEM and corresponding EDS results of sample (a)#4, (b)#5, (c)#8, and (d)#9 after 180 hrs simulated flue gas corrosion test at 650°C

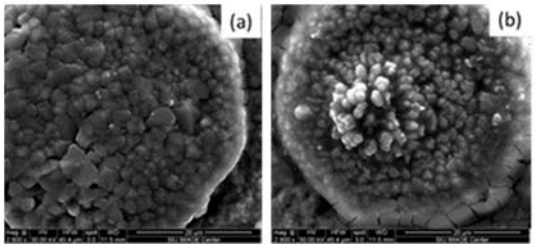

Figure 98 SEM images of TiC coating on stainless steel substrate of (a) sample #8, and (b) sample #9

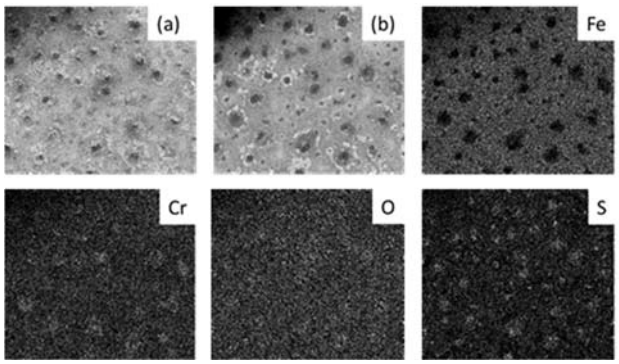

Figure 99 (a)SEM (b) backscattering, and EDS mappings for sample #10 (uncoated sample) after 180 hrs simulated flue gas corrosion test at 650°C

180 hr simulated flue gas corrosion test at700 °C for Ti coated 304H stainless steels

Additional corrosion tests were conducted for Ti coated 304 stainless steel samples as well as pristine 304 substrates under simulated flue gas condition at 700°C for 180 hrs. SEM images and EDS results of the Ti metal coated samples after corrosion test (#1-#3, #6) are a shown in Figure 100 (a) to (d), and (e) to (h) respectively. Small oxidation grains were observed throughout the surfaces of the Ti metal coated samples where substrate was not coated with Ti coating. Spallation of oxidation scale was observed on sample #2 and #6. Additionally, flakes were observed on surface of sample #1 where Ti coating was not present. The flake structures were later confirmed as iron oxide flakes by EDS results. SEM and EDS results of the iron oxide flakes are shown in Figure 101 (a) and (b). Note the additional layered structure in between the iron oxide flakes and the substrate matrix. By combining backscattering result and EDS results, it is suspected that the additional layer is also composed of iron oxide.

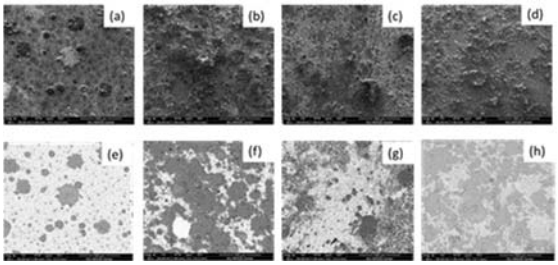

Figure 100SEM images of sample (a)#1, (b)#2, (c)#3, and (d)#6 after 180 hrs simulated flue gas corrosion test at 700^{o}C, and corresponding backscattering images (e) to (h).

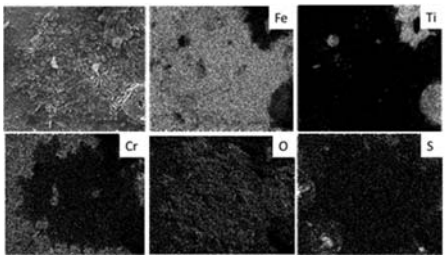

Figure 101 (a) SEM image and (b) EDS results of iron oxide flakes on sample #1.

SEM images of samples #4, #5, and #7 to #9 are shown in Figure 64 (a) to (e). Corresponding SEM backscattering images of the samples are as shown in Figure 64 (f) to (j). Compared to Ti metal coated samples, surface of samples coated with TiC (32wt% Carbon) and TiB_2 nanopowders are considerably smoother. No significant oxidation/ corrosion pattern or spallation of oxidation scales were observed on surface of sample #4, #5, and #7. Considerable amount of sulfurization and oxidation grains were observed on surface of sample #8. Corrosion islands were found on surface of sample #9, which seemed to be spalling off from the surface of the substrate. EDS results for sample #9 are shown in Figure 102. Note that Sulfur and oxygen amount is significantly lower at Ti coating area. SEM and EDS results of the pristine 304 stainless steel after being tested in simulated flue gas condition at 700^{0}C are shown in Figure 103. The SEM image shows that significant corrosion had occurred on the surface of the 304H stainless steel. Large oxidation and sulfurization grains were obviously seen, accompanied with corrosion pits and spallation of oxidation scales.

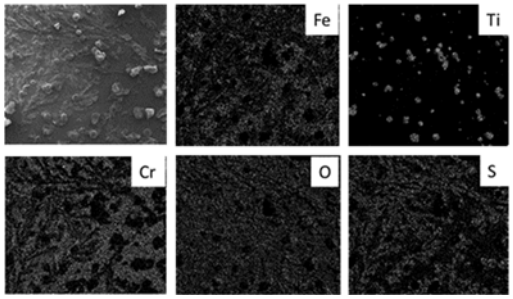

Figure 102. SEM and corresponding EDS results of sample #9 after 180 hrs simulated flue gas corrosion test.

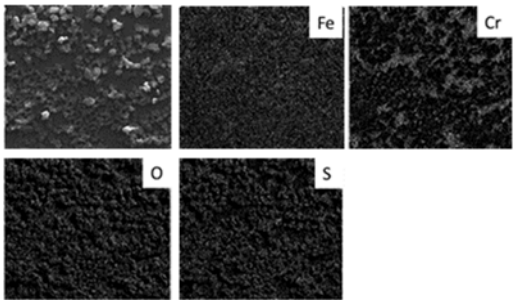

Figure 103. SEM and corresponding EDS results of uncoated sample after 180 hrs simulated flue gas corrosion test

Cross sectional SEM and EDS were conducted for the samples in order to study penetration of oxide scale or possible sulfurization. Cross sectional SEM images of sample #3, #5, #7, #9, and uncoated substrate after simulated flue gas corrosion test at 600^{0}C and 700^{0}C are as shown in Figure 65. Further examination of the cross section of sample was conducted with EDS analysis. For example, sign of oxidation/ sulfurization was observed at surface of the stainless steel substrate of sample #3 after 700^{0}C corrosion test according to cross sectional SEM image, as shown in Figure 104(a). EDS line scan result as shown in Figure 104(b) indicated high amount of oxygen (41.3 at%) at the surface along with small amount of sulfur (0.06 at%). However, Ti coating appeared to have stopped the oxidation and sulfurization from penetrating into the substrate, as no oxygen or sulfur was detected at the next EDS scan point.

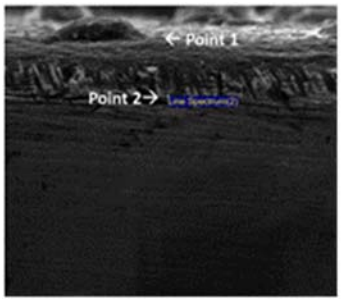

1

Element	Weight%	Atomic%
C K	39.46	52.72
O K	41.19	41.31
Si K	0.25	0.14
S K	0.12	0.06
Ti K	3.73	1.25
Cr K	6.18	1.91
Mn K	1.13	0.33
Fe K	7.94	2.28
Totals	100.00	

2

Element	Weight%	Atomic%
Si K	0.90	1.76
Cr K	18.90	19.93
Fe K	71.75	70.43
Ni K	8.45	7.89
Totals	100.00	

Figure 104. 103 (a)SEM and (b) EDS line scan result for sample #3 after 700^{o}C corrosion test

Grain growth on Ti coating at elevated temperature

During corrosion test with elevated thermal treatment, changes in morphology of the Ti coatings were observed. Figure 105 shows SEM images of the Ti coatings thermally treated at 650^{0}C and 700^{0}C at 2800 times magnification: (a) Sample #2, (b) sample #5, (c) sample #7, and (d) sample #9. For sample #2 and #5, increased length of grain can be easily observed. At 700^{0}C, a few longer grains sticking out from the coating particle was observed while the surface of the coating particle was still smooth at 650^{0}C. For sample #9, grains growth can already be observed at 650^{0}C, however, at 700^{0}C, larger overall grains were presented.

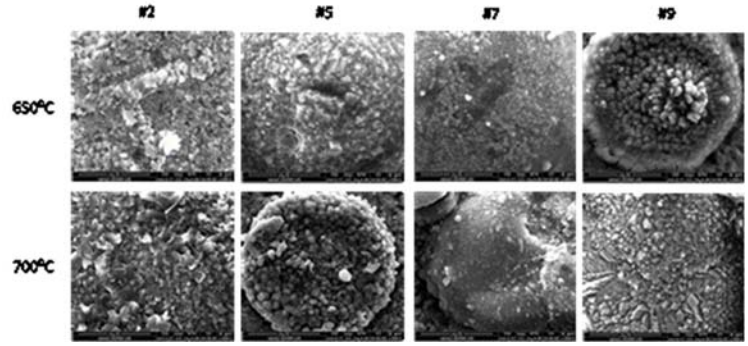

Figure 105. SEM images of titanium coatings on samples #2, #5, #7, and #9 at 650 ^{o}C and 700 ^{o}C at 2800X magnification.

CORROSION STUDIES

430 Ferritic Steel

Summary Findings

The effect of the coatings in terms of affording corrosion resistance during exposure to 750 ^{o}C air was similar to that of 304H. Figure 106 contains optical and electron microscopy images of the samples with different coating exposed to the high temperature air. The three samples looked darker after 180 hrs of air corrosion test, however, no sign of cracking or peeling of coating and no obvious oxidation pattern were observed. Further SEM secondary and back-scattering imaging analysis also showed no significant sign of oxidation. In addition, no significant change in surface morphology of coatings was observed for TiC coated substrates. Porous Ti structures found on TiB_2 coated sample were found to have decrease in area after 180 hrs of air corrosion test. However, from the back-scattering images, no sign of chromium or manganese precipitation was observed for these sample compared to the original samples before air corrosion test. Ti metal coated samples exhibited grain coarsening and is not further discussed in the summary.

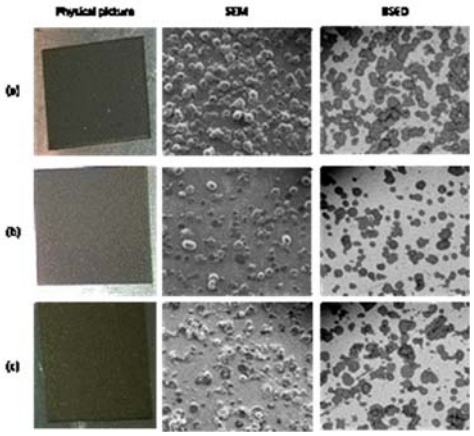

Figure 106. Physical picture, SEM and BSED images 430 ferritic steels coated with (a) TiC synthesized at 1400^{o}C, (b) TiC synthesized at 1500^{o}C, and (c) TiB2 after 180 hrs air corrosion test at 750^{o}C.

The cross section of post corrosion substrates for sample coated with (a) TiC synthesized at 1400^{0}C, (b) TiC synthesized at 1500^{0}C (c) TiB_2 were analyzed by SEM and EDS (Figure 107). The results were very similar to that obtained with coatings on 304H (Figure 61). Ti coating can be observed on the surfaces of 430 steel substrates. In addition, from the oxygen maps, a clear boundary of oxygen content variation between surface and cross section of the samples, and no significant sign of oxygen penetration was observed. The major difference between the 304H and 430 substrates exposed to 750 ^{o}C air was that in the case of 430, the Ti coating was better for the TiC prepared at 1400 ^{o}C with 32 %C coated TiO_2 and as a result, the Cr and O do not overlap while they overlap for the TiC prepared at 1500 ^{o}C with 35 %C coated TiO_2. In the case of 304H the reverse was true. Nonetheless, it appears that the TiC coatings performed better than TiB_2 coatings in terms of oxygen penetration (Figure 107(c)). Elemental composition as a function of depth was evaluated for substrate coated with TiC synthesized at 1400^{0}C using line scan EDS. Results are as shown in Figure 108. High Ti composition was observed at Ti coated areas as well as higher amount of oxygen. As the analysis was conducted deeper into the 430 steel substrate,

rapid decrease in oxygen amount can be observed which is an indication of low oxygen penetration.

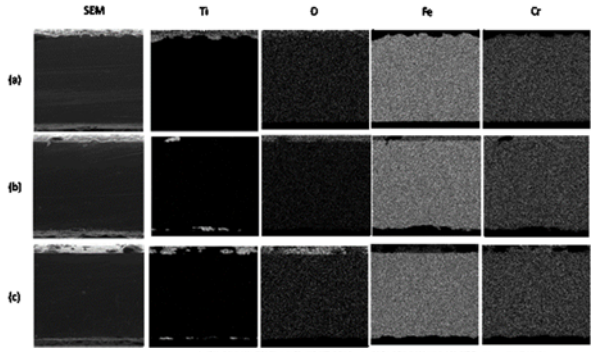

Figure 107. Cross section SEM and elemental maps for 430 ferritic steels coated with (a) TiC synthesized at 1400°C, (b) TiC synthesized at 1500°C, and (c) TiB2 after 180 hrs air corrosion test at 750°C.

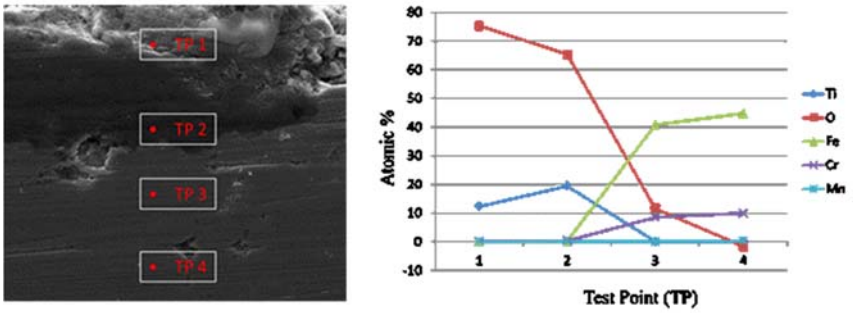

Figure 108. Elemental composition for Ti coated 430 ferritic steel coated with TiC synthesized at 1400°C after 180 hr air corrosion test.

No simulated ash corrosion studies were conducted but in depth simulated flue gas studies were conducted on the various 430 substrates. Figure 109 optical images of these substrates-coated and uncoated. In Figure 109(a), even coatings can be observed on the coated substrates, and a smooth surface morphology was also observed on the pristine 430 steel sample. Figure 109(b) shows the picture of substrates after 180 hrs of simulated flue gas test at 750°C. Change in color on the substrates were observed. Surface roughening was also observed for the substrates. Significant surface darkening was observed on the 430 substrate without coating. Additional surface morphology change was observed on substrates after 800 hrs of testing, as shown in Figure 109(c). Spallation was observed on the 430 substrate without coating.

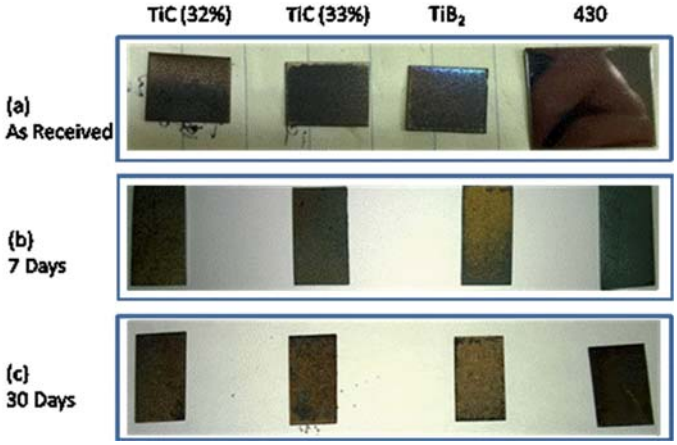

Figure 109. Pictures of 430 steel substrates and coated 430 steel substrates (a) as-received, and substrates after (b) 180 hrs (7 days) and (c) 800 hrs (30 days) of simulated corrosion test at 750°C.

Figure 110(a) to (d) are EDS maps for the various substrates exposed to 180 hrs of simulated flue gas at 750 ^{o}C. Below the top layer of Ti, a layered structure with higher concentration of chromium and oxygen, with minimal amount of manganese was observed at the interface between the coating materials and the 430 steel substrate. This is in agreement with our observations for the formation of chromium oxide layer in 304 H. It should be noted that the thickness of chromium oxide layer observed on the cross section of TiC (32%) coated substrate is significantly thinner than the layer observed on TiC (33%) and TiB_2, an indication of better protection since the Cr is not exposed to the oxygen penetrating the Ti layer. This may be a result of improved coating. Elemental distributions of iron, chromium, oxygen and manganese for the 430 substrate without coating were uniform throughout the analyzed area. A EDS mapping data was applied to plot the elemental concentration as a function of depth. Figure 111 shows the elemental distribution curves along with an inset indicating area and direction of scan for TiC (32%) coated substrate after 180 hrs of simulated flue gas test at 750^{0}C. Drastic decrease in amount of titanium and increase of iron can be observed in the figure, indicating the depth of the interface of the coating and the substrate from the surface of the coating. An oxygen peak as well as a chromium peak can also be observed at the interface, indicating the chromium oxide layer formed between the coating and the substrate. Elemental distribution curves were generated for all the substrates after 180 hrs of simulated flue gas test for comparison.

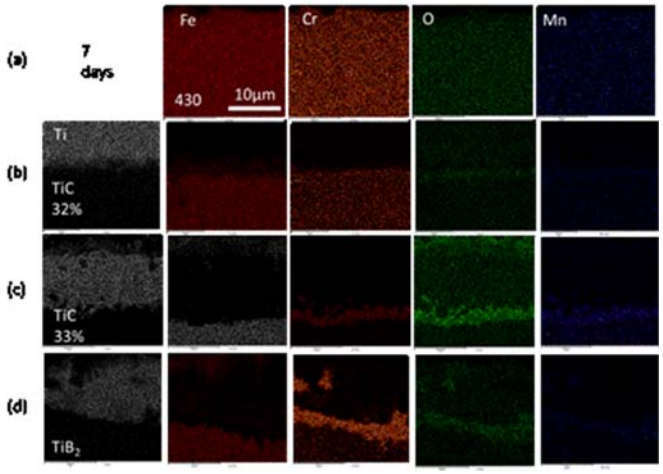

Figure 110. EDS mapping results for cross section of coated and pristine substrates after 180 hrs of simulated corrosion test at 750^{o}C.

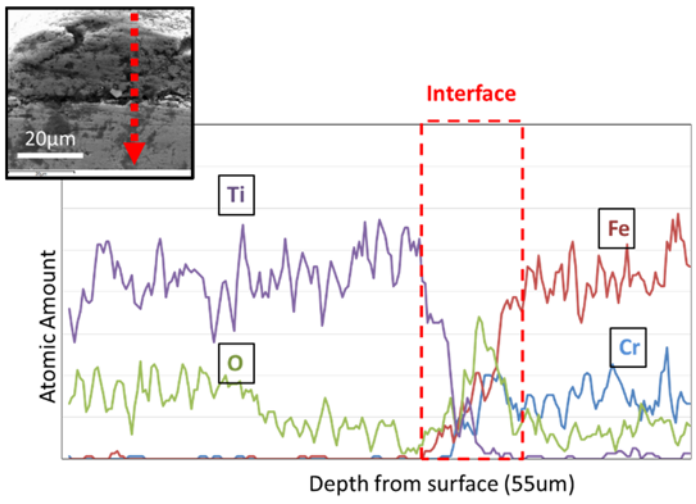

Figure 111. Elemental distribution curves for cross section of TiC (32%) coated substrates after 180 hrs of simulated corrosion test at 750^{o}C.

Figure 112 is a summarized SEM and surface distribution of the various elements present in the 430 steel along with the Ti on the surface of samples exposed to simulated flue gas for 800 hrs at 750 ^{o}C. Amount of oxygen was also found to be lower on the coated areas as compared to areas not coated with the coating materials. However, sulfur was found to present at areas with the presence of iron (Figure 113). Therefore, it was suspected that sulfur from the simulated flue gas environment had reacted with iron from the steel substrates.

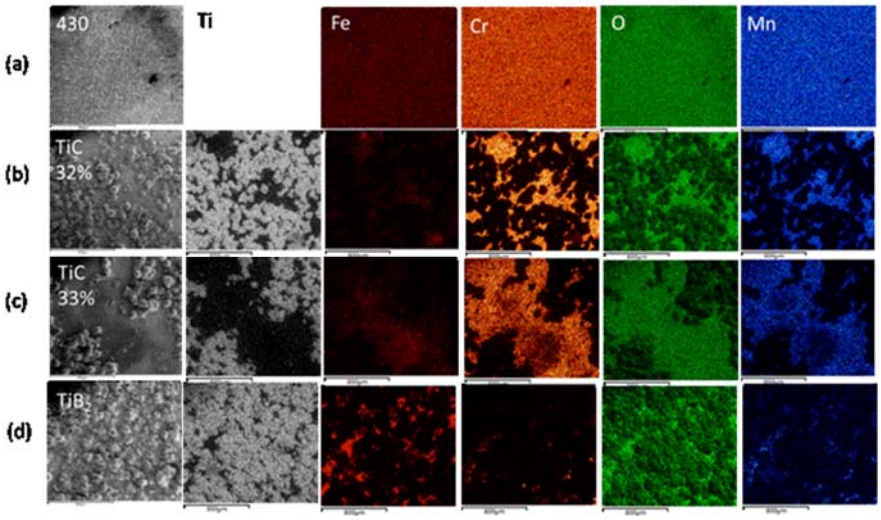

Figure 112. SEM images and EDS mapping results for (a) 430 substrate, (b) TiC (32%) coated, (c) TiC (33%) coated, and (d) TiB2 coated substrates after 800 hrs of simulated corrosion test at 750^{o}C.

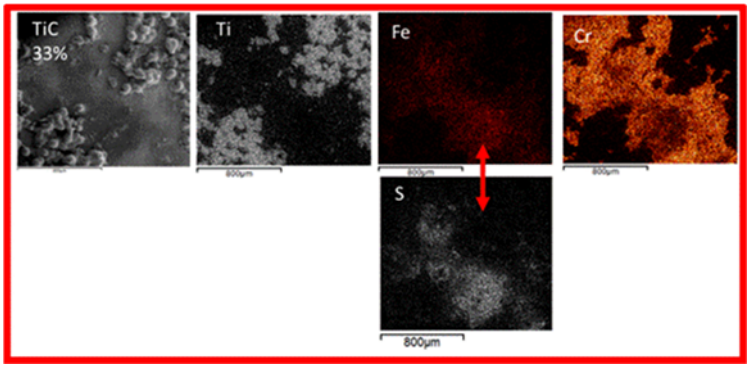

Figure 113. SEM and EDS mapping results for Ti, Fe, Cr, and S for TiC (33%) coated substrates after 800 hrs of simulated corrosion test at 750^{o}C.

Cross section analysis for substrates after 800 hrs of simulated flue gas test at 750^{0}C is shown in Figure 114. Clear distinction between distribution of titanium and iron can again be observed for the coated substrates. Presence of chromium oxide layer at the interface between the coating and substrate was further confirmed with the EDS mapping results for the coated substrates. However, compared with EDS analysis results after 180 hrs of corrosion test, a thicker layer of chromium oxide was observed, whereas the thickness of the chromium oxide decreased for the TiC (33%) and TiB_2 coated substrates. This change in thickness of the chromium oxide is believed to be related to evaporation of chromium oxide at prolong exposure to the testing environment (presence of water vapor). The oxygen concentration as a function of depth has also been evaluated for both 800 hr (Figure 115) and 180 hr (Figure 116) test substrates. Lower amount of oxygen can be observed at areas below the interface (zero by 45 µm depth) compared to areas above the interface

for the coated substrates (where oxygen peak was present). Amount of oxygen for the 430 substrate without coating was relatively uniformly distributed throughout the analyzed cross sectional area.

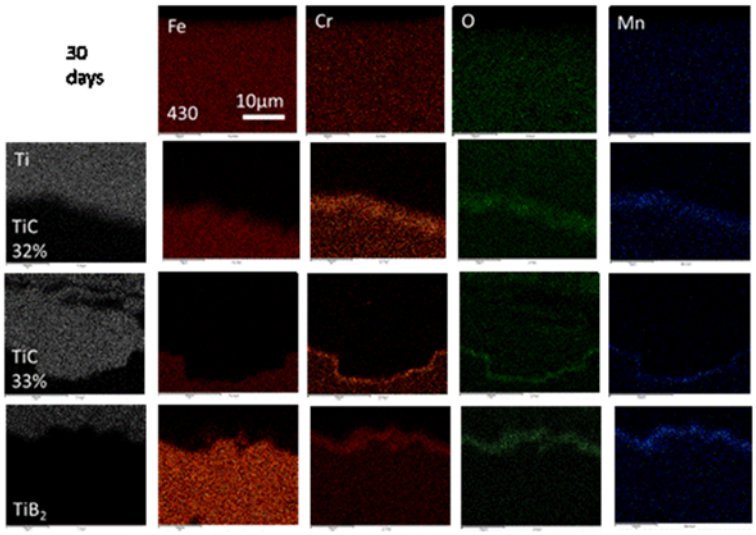

Figure 114. EDS mapping results for cross section of coated and pristine substrates after 800 hrs of simulated corrosion test at 750°C.

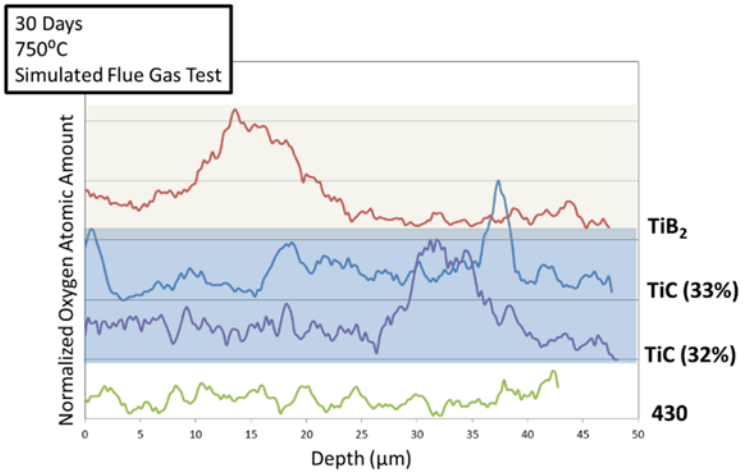

Figure 115. Oxygen distribution curves for cross section of coated substrates and pristine 430 stainless steel after 800 hrs (30 days) of simulated corrosion test at 750°C.

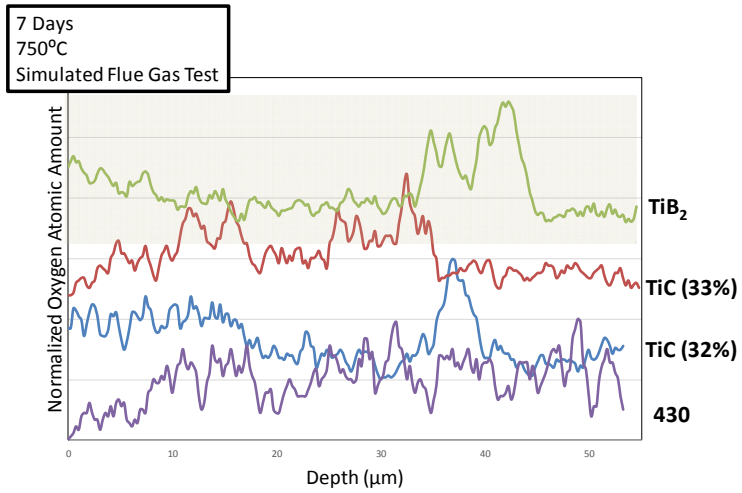

Figure 116. Oxygen distribution curves for cross section of coated substrates and pristine 430 stainless steel after 180 hrs (7 days) of simulated corrosion test at 750°C

The data clearly show that Ti based coatings are effective corrosion resistant coating although the HVOF process needs to be optimized further. The TiC coatings are performing better than the

TiB_2 coatings. The following figure provides a summary of the findings of the simulated flue gas corrosion studies on 430 ferritic steels. Additional data is discussed in the following sections.

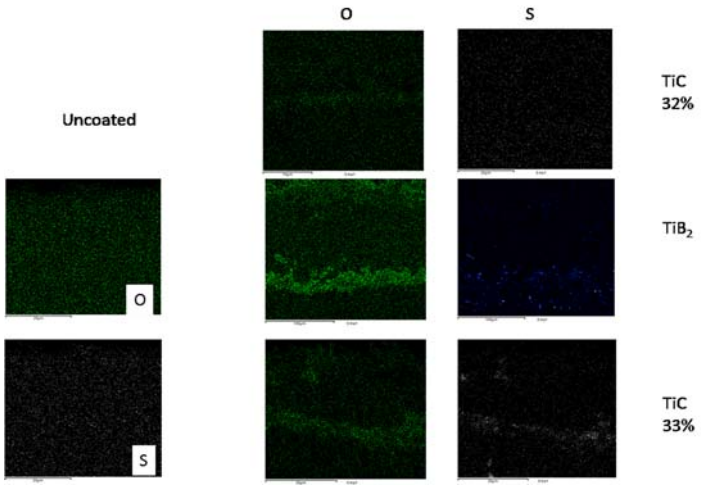

	750°C- 7 Days	750°C- 30 Days
TiC (32%)	Slight increase of O at interface of coating and substrate	Sulfur amount increased at area without coating
TiC (33%)	Layer composed of O and S observed at interface of coating and substrate	Significant less amount of oxygen and sulfur at coated area
TiB_2		small concentrated S spots
430	• Even distribution of Fe, Cr, Mn, O, and S. • Presence of Magnetite.	• Presence of Hematite and Cr_2O_3.

Air Corrosion

Impact of air corrosion on coated and uncoated substrates

The Ti coated (based on Table 6 parameters) stainless steel substrates and the 430 steel substrate were heat treated at 750^0C in air in order to study corrosion behavior/ resistance of the samples at high temperature environment. Table 3 contains the mass change (in %) of the substrates after 180 and 800 hrs of exposure to air at 750 ^{o}C. Physical photos of the samples #1-#10 after 180 hrs of air corrosion are shown in Figure 117. The data in Table 13 show that there is a loss of mass of the coated samples in the first 180 hrs. However, the mass loss is not observed on all the coated substrates after 800 hrs of exposure to high temperature air. In fact, all the samples except for the coating #8 show mass gain after the first 180 hrs. One of the reasons for this initial mass loss may be due to carbon particles on the coated substrates (SEM images). These carbon particles, presumably have their source in the hydrocarbon fuel during coating. The loss of this carbon during air oxidation may have led to this observed loss since a mass gain should have been observed. The uncoated 430 steel gained mass with time during exposure to high temperature air.

Table 13 Air Corrosion Studies – Mass Change

	Coating	Coating time (min)	200 hrs	800 hrs
1	Ti Metal	1	-0.033	-0.010
2	Ti Metal	3	-0.030	0.020
3	Ti Metal	5	-0.110	-0.079
4	TiC from 32 % C coated TiO_2 at 1400 ^oC	5	-0.057	-0.022
5	TiC from 32 % C coated TiO_2 at 1400 ^oC	10	-0.038	0.021
6	Ti Metal	10	-0.047	0.011
7	TiB_2	8	-0.081	-0.054
8	TiC from 33 % C coated TiO_2 at 1500 ^oC	6.5	-0.017	-0.067
9	TiC from 33 % C coated TiO_2 at 1500 ^oC	10	-0.026	0.006
10 (430)	uncoated	-	0.016	0.017

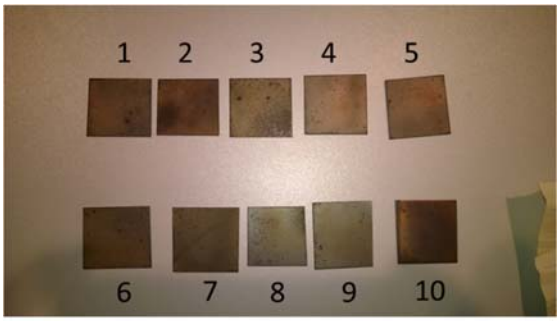

Figure 117. Physical photo of samples #1-#10 after 180 hrs of air corrosion test at 750^oC.

For samples coated from Ti metal as source material, grain coarsening was observed on the titanium coating from the SEM image shown in Figure 118 (a) for sample #1 (Ti metal coated for 1 min), and (b) for sample #3 (Ti metal coated for 5 min). Moreover, larger crystals with rectangular shape were also observed from Figure 118(b). Also noteworthy is that, small particles of iron oxide were presented on the substrate at area without Ti coating. However, no sign of significant oxidation pattern was observed.

EDS analysis was conducted to study the composition of the rectangular grain structure found on Ti coating of sample #3 (Ti metal coated for 5 min), and the result is as shown in Figure 119. According to EDS the grain structures are composed of mainly titanium. However, carbon content is higher where the rectangular structures are present compared to the rest of the Ti coating.

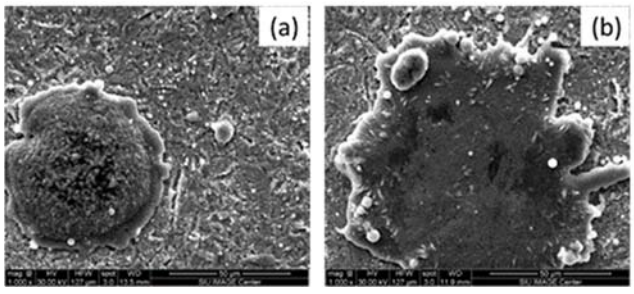

Figure 118. SEM image of surface of Ti coated sample with Ti metal as source material: (a) sample #1 (Ti metal coated for 1 min), and (b) sample #3 (Ti metal coated for 5 min)

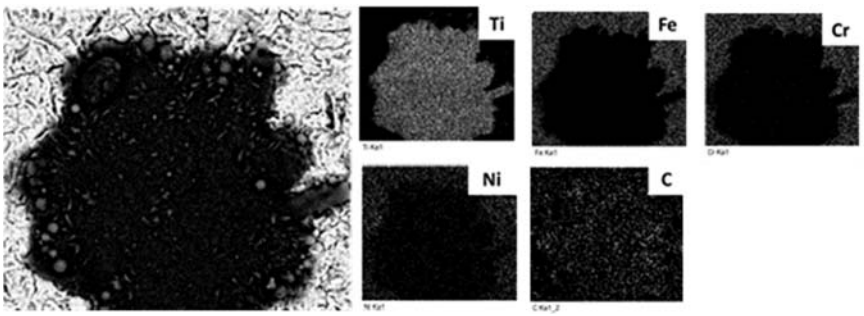

Figure 119. EDS mapping result with regards to Ti, Fe, Cr, Mn, and Ni for Ti coated sample coated with Ti metal by HVOF method for 5 minutes after 180 hrs of air corrosion test.

SEM images of the TiC coated samples are shown in Figure 120. No significant oxidation pattern was found on any of the coated samples compared to the uncoated 304H substrate. However, back-scattering images (BSED) showed presence of different phases at specific areas especially where Ti coating is less populated. EDS results confirmed that the newly formed phase are rich in Cr and O element, indicating the formation of chromium oxide, as shown in Figure 121. Finally, the uncoated 430 steel after 180 hrs of air corrosion test at 750^{0}C was also analyzed with SEM and EDS. Clear oxidation pattern can be observed on the surface of the 430 steel (Figure 122).

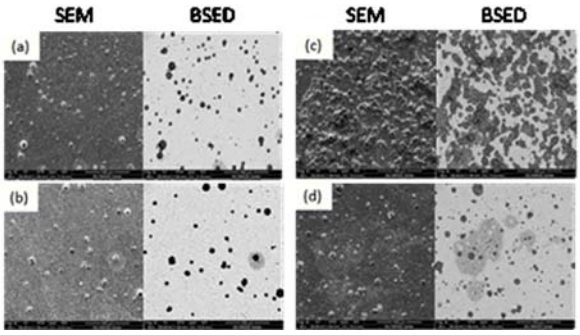

Figure 120. SEM/ BSED images of Ti coated samples with TiC as source material after 180 hrs of air corrosion test: (a) sample #3, (b) sample #4, (c) sample #8 and (d) sample #9.

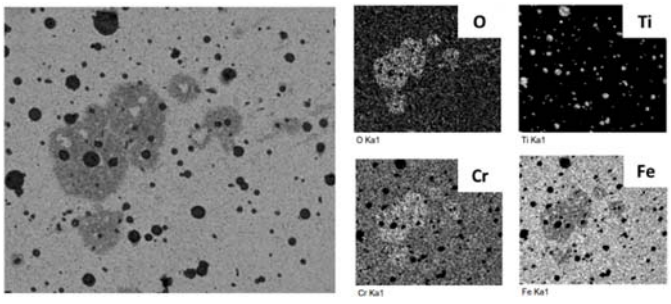

Figure 121. EDS result Ti coated samples coated by HVOF using TiC powders as source material after 180 hrs of air corrosion test: Sample #9.

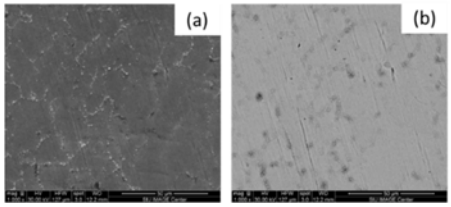

Figure 122. (a) SEM image and (b) Back-scattering SEM image of 430 stainless steel after 180 hrs of air corrosion test at 750^{o}C.

Air corrosion tests were then conducted on the coatings described in Table 7. Weight changes of the Ti coated samples were recorded before and after 180 hrs of air corrosion test (Table 14).

0.32% and 0.04% weight gain was observed for substrates coated with TiC nanopowders synthesized at 1400^{0}C and 1500^{0}C, respectively. 0.41% of weight loss was observed for substrate coated with TiB_2.

Table 14. Weight information of Ti coated 430 stainless steels before and after 180 hrs air corrosion test at 750^{0}C

	TiC1400	TiC1500	TiB2
	Weight (g)		
Gain	0.0036	0.0005	-0.0053
Gain Percentage	0.32%	0.04%	-0.41%

Figure 106 shows the physical picture (first column), SEM secondary images (second column), and back-scattering (third column) images of Ti coated substrates after 180 hrs of air corrosion test for substrates coated with (a)TiC synthesized at 1400^{0}C (b)TiC synthesized at 1500^{0}C, and (c)TiB_2. Cross sectional SEM and EDS mapping results of the three samples are shown in Figure 107 for sample coated with (a) TiC synthesized at 1400^{0}C, (b) TiC synthesized at 1500^{0}C (c) TiB_2. Ti coating can be observed on the surfaces of 430 steel substrates. Elemental composition depth profile was created for substrate coated with TiC synthesized at 1400^{0}C using line scan EDS (Figure 108).

Simulated Flue Gas Corrosion

Simulated flue gas corrosion studies were conducted for temperatures up to 750^{o}C. Figure 109(a) to (c) show the pictures of the as received 430 substrates before and after simulated flue gas corrosion test at 750^{0}C. Surface morphology of the substrates were also analyzed using SEM and EDS. Figure 123 (a) to (d) show the SEM and EDS maps with regards to titanium, iron, chromium, oxygen and manganese for substrates after 180 hrs of simulated flue gas test at 750^{0}C. For the coated substrates, distribution of titanium could be observed on the surface of the coated substrates according to Ti maps. Presence of Fe, Cr, O, and Mn were observed at areas not covered by titanium based coating. It was also observed that amount of oxygen is significantly lower on the Ti coated areas compared to areas without presence of titanium. Uniform distribution for most of the targeted elements were observed from the surface of 430 substrates without coating except chromium. Distribution of chromium was found to correlate to the surface morphology change observed from the SEM image of the substrate. After 180 hrs of exposure, no noticeable amount of sulfur deposition was observed on the surface for all 4 substrates tested. SEM and EDS mapping result for substrates after 800 hrs of simulated flue gas test at 750^{0}C are shown in Figure 112(a) to (d). Similar distribution of elements for titanium, iron, chromium, and manganese were observed on the surface of the coated substrates. As expected, the oxygen content was also found to be lower on the coated areas compared to areas not coated with the coating materials. However, sulfur was found to present at areas with the presence of iron (Figure 113). Therefore, it was suspected that sulfur from the simulated flue gas environment had reacted with iron from the steel substrates.

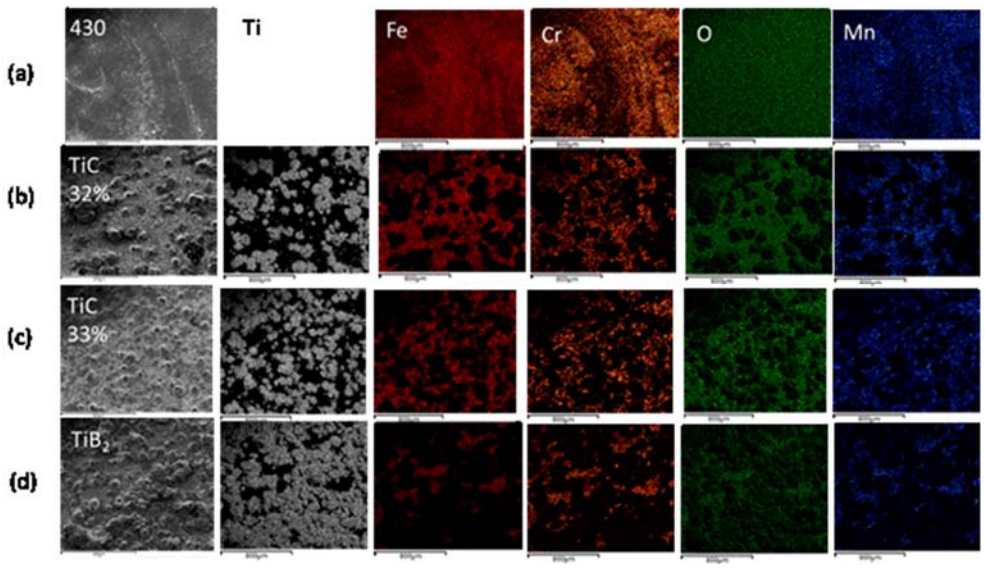

Figure 123. SEM images and EDS mapping results for (a) 430 substrate, (b) TiC (32%) coated, (c) TiC (33%) coated, and (d) TiB2 coated substrates after 180 hrs of simulated corrosion test at 750^{o}C.

Other than surface morphology analysis, SEM and EDS analysis were also performed along the cross section of the substrates. Figure 124 shows the (a) secondary electron and (b) backscattering electron SEM images for substrates after 180 hrs of simulated flue gas test at 750^{0}C. From the backscattering images of the coated samples, a layer with color lighter than the Ti coating, but darker than the substrate could be observed at the interface of the coating and the substrate. Considering the oxidation behavior of 430 steel substrates and the theory of the generation of backscattering electron images, the observed layer is expected to be a layer of chromium oxide. On the other hand, for the 430 substrate, a uniform cross section was observed indicating either uniform corrosion or no corrosion of which the former holds after other analysis.

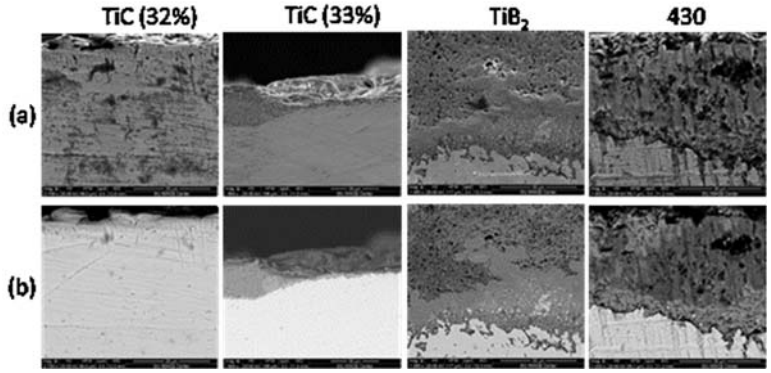

Figure 124. SEM (a) secondary electron and (b) backscattering electron images for cross section of coated and pristine substrates after 180 hrs of simulated corrosion test at 750^{o}C.

Figure 110(a) to (d) show the corresponding EDS maps for areas shown in Figure 118. For the coated substrates, distribution of titanium can be observed on the top of the stainless steel substrates. Figure 111 shows the elemental distribution curves along with an inset indicating area and direction of scan for TiC (32%) coated substrate after 180 hrs of simulated flue gas test at 750^{0}C. In order to further study, the oxidation behavior of the substrates, oxygen distribution of

the substrates was normalized and superimposed as shown in Figure 116. Lower amount of oxygen can be observed at areas beyond the interface compared to areas above the interface for the coated substrates (where oxygen peak was present). Amount of oxygen for the 430 substrate without coating was relatively uniformly distributed throughout the analyzed cross sectional area. Figure 125 shows the (a) secondary electron and (b) backscattering electron SEM images for substrates after 800 hrs of simulated flue gas test at 750^0C. Clear interface between the coating and substrates can be observed from both secondary electron and backscattering electron images for the coated substrates. Chromium oxide layers as observed from substrates after 180 hrs of testing were also observed from the coated substrates. In addition, EDS maps from the cross section analysis for substrates after 800 hrs of simulated flue gas test at 750^0C is shown in Figure 114. Clear distinction between distribution of titanium and iron can again be observed for the coated substrates. Presence of chromium oxide layer at the interface between the coating and substrate was further confirmed with the EDS mapping results for the coated substrates. Analysis result of the cross section of the 430 substrate without coating on the other hand, showed uniformly distributed iron, chromium, oxygen, and manganese throughout the tested areas. Oxygen distribution curves were also generated from the EDS mapping results for the substrates after 800 hrs of corrosion test, as shown in Figure 115.

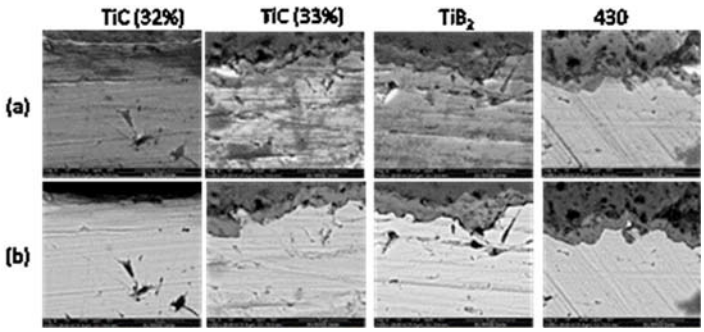

Figure 125. SEM (a) secondary electron and (b) backscattering electron images for cross section of coated and pristine substrates after 800 hrs of simulated corrosion test at 750^oC.

Other than electron microscopy analysis, X-ray diffraction analysis was also performed for the substrates. Figure 126 shows the XRD pattern for 430 substrates without coating before and after 180 and 800 hrs of corrosion tests. For the pristine 430 substrates, peaks for 430 steels were observed. After 180 hrs of testing, magnetite peaks were observed. This indicated the surface of 430 substrates being oxidized to Fe_3O_4 after being exposed at the corrosive environment simulated. Phase transformation of magnetite to hematite was observed for the 430 substrates after 800 hrs of testing. The phase transformation from Fe_3O_4 to Fe_2O_3 on the 430 substrate clearly indicates further oxidation of the substrates after prolong exposure to the corrosive environment. For the 430 peaks as well as the Cr_2O_3 peaks, as temperature increases, decrease in width and increase in height for the peaks could be observed. This indicates either an increase of particle size, or increase in crystallinity of the phases. On the other hand, it has been reported that it can be hard to distinguish between the XRD peaks for hematite and eskolaite (Cr_2O_3) due to the similarities in lattice parameters of the materials. XRD patterns for the TiC (32%) coated substrate before and after corrosion tests are shown in Figure 127. From the XRD pattern for the as-received TiC (32%) coated substrate, Ti_3O_5 peaks as well as TiC peaks were observed. After 180 hrs and 800 hrs of corrosion test, graduate transformation of Ti_3O_5 to TiO_2 (rutile) as well as decrease of TiC were observed. Rutile TiO_2 was reported as the most thermal dynamically stable form titanium oxide.

From the XRD patterns of the TiC (33%) coated substrates, as shown in Figure 128, similar results to the TiC (32%) coated substrates were observed- Ti_3O_5 and TiC peaks from the as-received substrates, and graduate transformation to rutile TiO_2 and decrease of TiC after 180 hrs and 800 hrs of corrosion test. XRD results for the TiB_2 coated substrates are as shown in Figure 129. TiB_2 peaks as well as Ti_3O_5 peaks were both observed from the as-received substrates. Similar phase transformation of Ti_3O_5 to TiO_2 was also observed for the TiB_2 coated substrate after 180 hrs of testing.

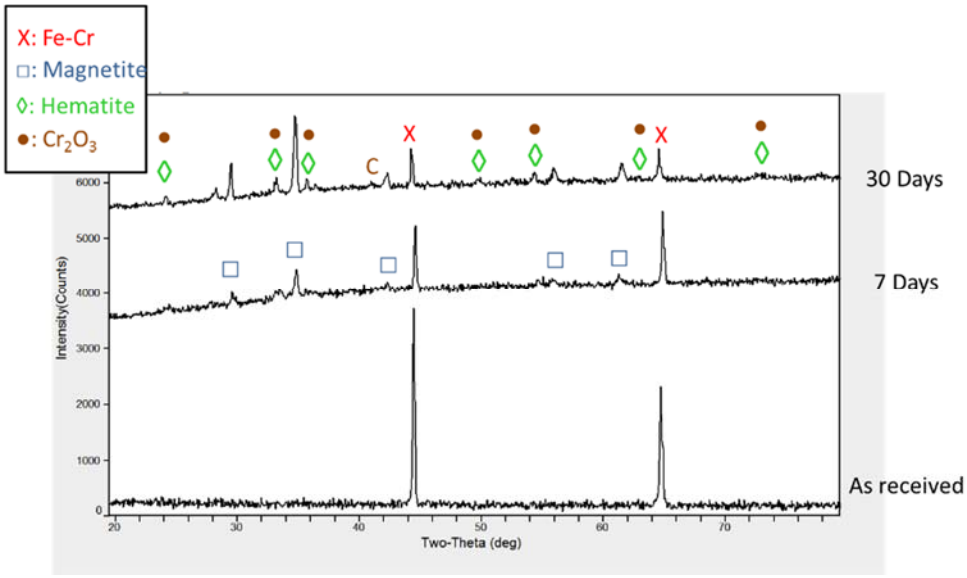

Figure 126. XRD pattern for pristine 430 stainless steels before and after 180 hrs (7 days) and 800 hrs (30 days) of simulated corrosion test at 750°C.

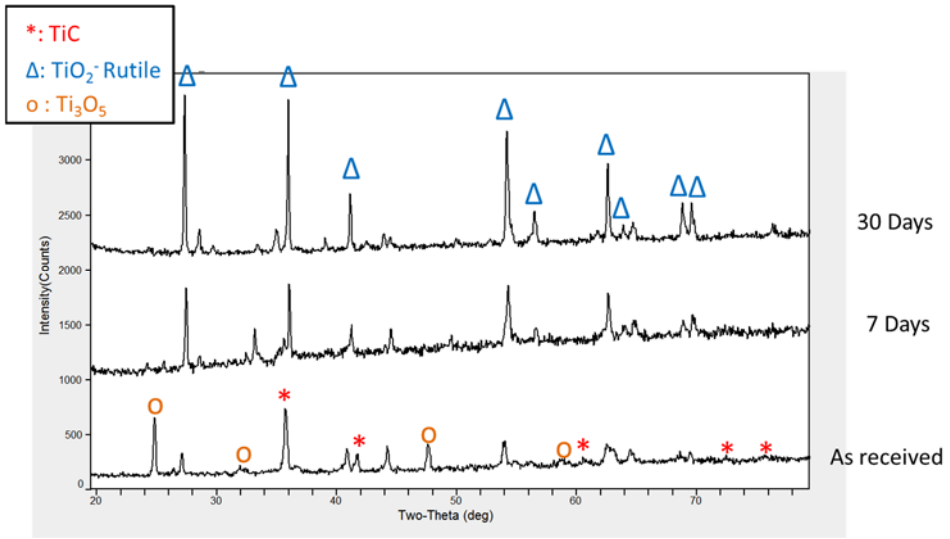

Figure 127. XRD pattern TiC (32%) coated substrates before and after 180 hrs (7 days) and 800 hrs (30 days) of simulated corrosion test at 750°C.

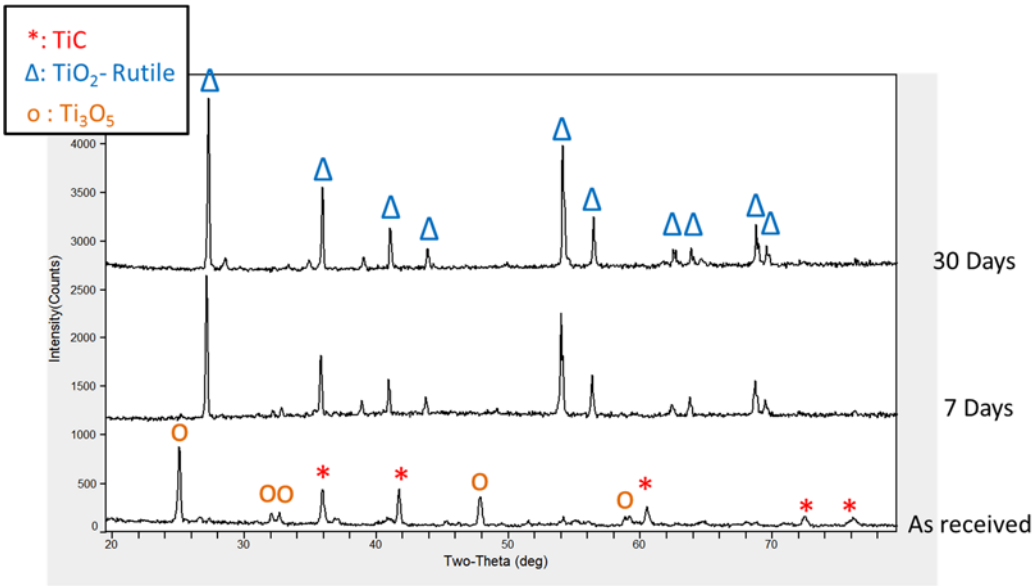

Figure 128. XRD pattern TiC (33%) coated substrates before and after 180 hrs (7 days) and 180 hrs (30 days) of simulated corrosion test at 750°C.

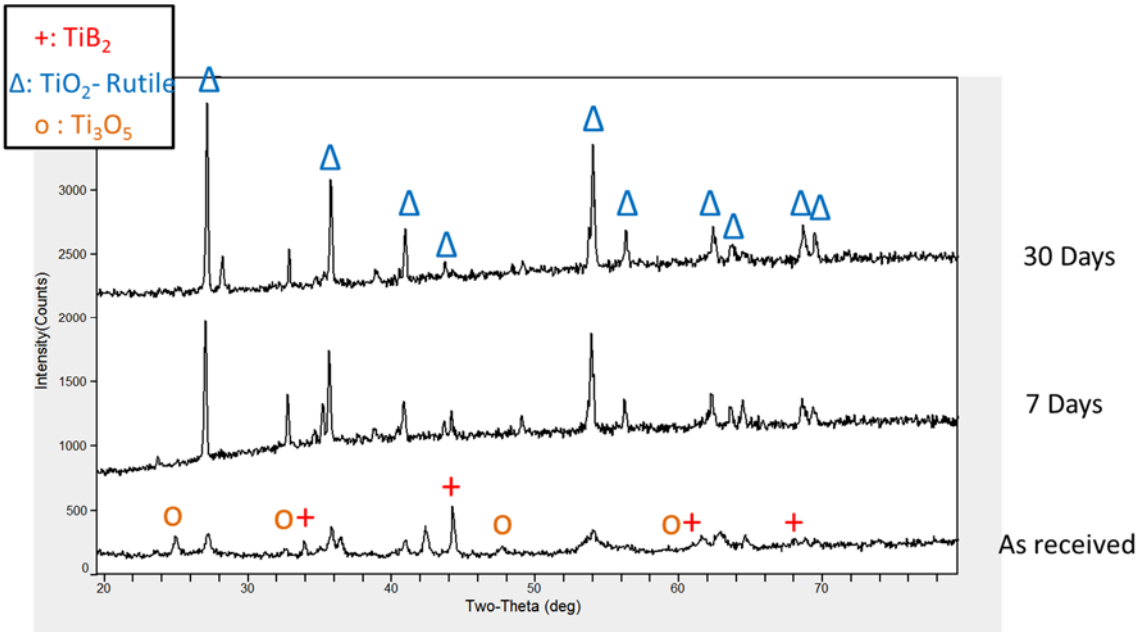

Figure 129. XRD pattern TiB2 coated substrates before and after 180 hrs (7 days) and 180 hrs (30 days)of simulated corrosion test at 750°C.

CORROSION STUDIES

P91

Summary Findings

Since the Ti based coatings afforded good corrosion resistance to both 304H (high Cr and high Ni content) and for 430(high Cr content) steels, it was decided to select a low Cr content steel instead of a high Ni content steel. Thus, P91 was chosen as the final substrate. In this study, in addition to air corrosion, simulated ash corrosion and simulated flue gas corrosion studies, an additional set of corrosion studies in the presence of steam and air were conducted.

Figure 130 and 131 compares the corrosion behavior of the 430 and P91 steels in simulated flue gas at 750 ºC, where Figure 130 is the surface analysis and Figure 131 is the cross sectional analysis. P91 clearly has a higher concentration of Oxygen along with iron. In addition, the surface deterioration is more evident on the P91 surface. The cross section analysis shows the presence of iron on the surface with Cr concentration increasing below the surface. It is important to note the differences in the scales used in Figure 131. It clearly shoes that the oxygen penetration is more severe and to a greater depth for the low Cr steel under these conditions. The surface spallation is more evident when viewed along the cross-section.

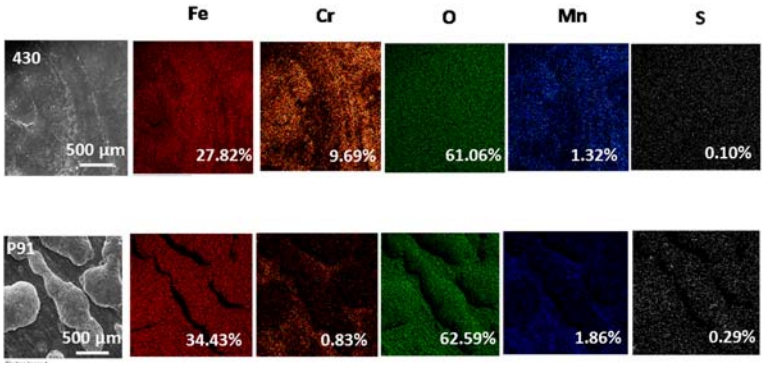

Figure 130. Elemental Distribution on the surface after 800 hrs of exposure to simulated flue gas at 750ºC.

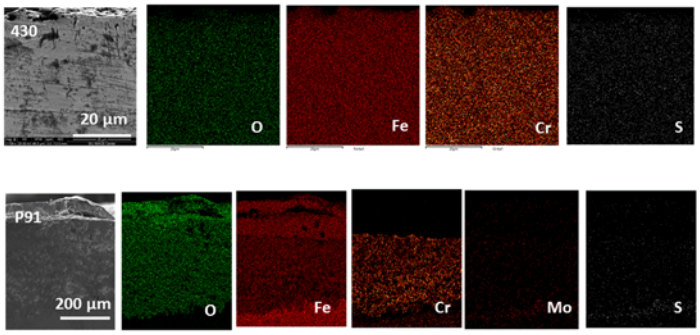

Figure 131. Elemental Distribution along the cross-section after 800 hrs of exposure to simulated flue gas at 750ºC.

Figure 132 quantifies the distribution of the elements along the cross section of the P91 substrate exposed to simulated flue gas at 75-0 ºC. The figure clearly shows that the top 45 µm is primarily composed of hematite followed by a dominant magnetite phase for the lower 90 µm with another 200µm consisting of magnetite and hematite to a total of 335µm oxygen penetration into the substrate.

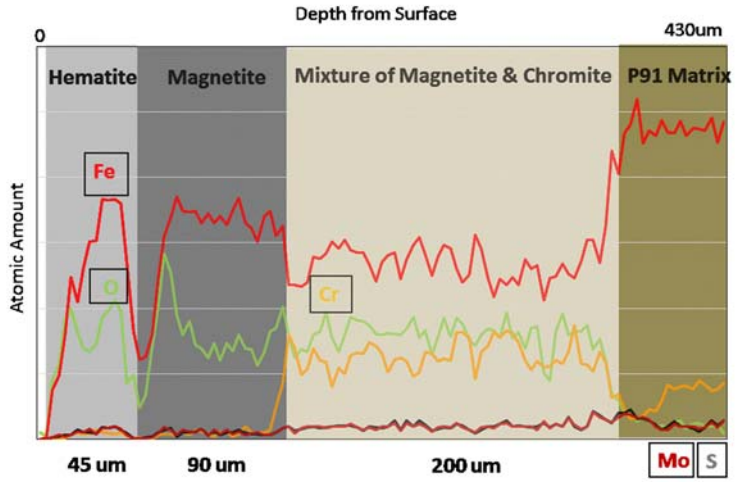

Figure 132. Elemental depth profile of the post corrosion test on uncoated P91 substrate exposed to 750 °C simulated flue gas for 800 hrs.

Figure 133 (top) shows the surface elemental distribution of the post exposure TiC coated P91. The uniformity of Ti coating clearly shows the benefits. No surface degradation is observed. In addition, the surface contains on 1.08 % Fe (indicating better coating parameters are required). Comparing Figure 131 with Figure 133 (bottom), the efficacy of corrosion resistance by the coatings is amply clear. The oxygen penetration is only 29 µm and the Cr oxide layer is only 5µm. Finally, iron does not exhibit duplex oxidation behavior as seen in the uncoated P91. Similar trends are observed in other coatings as well. Figure 134 further illustrates the stark difference in corrosion resistance due to the coating when compared to uncoated surface (Figure 132). Prior to discussing further results, it is important to note that dense uniform coating is necessary for enhanced corrosion protection and thus further studies is necessary to optimize the HVOF coating process. Figure 135 clearly demonstrates this fact. The dense coating does not allow O or S penetration into the substrate it is protecting

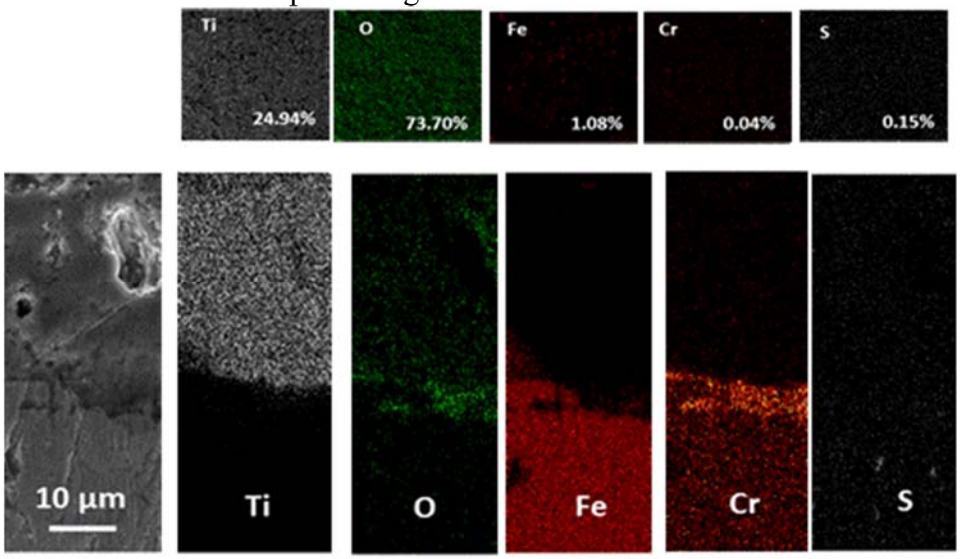

Figure 133. Analysis of post exposure TiC coated P91 – Simulated flue gas at 750 °C, 800 hrs. (Top) elemental distribution on the surface. (bottom) elemental distribution along the cross section.

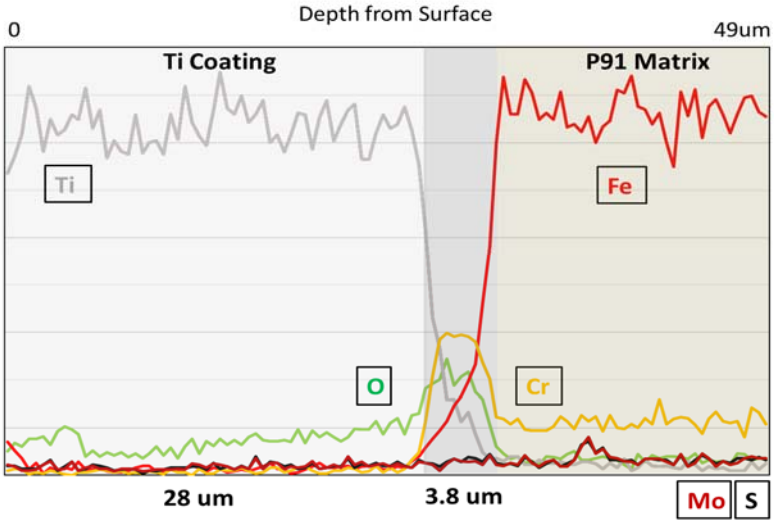

Figure 134. Figure 132. Elemental depth profile of the post corrosion test on TiC coated P91 substrate exposed to 750 ^{o}C simulated flue gas for 800 hrs.

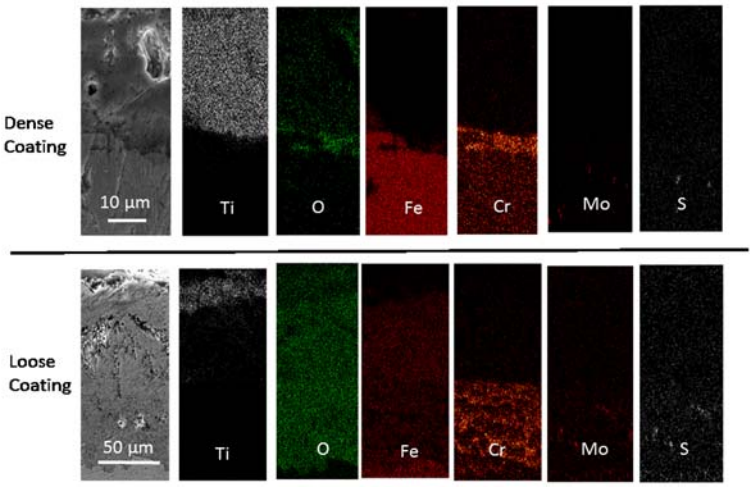

Figure 135. Comparison of corrosion in dense vs loose TiC coating. Coated P91 subjected to 800 hrs of simulated flue gas at 750 ^{o}C.

Having discussed the issue of the uniformity a complete coverage of the coating, the effect of exposure temperature on the corrosion is shown in Figure 136. Please note that the samples were not completely coated unfirmly and thus some of the data shown here may seem inconsistent with the data shown previously. It is seen in the figure that the extent of corrosion as determined by the oxygen penetration increases with temperature. In addition, it is observed that while the S prefers to bond with iron, it also bonds with the Cr. The S seems to penetrate the top surface and attempt to bond with the Fe below the Cr oxide layer and not with the surface Fe. This probably due to the oxidation of the iron sulfide if formed in this region. However, the care was taken such that the temperature comparison holds. In terms of the type of coating, TiC was found to perform better than TiB_2 coatings. However, Ti and TiC coating performed equally well as can be seen in Figure 137. However, the cost of Ti metal vs TiC produced by the carbo thermal process clearly shows the economic benefit of using TiC coatings.

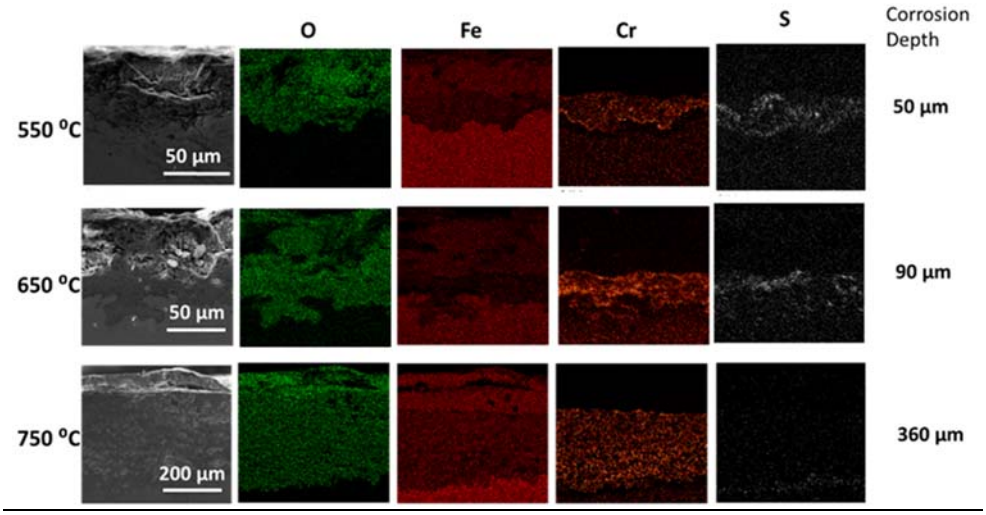

Figure 136. Effect of temperature on the corrosion of TiC coated flue gas in simulated flue gas

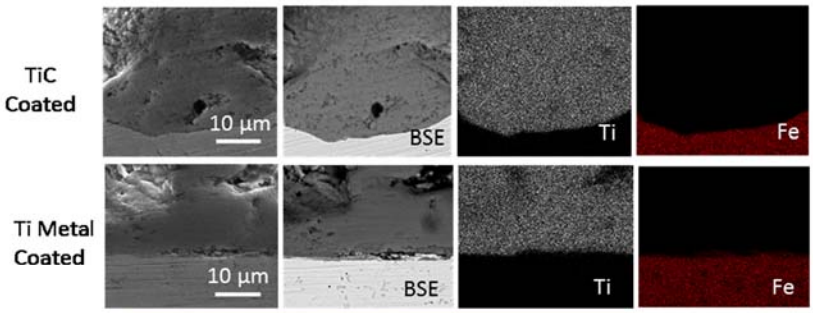

Nanoparticles	Particle Size	Price/ kg (Sigma Aldrich)
Ti Metal	<100 nm	$21,900
TiC commercial	<200 nm	$5,300
P-25 TiO_2	21 nm	$1,365
TiC synthesized	100 nm- 200 nm	

Figure 137. Comparison of corrosion resistance of TiC coated and Ti metal coated P91

Figure 138 compares the corrosion behavior of uncoated and TiC coated P91 substrates exposed to steam and air at 700 °C for 180 hrs. The effectiveness of TiC coating on retarding the progress of corrosion is clearly evident in the figure. The depth of oxygen penetration is significantly higher in the case of the uncoated P91 substrate. Figure 139 compare the oxidation prevention of the substrate in 700°C air due to the coating in comparison with the uncoated substrate. In spite of nearly identical thickness of the oxygen layer, the oxygen is primarily in the Ti layer for the coated substrate and the overall content is significantly lower than that of the uncoated substrate. Compared to pristine substrates tested in steam and air environment surface of the pristine P91 substrates after air oxidation test are considerably smoother. The large iron oxide observed on the surface of the pristine substrates after steam and air corrosion test was not observed on this batch of substrate. No significant surface scale formation was observed

The effectiveness of the Ti coatings in rendering corrosion protection in severe conditions existing in the boiler has been clearly demonstrated. However, it has also been noted that the uniformity

and completeness of the coating is equally important and thus it is necessary to understand and optimize the HVOF thermal spray coating. In order to gain a better understanding of the impact of coating parameters on the quality of coating and thus the corrosion resistivity, HVOF coating parameters shown in Table 8 was used. Two different flow rates for the N_2 carrier were utilized during this batch of substrate coating: Low (1.8 LPM), and High (3.6 LPM), while spraying distance remained the same at 27cm. Detailed conditions of the as-received substrates Two different coating materials were applied to the substrates: TiC (32% synthesized at 1500^0C for 2 hours), and Ti metal. Substrate A and E were control substrates with and without application of glass blasting. Substrates B, C, D, and F were coated on both sides of the substrates with different coating parameters such as coating durations, carrier flow rates, and whether or not the substrate was glass blasted.

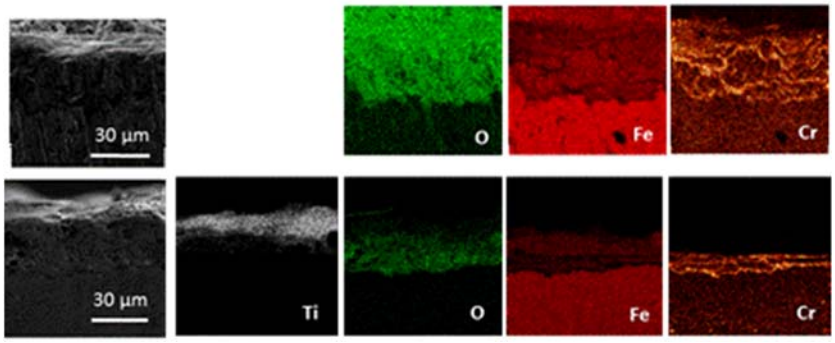

Figure 138. Comparison of corrosion between uncoated and TiC coated samples exposed to steam and air at 700 ^{o}C.

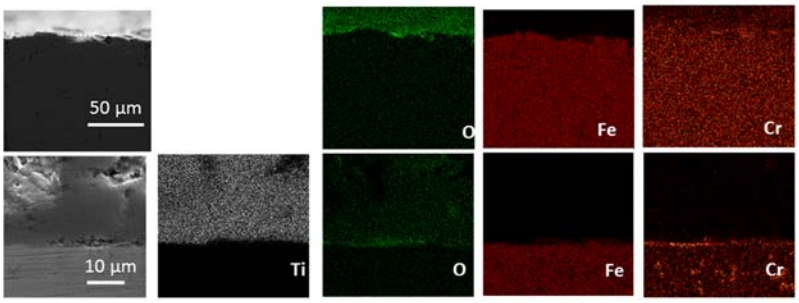

Figure 139. Comparison of corrosion between uncoated and TiC coated samples exposed to air at 700 ^{o}C.

Figure 140 compares the effect of coating time and flow rate on the as received P91 substrates on the ultimate corrosion resistance in simulated flue gas at 750 ^{o}C. Excellent corrosion resistance is provided by all the coatings although low N_2 and 12 minute coating appears to be the best. Figure 141 compares the effect of N_2 flow rate for 12 minutes on the performance in terms of corrosion resistance. Glass blasted substrate coated for two consecutive 12 minutes at high N2 flow provided the best resistance Finally, Figure 142 compares the performance of TiC and Ti metal coated at high and low N_2 flows for 3 and 12 minute, respectively. The performance of the two different coatings were very similar with the low N_2 flow but 12 minutes of coating was more effective than the alternate condition for both coating materials.

The following sections provide detailed analysis of the various tests conducted and the corrosion performance measured.

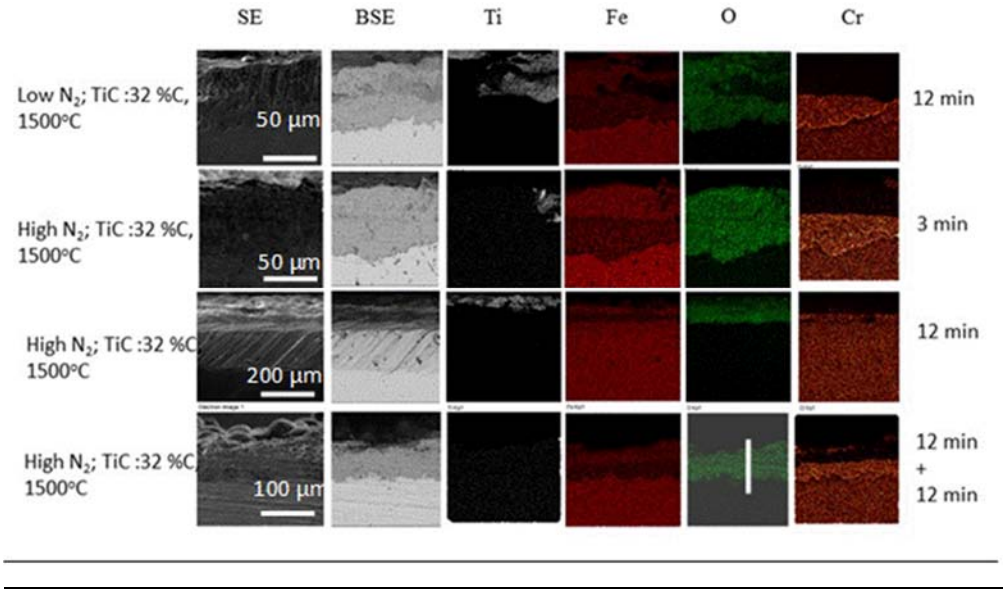

Figure 140. Effect of coating time and N_2 flow rate of corrosion resistance.

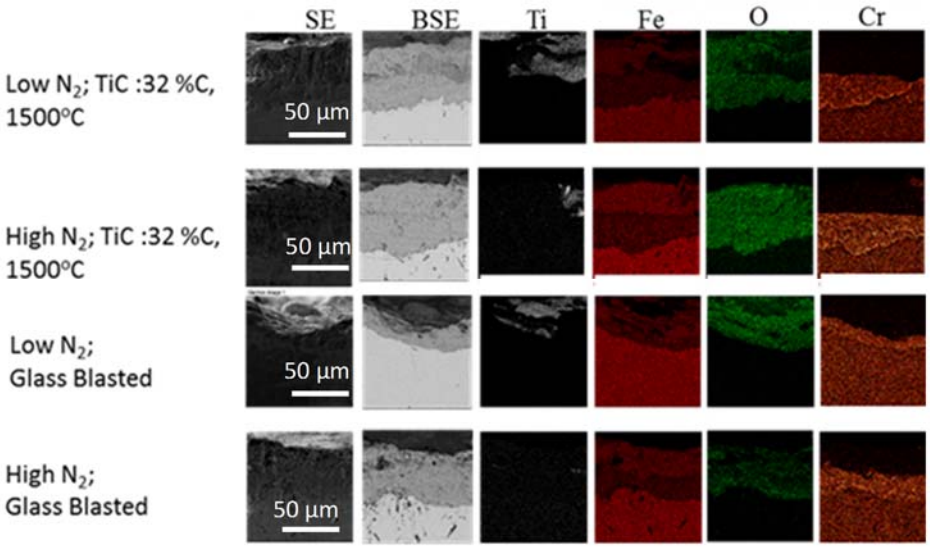

Figure 141. Effect of surface treatment and N2 flow rate of corrosion resistance.

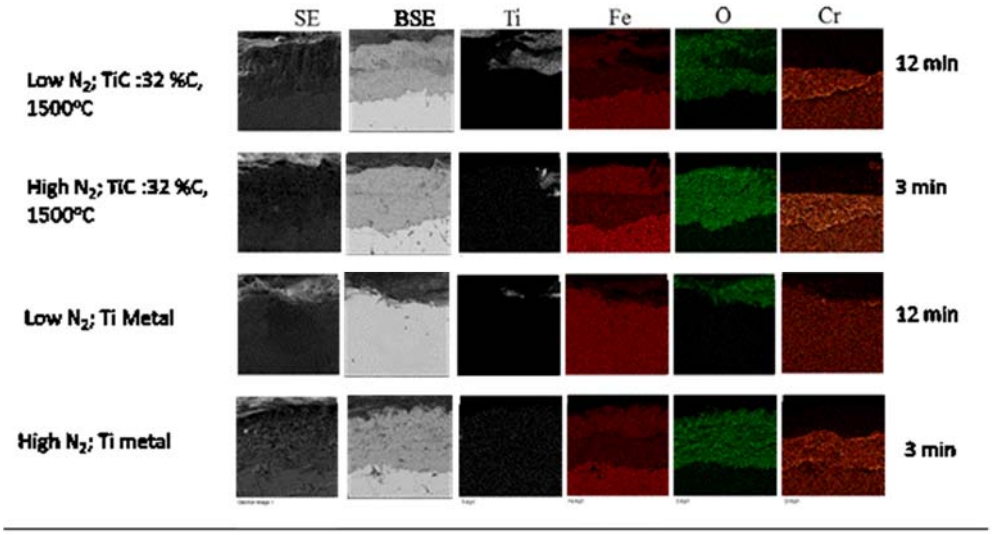

Figure 142. Effect of coating material, flow rate and coating time on the corrosion resistance.

Simulated Flue Gas Corrosion

Photos of the P91 substrates after 800 hrs of simulated flue gas corrosion test are as shown in Figure 143. All substrates showed changes in color and surface morphology compared to as-received substrates. Large bumps were observed on surface of part of the substrates, such as substrate A. Spallation of surface scale were also observed on substrates after corrosion test. For the simulated flue gas analysis, corrosion analysis at 700 °C is conducted first since the steam and air corrosion and oxidation resistance are conducted at 700 °C, followed by 750 °C and then 650 °C. Experiments were conducted at 550 and 650 C but are not discussed here for the sake of brevity.

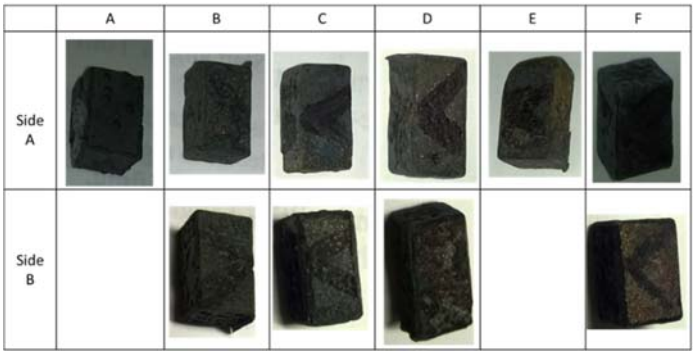

Figure 143. Photos of the P91 substrates after 800 hrs of simulated flue gas corrosion test.

Substrates A and E after 800 hrs simulated flue gas corrosion test at 700 °C

Figure 130 shows the SEM (a) secondary electron images and (b) back scattering electron images for substrates A, and E at low and high magnifications. Both substrates were not coated with Ti coatings. Heavy signs of corrosion were observed on surface of both substrates. Large iron oxide

particles (>25um) were observed on substrate whereas uniform distribution of iron oxide island structures were presented on surface of substrate E. At higher magnifications, surface consists of small iron oxide particles was observed from substrate A. On the surface of substrate E, extrusion of structures was observed, and later identified with EDS as consisting higher amount of oxygen compared to the matrix of the substrate.

Figure 144 shows the EDS mapping and quantitative elemental analysis results for substrate A after 800 hrs of simulated flue gas test. Uniform distribution of oxygen was observed throughout the surface of the substrate. Iron and chromium were also found uniformly distributed except only iron was observed on the large iron oxide particles. This may be indication of corrosion resistance from chromium oxide forming at locations consisted sufficient amount of chromium. Significant increase in amount of oxygen (23.43 at% to 55.33 at%) and decrease in iron (67.20 at% to 18.09 at%) were also observed according to the quantitative elemental analysis results.

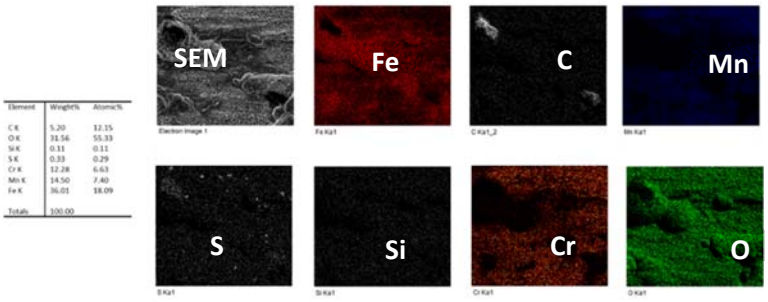

Figure 144. SEM image and corresponding EDS mapping results for substrate A after 800 hrs of simulated flue gas corrosion test at 700 °C.

EDS mapping results of the glass blasted substrate E, as shown in Figure 145 show that the extruded structures were iron and oxygen-rich structure. Quantitative elemental analysis results also showed high percentage of oxygen (50.77 at%) on the surface of the substrate after 800 hrs of simulated corrosion test.

Element	Weight%	Atomic%
C K	5.07	12.65
O K	27.09	50.77
Si K	0.19	0.20
P K	0.02	0.02
S K	0.12	0.12
Cr K	0.01	0.01
Mn K	0.07	0.04
Fe K	67.42	36.20
Totals	100.00	

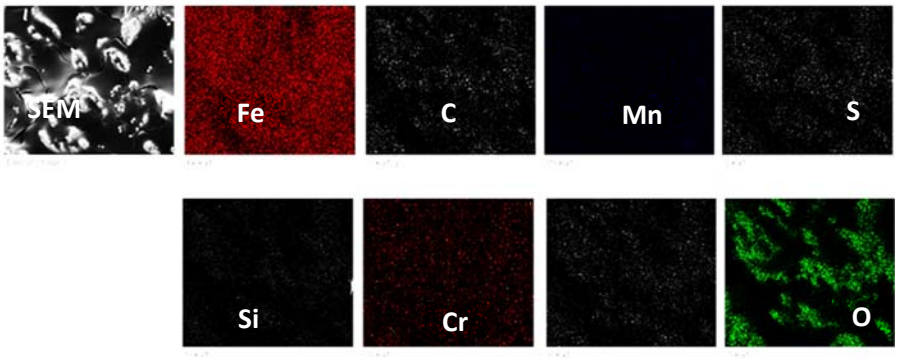

Figure 145. SEM image and corresponding EDS mapping results for substrate E after 800 hrs of simulated flue gas corrosion test at 700 °C.

Substrates B after 800 hrs simulated flue gas corrosion test at 700 °C

SEM secondary electron images and back scattering electron images for both sides of substrate B (B-A and B-B) are shown in Figure 146 (a) and (b). Side A of substrate B (B-A) was coated with TiC powders at low N_2 carrier flow for 12 minutes, and side B (B-B) was coated with high carrier flow for 3 munities. According to previous SEM analysis results on the as-received substrate B, a more uniform Ti coating was observed for side B of the substrate before corrosion test. Similar surface morphology can be observed after 800 hrs of simulated flue gas corrosion test, along with existence of large iron oxide particles (>100um in diameter) on both sides of the substrates.

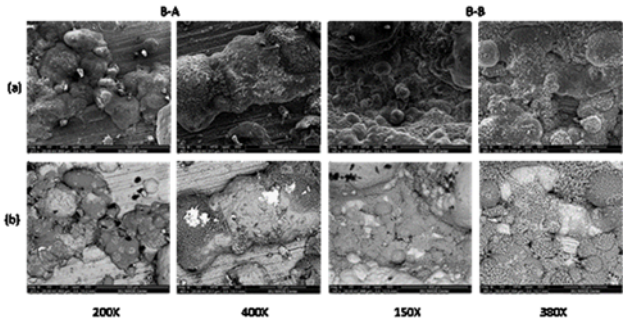

Figure 146 SEM (a)Secondary electron and (b)Backscattering electron images of both sides of substrate B (B-A and B-B) after 800 hrs of simulated flue gas corrosion test at 700 °C at low and high magnification.

EDS mapping and quantitative elemental analysis results for substrate B are shown in Figure 147 (a) side A, and (b) side B. It was observed that amount of iron, manganese, and chromium (side A) are significantly lower at areas covered by Ti coating. Amount of manganese and chromium were also found to be significantly lower on the iron oxide particles compared to substrate matrix. This may be indication of slower diffusion rate of manganese and chromium compared to iron under the corrosive condition.

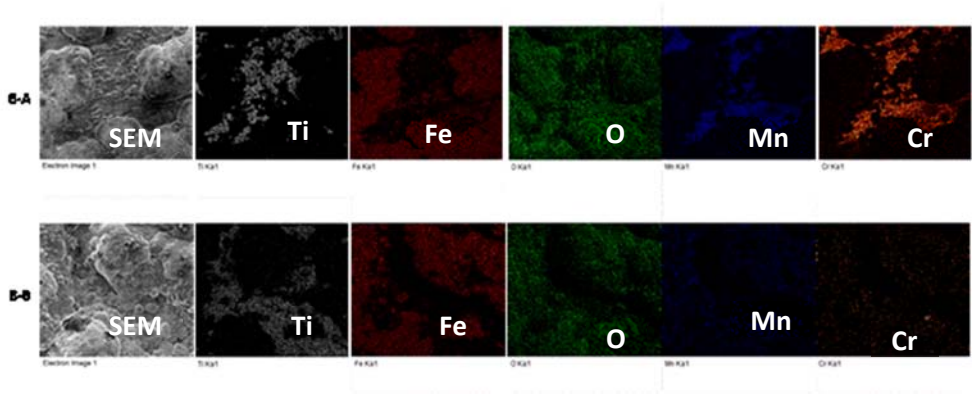

Figure 147. SEM image and corresponding EDS mapping results for substrate E after 800 hrs of simulated flue gas corrosion test at 700 °C.

Substrates C after 800 hrs simulated flue gas corrosion test at 700 °C

SEM secondary electron images and back scattering electron images for both sides of substrate C (C-A and C-B) after 800 hrs of simulated flue gas test are shown in Figure 148 (a) and (b). Side A of substrate C (C-A) was coated with titanium metal at low N_2 carrier flow for 12 minutes, and side C (C-B) was coated with high carrier flow for 3 munities. Large iron oxide particles as observed from substrate B was not found on surface of substrate C. At higher magnification,

island-like structure was observed from side A, while column structures partially covered by iron oxide was presented on side B. The column structures were identified as titanium-rich. EDS mapping results for both sides of substrate C (C-A and C-B) after 800 hrs of simulated flue gas test are shown in Figure 149 (a) and (b). Traces of Titanium was not observed on the surface of side A, only Fe, Cr, Mn, and O was observed. On the other hand, Ti coatings were observed on surface of side B. Distribution of iron was found mostly concentrated at areas without Ti. This indicates the formation of iron oxide took place mainly at areas without Ti coating.

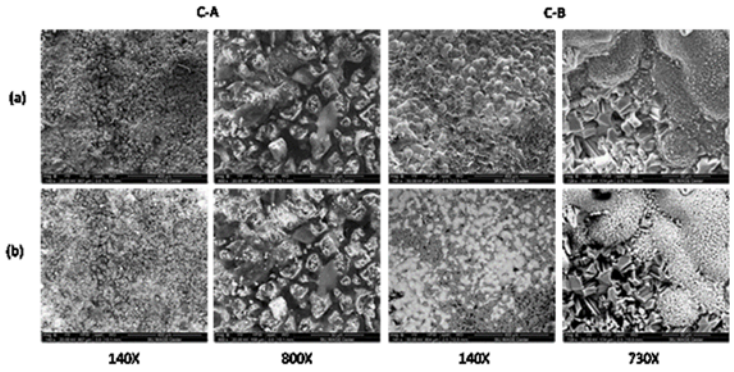

Figure 148 SEM (a)Secondary electron and (b)Backscattering electron images of both sides of substrate C (C-A and C-B) after 800 hrs of simulated flue gas corrosion test at 700 °C at low and high magnification.

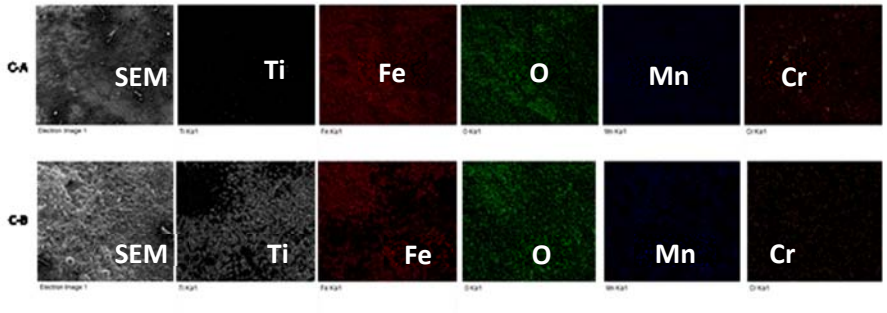

Figure 149. SEM image and corresponding EDS mapping results for substrate E after 800 hrs of simulated flue gas corrosion test at 700 °C.

Substrates D after 800 hrs simulated flue gas corrosion test at 700 °C

SEM secondary electron images and back scattering electron images for both sides of substrate D (D-A and D-B) after 800 hrs of simulated flue gas test are shown in Figure 150 (a) and (b). Both sides of the substrates were coated with TiC powders at high N_2 carrier flow. Side A of the substrate D (D-A) was for 12 minutes, and side D (D-B) was coated for 12+12 minutes. Compared to SEM images taken for both sides of substrate D before the corrosion test, the Ti structure on the surface transformed from droplet-like structures throughout the surface to grains with sharp edges distributed by the newly formed iron oxide particles. According to our studies on Ti coatings on 304 and 430 stainless steels, the grains observed on these surfaces are expected as grains of titanium oxide. Also, large iron oxide particles (>50um in diameter) were observed tightly adjacent

to the titanium oxide grains. Higher number of iron oxide particles over 100um in diameter were observed on surface of side A compared to side B.

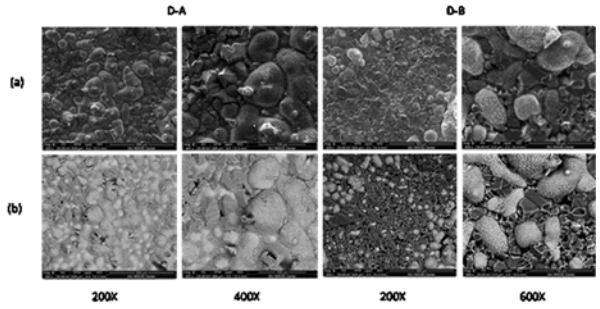

Figure 150. SEM (a)Secondary electron and (b)Backscattering electron images of both sides of substrate D (D-A and D-B) after 800 hrs of simulated flue gas corrosion test at 700 °C at low and high magnification.

EDS results show good agreement with aforementioned observation from the SEM images. EDS mapping results for both sides of substrate D (D-A and D-B) after 800 hrs of simulated flue gas test are shown in Figure 151 (a) and (b). Similar to previously analyzed Ti coated substrates, a clear interface between Ti and Fe can be observed from the elemental maps for both side A and B for this substrate. Chromium was considered absent according to our EDS analysis results on both sides of the substrate.

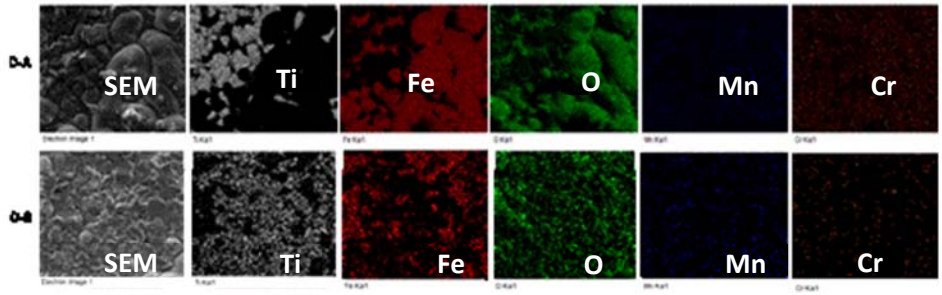

Figure 151 SEM image and corresponding EDS mapping results for substrate E after 800 hrs of simulated flue gas corrosion test at 700 °C.

Substrates F after 800 hrs simulated flue gas corrosion test at 700 °C

SEM images of both sides of substrate F (F-A and (F-B) at low and high magnification are as shown in Figure 152: (a)Secondary electron, and (b) back scattering electron images. Both sides of the substrate were glass-blasted and then coated with TiC powders as source, but with low N_2 carrier flow for side A, and high carrier flow for side B. Both coated for 12 minutes. No obvious formation of large iron particles was observed on the surface of substrate F compared to substrate B, C, and D. At higher magnification (400X), it was observed that side A consisted of column structures extruding out from the matrix. The column structures were characterized as iron oxide from EDS result. Side B, on the other hand, had iron oxide particles less than 100 μm in diameter surrounded by grains with sharp edges. EDS data of the surface is shown in Figure 153.

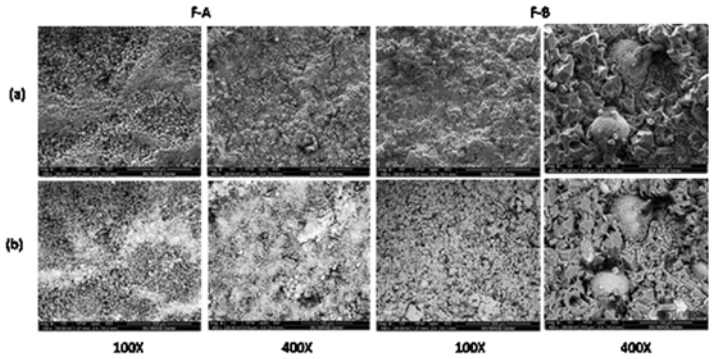

Figure 152. SEM (a)Secondary electron and (b)Backscattering electron images of both sides of substrate F (F-A and F-B) after 800 hrs of simulated flue gas corrosion test at 700 °C at low and high magnification.

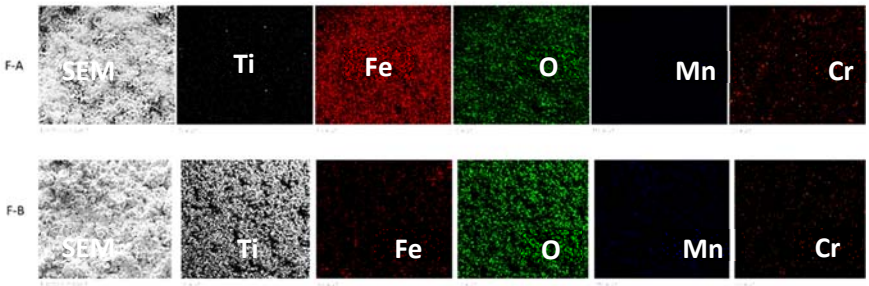

Figure 153. SEM image and corresponding EDS mapping results for substrate F after 800 hrs of simulated flue gas corrosion test at 700 °C.

Substrate A after 800 hrs simulated flue gas corrosion test at 750°C

Figure 154 shows the SEM and EDS mappings of cross section of substrate A (Control, no coating) after 800 hrs of simulated flue gas corrosion test at 750°C. Clear oxidation scale can be observed from the oxygen maps. An Fe oxide layer (partially chipped off) was observed at the surface of the substrate where only very little amount of Cr was detected. At area below the iron oxide layer, higher concentration of Cr and lower amount of Fe was observed within the O rich area compared to the matrix which was not attacked by oxidation. This indicated the formation of chromium oxide protection layer close to surface of the P91 substrate. The Fe oxide layer observed from this cross section analysis is in agreement with the iron oxide scale observed from surface of the substrate observed after 180 hrs of testing (Figure 155). Based on this data it is clear that the Cr content on pristine P91 steel was not sufficient to form uniform chromium oxide layer throughout surface of the steel under the tested condition

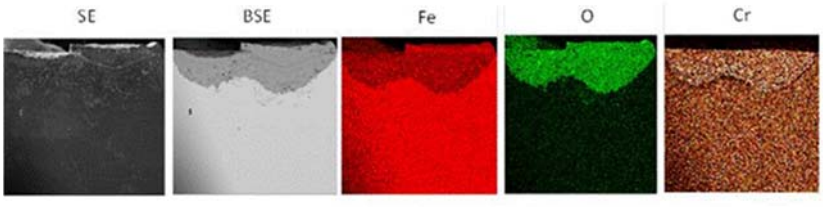

Figure 154. SEM- Secondary Electron (SE), Backscattering Electron (BSE) images and EDS mapping results of cross section of substrate A after 800 hrs of simulated flue gas corrosion test at 750°C.

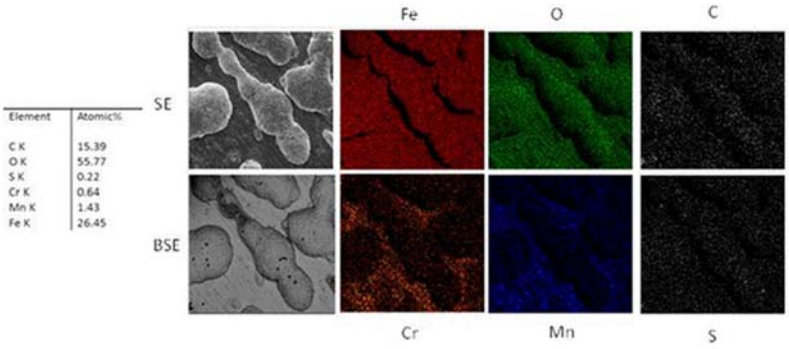

Figure 155. SEM (Secondary and Backscattering electron) images and corresponding EDS mapping results for surface of substrate A after 180 hrs of simulated flue gas corrosion test at 750°C.

Substrate E after 800 hrs simulated flue gas corrosion test at 750°C

Substrate E was glass blasted substrate without coating. Figure 156 shows the SEM images and EDS mappings for cross section of substrate E after 800 hrs of simulated flue gas corrosion test at 750°C. A loose iron oxide layer was observed from the surface of the substrates. The surface of the substrate is dominated by iron oxide scale even after 180 hrs of exposure (Figure 157). Quantitative elemental analysis results also showed 55.25 at% oxygen, 28.9 at% iron, and negligible amount (0.02 at %) of chromium on the surface of the substrate after 180 hrs of simulated corrosion test. Chromium oxide layer was also observed underneath the iron oxide layer. Higher concentration of chromium was observed at the interface between the chromium oxide layer and matrix of the substrate not attacked by oxidation.

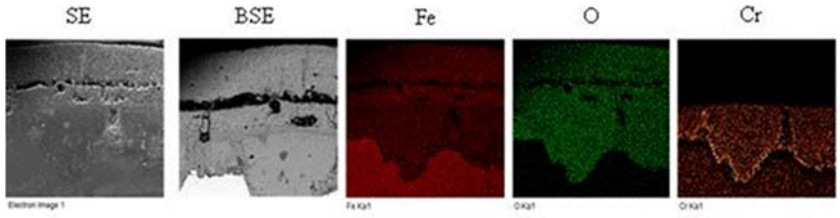

Figure 156. SEM- Secondary Electron (SE), Backscattering Electron (BSE) images and EDS mapping results of cross section of substrate E after 800 hrs of simulated flue gas corrosion test at 750°C.

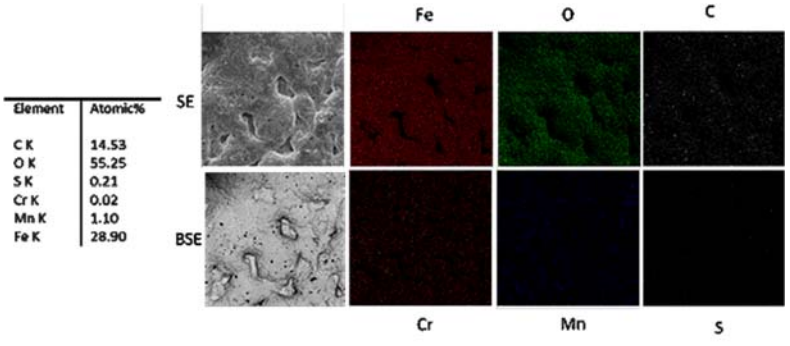

Figure 157. SEM (Secondary and Backscattering electron) images and corresponding EDS mapping results for surface of substrate E after 180 hrs of simulated flue gas corrosion test at 750°C.

SEM images and EDS mapping analysis results for the cross section of substrates without coatings- A and E are as shown in Figure 158. A spalling layer of iron oxide was observed for both substrates,

whereas a second iron oxide layer (deeper from the surface) was still intact with the P91 steel matrix. A chromium oxide layer was also observed underneath the second iron oxide layer. From the oxygen maps and chromium maps, it can be observed for both substrates that depth of oxygen penetration matches the depth of the chromium rich layer near the surface of the substrate. This indicated the formation of chromium oxide layer in both P91 steel substrates retarded the oxidation penetration from the simulated flue gas corrosion environment.

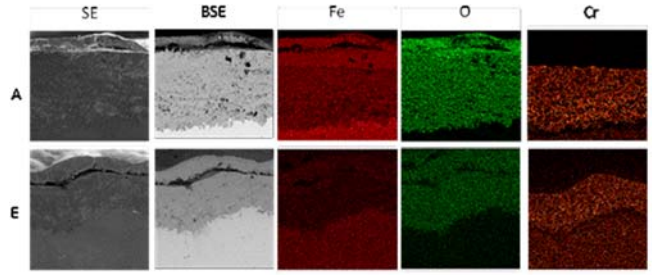

Figure 158. SEM- Secondary Electron (SE), Backscattering Electron (BSE) images and EDS mapping results of cross section of substrate A after 180 hrs of simulated flue gas corrosion test at 750°C.

Substrate B, C, and D after 800 hrs simulated flue gas corrosion test at 750°C

Figure 140-142 shows the SEM and EDS mappings of cross section of substrate B, C, and D after 800 hrs of simulated flue gas corrosion test at 750°C. Substrate BA was coated with TiC powders at low N_2 carrier flow for 12 minutes, and substrate BB was coated with high carrier flow for 3 munities. Substrate CA was Ti metal coated with low N_2 carrier flow for 12 minutes, and substrate CB was coated with high N_2 carrier flow for 12 minutes. Substrate DA was TiC coated for 12 minutes, and DB was coated for 12+12 minutes.

Presence of iron oxide layer over the chromium oxide layer was observed at the surface for all the titanium coated substrates. Also, a clear interface between titanium layer and the chromium oxide layer was observed from the EDS mapping results. Separation of iron oxide layer at the surface of substrates was observed for substrates CA, CB, DA, and DB. No chromium was observed at the separated layer. Also, at the interface between the chromium rich layer and the P91 steel matrix, localized area with higher concentration of chromium was observed. According to the depth of oxidation penetration, it was observed that better oxidation protection was achieved from substrates coated with higher N_2 carrier flow with same coating material, or substrate coated for longer period of time under same coating conditions.

Cross section SEM/ EDS analysis for the titanium coated substrates (substrate B, C, D, and F) after 180 hrs simulated flue gas corrosion test at 750°C (Figure 159). Compared to substrates tested for 800 hrs under simulated flue gas corrosion test at 750°C, iron oxide layer at the surface of substrates were still intact as compared to the spalling iron oxide layers previously observed. However, oxygen penetration can be observed. Note the sharp interface for chromium near the surface of the substrates. It was suspected that the spalled/ separated iron oxide layer observed from the substrates after 800 hrs simulated flue gas test at 750°C was gradually separated from the P91 matrix from chromium interface after prolong exposure to corrosion environment.

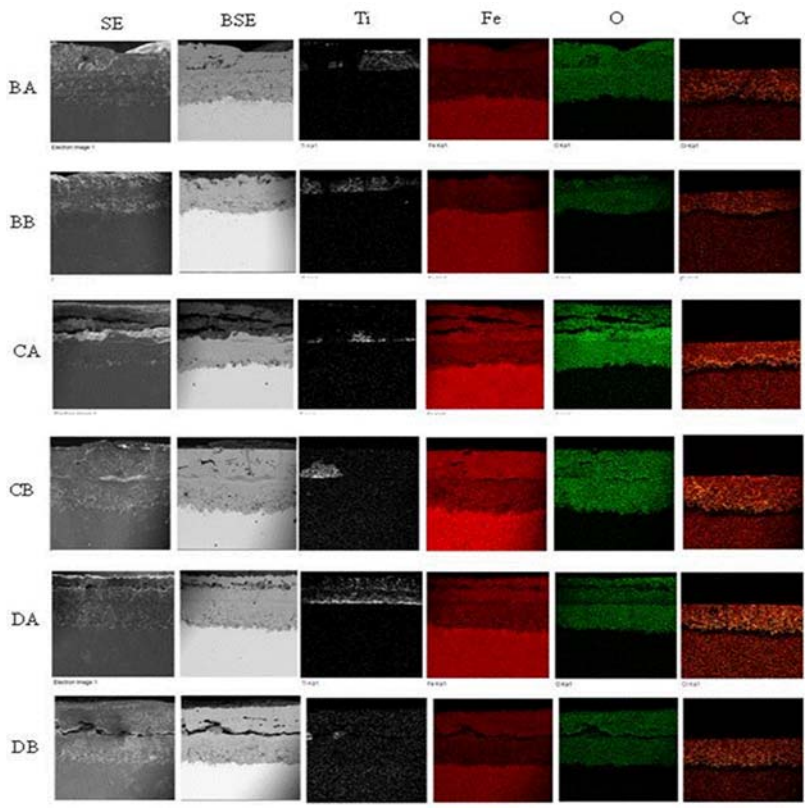

Figure 159. SEM- Secondary Electron (SE), Backscattering Electron (BSE) images and EDS mapping results of cross section of substrate BA, BB, CA, CB, DA, and DB after 180 hrs of simulated flue gas corrosion test at 750°C.

A layer of mixture of titanium, iron and oxygen was observed at the surface of substrate DA. The titanium layer appeared to have a clear interface with the chromium oxide layer near surface of the substrate. Top surface SEM and EDS mapping results for samples B, C and D after 180 hrs simulated flue gas corrosion test at 750°C are shown in Figure 160. Substrate BA was coated with TiC powders at low N_2 carrier flow for 12 minutes, and BB was coated with high carrier flow for 3 munities. The surface coverage of TiC for the A surface is much greater for side A. For both sides of sample C (coated with Ti metal), distribution of iron was found mostly concentrated at areas without Ti. Unlike the TiC coated sample B, surface of substrate CB (High N2 flow rate and 3 minute coating) was uniformly coated with titanium coating, while substrate CA was partially coated. A few large iron oxide scale was observed on surface of substrate CA, while surface of substrate CB was relatively smoother, with no sign of iron oxide formation. At the analyzed area, surface of substrate DA was more thoroughly coverer by titanium, and therefore less iron oxide scale was observed from the EDS results. On substrate DB, high concentration of chromium was observed at area not being coated by titanium, whereas chromium content is uniformly low on surface of substrate DA.

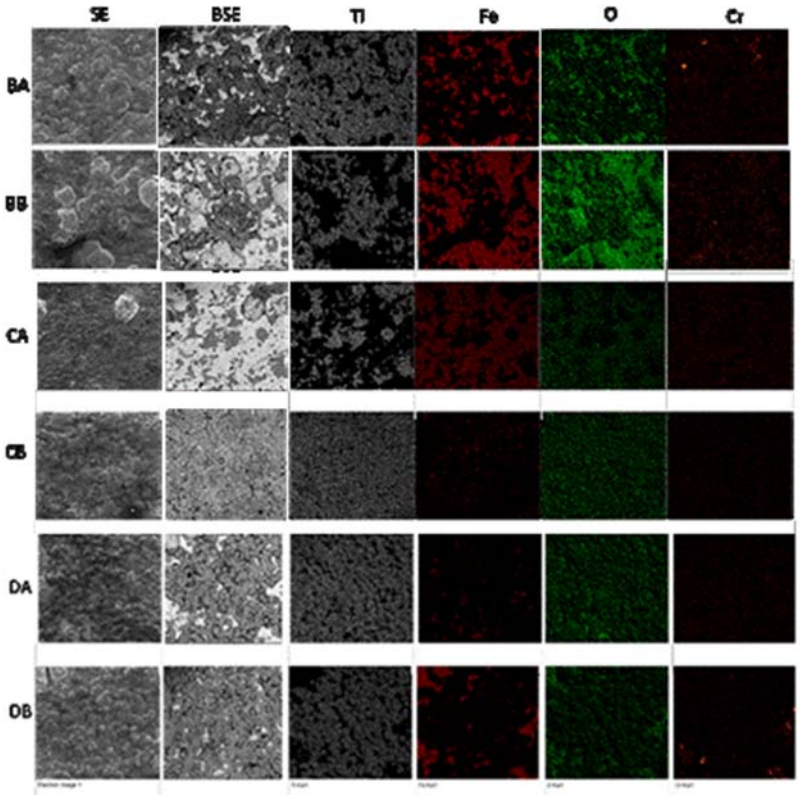

Figure 160. SEM (Secondary and Backscattering electron) images and corresponding EDS mapping results for surface of substrate BA and BB after 180 hrs of simulated flue gas corrosion test at 750°C.

Substrate F after 800 hrs simulated flue gas corrosion test at 750°C

Substrate F was glass blasted P91 substrate (substrate E) coated with titanium coatings. Both sides of the substrate were coated with TiC powders as source, but with low N_2 carrier flow for side A, and high carrier flow for side B, both coated for 12 minutes. Figure 161 shows the SEM and EDS mappings of cross section of substrate F after 800 hrs of simulated flue gas corrosion test at 750°C. Presence of iron oxide layer over chromium oxide layer was also observed for both substrates. However, for substrates FB, two layers of titanium were observed from the EDS mapping result. SEM images and EDS mapping results of the top surface for substrate FA and FB after 180 hrs simulated flue gas corrosion test at 750°C are shown in Figure 162. A dense titanium coated area was observed for substrate FB, where titanium coating was covering the entire coated area, and very little iron and chromium can be detected. Coatings on FA, however, was mixed with iron oxide scale formed after corrosion test.

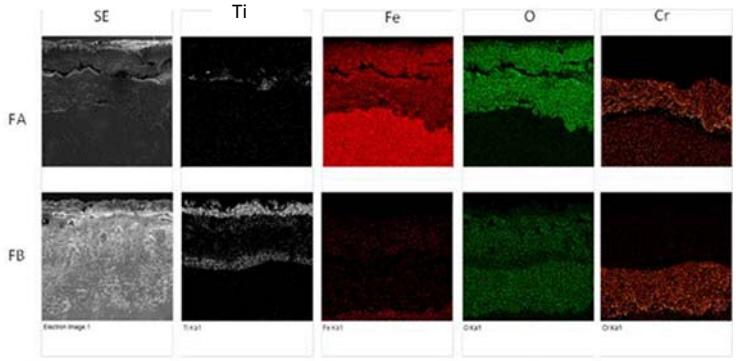

Figure 161. SEM- Secondary Electron (SE), Backscattering Electron (BSE) images and EDS mapping results of cross section of substrate F after 800 hrs of simulated flue gas corrosion test at 750°C.

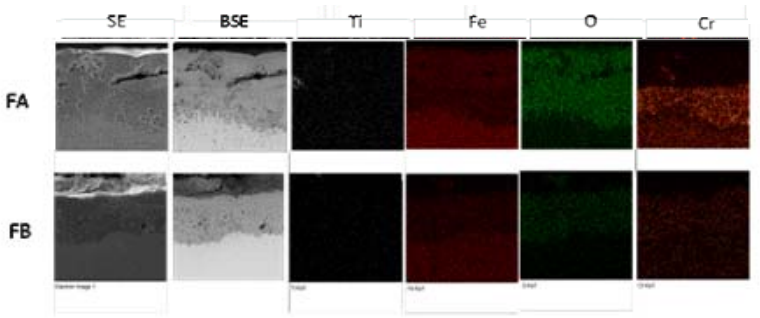

Figure 162. SEM images and corresponding EDS mapping results for cross section of F of substrate CA and FB after 180 hrs of simulated flue gas corrosion test at 750°C.

Substrates A and E after 180 hrs simulated flue gas corrosion test at 650°C

Figure 163 shows the SEM images and EDS mapping and quantitative elemental analysis results for substrate A after 180 hrs of simulated flue gas test at 650°C. Iron, oxygen, and carbon are the dominating elements on the surface of substrate. Porous structure due to sulfur attack can be observed at sulfur-rich area. Compared to substrates tested under simulated flue gas condition at 750°C, large iron oxide scales were not observed. EDS mapping results showed 57.2 at% oxygen, 4.3 at% chromium, and 24.46 at% iron on surface of the substrate, compared to 55.7 at% oxygen, 0.64 at% chromium, and 26.45 at% iron for same substrate tested under simulated flue gas condition at 750°C for 180 hrs. The drastic difference on amount of chromium detected is suspected to be due to formation and growth of large iron oxide scale formed on surface of substrate at simulated flue gas tests conducted at 750°C.

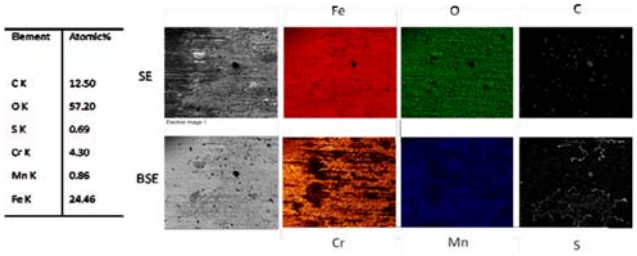

Figure 163. SEM (Secondary and Backscattering electron) images and corresponding EDS mapping results for surface of substrate A after 180 hrs of simulated flue gas corrosion test at 650°C.

SEM images and EDS mapping analysis results for the cross section of substrates without coatings-A and E are as shown in Figure 164. An iron oxide layer can be observed at the surface of both the substrates where no chromium was presented. Chromium oxide layer was observed underneath the iron oxide layer. From the oxygen maps and chromium maps, it can be observed for both substrates that depth of oxygen penetration matches the depth of the chromium rich layer near the surface of the substrate. This indicated the formation of chromium oxide layer in both P91 steel substrates retarded the oxidation penetration from the simulated flue gas corrosion environment. Compared to the cross section analysis result of the same substrates after 180 hrs of simulated flue gas corrosion test at 750°C, the spalling iron oxide was not observed on this set of substrates. Chromium distribution was also found to be less dense compared to the results previously reported for substrates after 750°C simulated flue gas testing environment. Figure 165 shows the SEM images (SE, BSE), EDS mapping and quantitative elemental analysis results for glass blasted substrate E after 180 hrs of simulated flue gas test at 650°C. Compared to substrate A under same testing condition, surface of substrate E is considerably rougher. Also, according to quantitative

analysis result, amount of iron was higher, and chromium was lower compared to substrate A. Chromium oxide observed on the surface were less continuous (more localized).

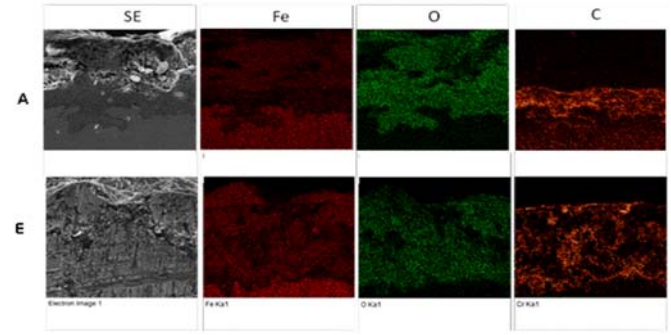

Figure 164. SEM- Secondary Electron (SE), and EDS mapping results of cross section of substrate A and E after 180 hrs of simulated flue gas corrosion test at 650°C

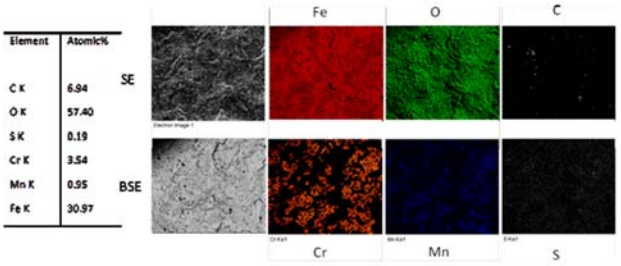

.Figure 165. SEM (Secondary and Backscattering electron) images and corresponding EDS mapping results for surface of substrate E after 180 hrs of simulated flue gas corrosion test at 650°C.

Substrates B, C and D after 180 hrs simulated flue gas corrosion test at 650°C

SEM images and EDS mapping data for both A and B sides of substrates B, C and D after 180 hrs simulated flue gas corrosion test at 650°C are shown in Figure 166. Titanium coatings covered most of the surfaces for both sides of sample B while substrate BA being covered more thoroughly. Iron oxide can be observed at areas not covered by titanium coating. Higher amount of oxygen compared to the surroundings was observed at where iron oxide presented. Chromium was found to be uniformly distributed throughout surface of substrate while chromium content on substrate BB is higher compared to substrate BA. From the SEM images, it was observed that titanium coating on substrate CA was not as uniform when compared to substrate CB. Flake-like structures can be observed at gaps on the surface not covered by titanium coating. EDS result also showed localized area with higher concentration of iron, chromium, and oxygen. The flake-like structures on surface of substrate CA were confirmed as iron and oxygen-rich structures.

For Sample D, titanium coating was not sufficient in covering the P91 substrates for substrate DA. Formation of iron oxide can be observed on the surface of substrate. However, no localized area with high concentration of chromium was observed. Titanium coatings on substrate DB on the other hand, covered part of the substrate and prevented formation of iron oxide at the covered area. Formation of chromium oxide was observed at some interface between the titanium coating and iron oxide formed after the corrosion test.

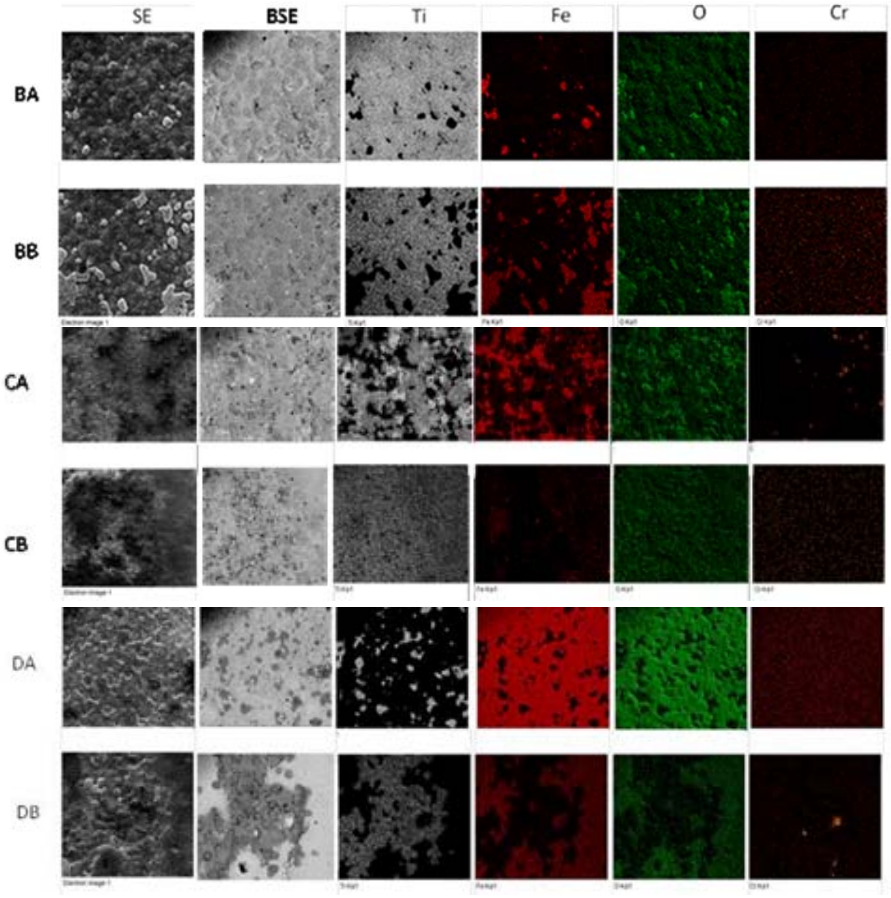

Figure 166. SEM images and corresponding EDS mapping results for surface of substrate B, C and D after 180 hrs of simulated flue gas corrosion test at 650°C.

Substrates F after 180 hrs simulated flue gas corrosion test at 650°C

Substrate F was glass blasted P91 substrate (substrate E) with TiC powders, with low N_2 carrier flow for substrate FA, and high carrier flow for substrate FB. Both coated for 12 minutes. SEM secondary, back scattering electron images and EDS mapping results for substrate FA and FB after 180 hrs simulated flue gas corrosion test at 650°C are shown in Figure 167. A dense titanium coating was again observed on substrate FB, which coincide previous observation for substrates after 180 hrs of corrosion test at 750°C. Iron and chromium amount on surface of substrate FB were considerably lower compared to results observed from surface of substrate FA. On surface of substrate FA, part of titanium coating was lifted by iron oxide formed beneath the coating. Localized spots with high chromium content were also observed from surface of substrate FA.

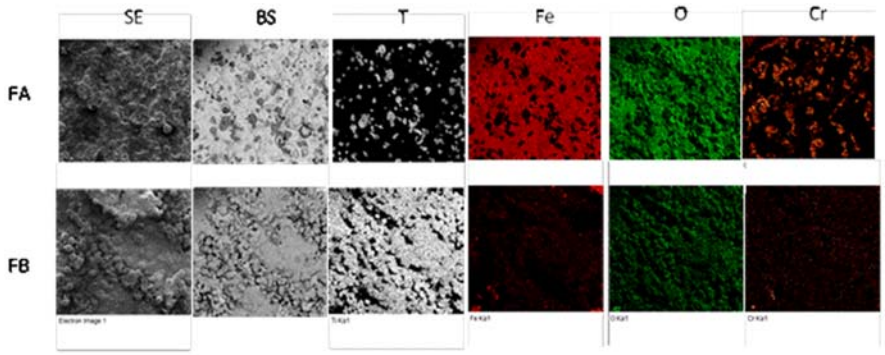

Figure 167. SEM images and corresponding EDS mapping results for surface of substrate A after 180 hrs of simulated flue gas corrosion test at 650°C

Cross sectional analysis

Cross section SEM/ EDS analysis for the titanium coated substrates (substrate B, C, D, and F) after 180 hrs simulated flue gas corrosion test at 650°C was also performed. Results for the analysis are shown in Figure 168. From the mapping results, it can be observed that the titanium coating prevented formation of iron oxide when sufficient amount and dense enough titanium layer was present (for example, BA, BB, CA). Following by the titanium coating, a layer with less amount of iron as compared to the matrix can be observed, followed by a chromium rich layer. Oxygen amount was found significantly decreased at area deeper into the substrate beyond the chromium rich layer.

Chromium distribution on the chromium rich layer on these substrates were not as dense as compared to substrates from simulated flue gas corrosion test at 750°C. Also, although surface layer separation was observed from substrate CB and DA, the Ti surface coating appeared to have retarded the oxidation of the substrates.

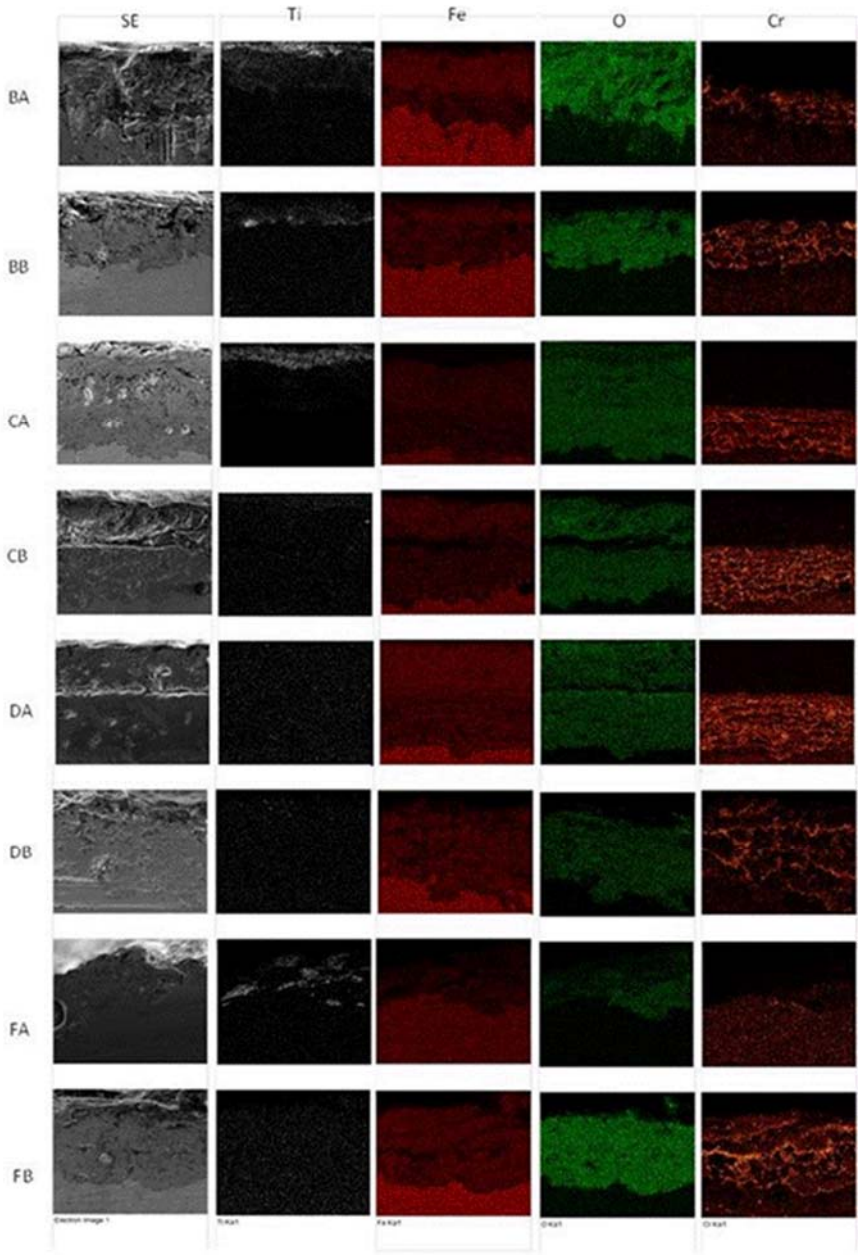

Figure 168. SEM images and EDS mapping results of cross section of substrate BA, BB, CA, CB, DA, DB after 180 hrs of simulated flue gas corrosion test at 650°C.

Steam and Air Corrosion test at 700 ^{0}C

Pristine P91 and P91 substrates coated using both Ti metal and TiC nanoparticles were tested in steam and air environment at 700 ^{0}C for 180 hrs. Substrates were analyzed using SEM/ EDS after the corrosion tests, and the results are reported as follows.

Pristine P91 substrates corrosion test in mixture of steam and air at 700°C

Figure 169 and Figure 170 shows the SEM images and corresponding EDS mapping results for surface and cross section, respectively of pristine P91 substrates with and without surface roughening (A and E) after 180 hrs of exposure to steam and air at 700°C. A rougher morphology can be observed on the surface of substrate E due to sand blasting. Iron oxide scales can be observed covering most surface of both substrates. XRD results showed Hematite phase on surface of both the substrates (Fe_2O_3). EDS elemental composition results of the substrates are as shown in Table 15. Slightly higher amount of iron on substrate E compared to substrate A (41.21% vs 37.69%) may be the result of higher amount of iron oxide formed on the surface of substrate E.

Table 15. Elemental composition of pristine P91 substrates with and without surface roughening (A and E) after 180 hrs of steam and air corrosion test at 700°C

Substrate A	
Element	Atomic%
O K	60.39
Cr K	0.52
Mn K	1.07
Fe K	37.69

Substrate E	
Element	Atomic%
O K	57.18
Cr K	0.31
Mn K	1.31
Fe K	41.21

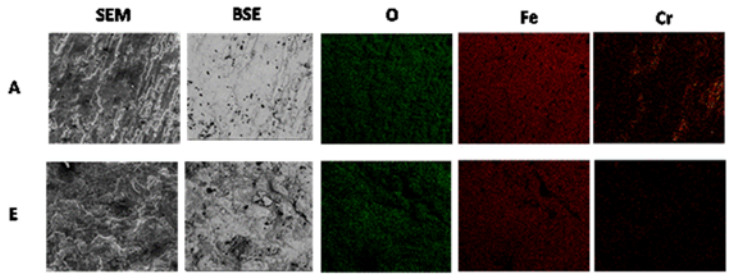

Figure 169. SEM images (Secondary and Backscattering electron) and corresponding EDS mapping results for surface of pristine P91 substrates with and without surface roughening (A and E) after 180 hrs in steam and air environment at 700°C.

From the cross section data, a duplex oxidation layer containing an iron rich upper layer and a Fe-Cr rich oxidation layer can be observed from cross section of both substrates. The Fe- Cr rich oxidation layer was thicker on substrate A compared to the layer on substrate E. A thin layer of high chromium content was observed at the interface of Fe- Cr rich oxidation layer and the P91 matrix (which was not observed on substrate A. Also, a gap could be observed near the interface of the upper oxidation scale and the Fr- Cr rich oxidation layer on substrate E. This could be due to the evaporation and depletion of the chromium content in the substrate according to literature.

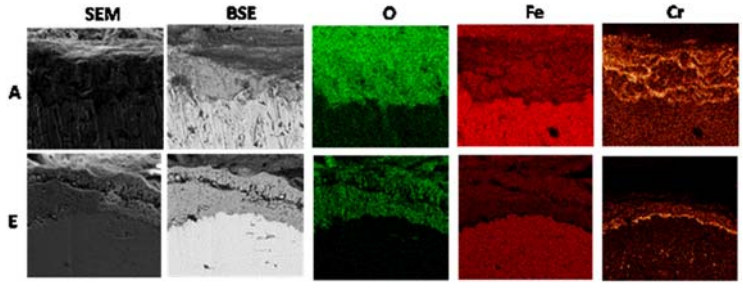

Figure 170. SEM images and corresponding EDS mapping results for cross section of pristine P91 substrates with and without surface roughening (A and E) after 180 hrs in steam and air environment at 700°C

Ti coated P91 substrates corrosion test in mixture of steam and air at 700°C

SEM analysis was conducted for the P91 substrate coated using Ti metal after 180 hrs of exposure to steam and air at 700°C, and the results for surface and cross section as well as corresponding EDS maps are as shown in Figure 171. When compared to the pristine P91 substrates, iron oxide scale observed on the surface of pristine P91 after corrosion test was not observed on the surface of the Ti coated substrate. From the SEM top view images (secondary and backscattering) as well as the Ti mapping, a uniform Ti coating can be observed. Small amount of iron and chromium can be observed at areas not coated with the Ti coating, otherwise, the two elements were absent at coated areas.

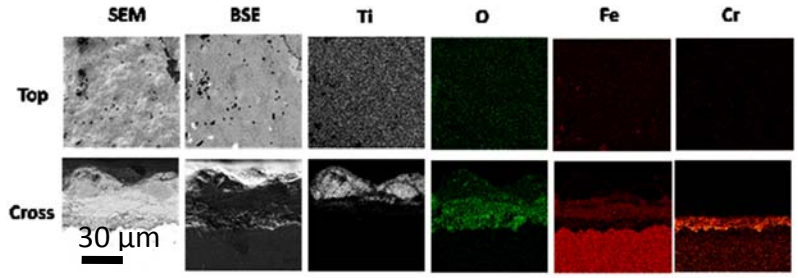

Figure 171. SEM images and corresponding EDS mapping results for surface and cross section of P91 substrate coated using Ti metal after 180 hrs in steam and air environment corrosion test at 700°C.

Cross sectional SEM analysis indicated oxidation penetration depth of less than 30 µm compared to the oxidation penetration of pristine P91 substrate (over 60 µm). The duplex oxidation layer was observed on the Ti coated substrate with a thicker iron oxide layer (~25 µm) compared to the Fr-Cr rich oxidation layer (~15 µm). Slightly higher concentration of Cr can be observed at the interface of the Fr- Cr rich oxidation layer and the P91 matrix.

TiC coated P91 substrates corrosion test in mixture of steam and air at 700°C

Figure 172 shows the SEM analysis results for TiC coated P91 substrate subjected to 700 ^{o}C steam and air environment for 180 hrs. Similar to the surface morphology observed on the Ti metal coated substrate, iron was only observed at areas without the Ti coating. Oxygen content is also noticeably higher at areas without coating. As with the Ti metal coated substrates, iron oxide scale observed on the surface of pristine P91 was not observed on the coated area of the TiC coated P91 substrates. Cross section analysis of the substrate showed a less than 20 µm thick oxidation penetration along with the iron oxide- Fe-Cr rich oxidation layer duplex oxidation layer under the Ti coating. The thickness of the upper iron oxide layer (~12 µm) and the Fe-Cr rich oxidation layer (~11 µm) was similar, unlike what was observed from the cross section analysis of the Ti coated P91 substrates. The oxygen penetration observed on both the coated substrates were suspected to have penetrated into the substrate from areas not coated with the coating.

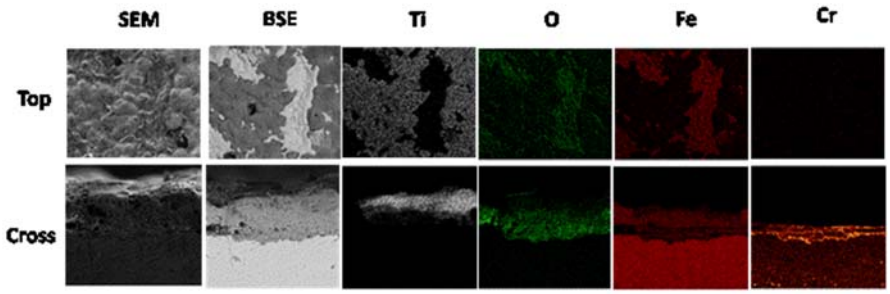

Figure 172. SEM images and corresponding EDS mapping results for surface and cross section of P91 substrate coated using TiC nanoparticles after 180 hrs testing in steam and air environment corrosion test at 700°C.

700 ^{o}C steam and air driven corrosion on Substrates F

Substrate F was glass blasted P91 substrate (substrate E) with TiC powders, with low N_2 carrier flow for substrate FA, and high carrier flow for substrate FB. Both coated for 12 minutes. SEM secondary, back scattering electron images and EDS mapping results for substrate FA and FB after 180 hrs corrosion test in a flow of 700°C steam and air are as shown in Figure 173.

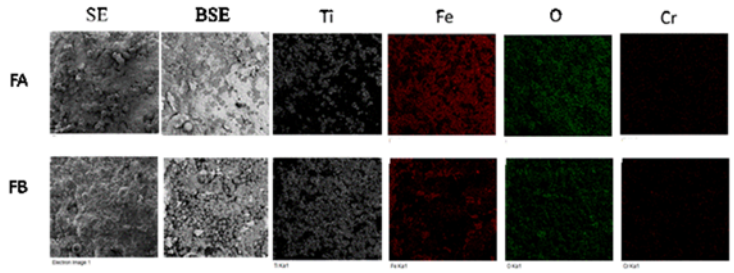

Figure 173. SEM images and corresponding EDS mapping results for surface of substrate FA and FB after exposure to steam an air at 700 ^{0}C for 180 hrs.

On the surface of both substrate FA and FB, Ti coatings consisted of coating particles were observed. Oxidation scales were observed forming at the vacancies of the particulate Ti coating. However, the formation of the oxidation scale was significantly retarded by the coating on the substrate FB, due to the higher density of the coating. Lateral growth of the oxidation scale was also observed on substrate FA, covering Ti coatings on the surface of the substrate.

From cross sectional analysis, the thickness of the oxidation layer was found to be thinner for areas covered with Ti coating, with an apparent thinner layer of oxygen distribution according to the EDS mappings. For substrates except DB and FA, a clear chromium oxide layer can be observed at the interface of the oxidation layer and the P91 matrix. This indicated the formation of chromium oxide as a protective layer for the P91 matrix, stopping oxygen from further penetrating into the matrix. For substrates BB, CB, and FA, traces of chromium oxide can be observed all the way to the surface, while the chromium distribution was found mostly concentrated underneath the surface iron oxide layer.

Figure 174 summarizes the findings of the steam and air oxidation studies.

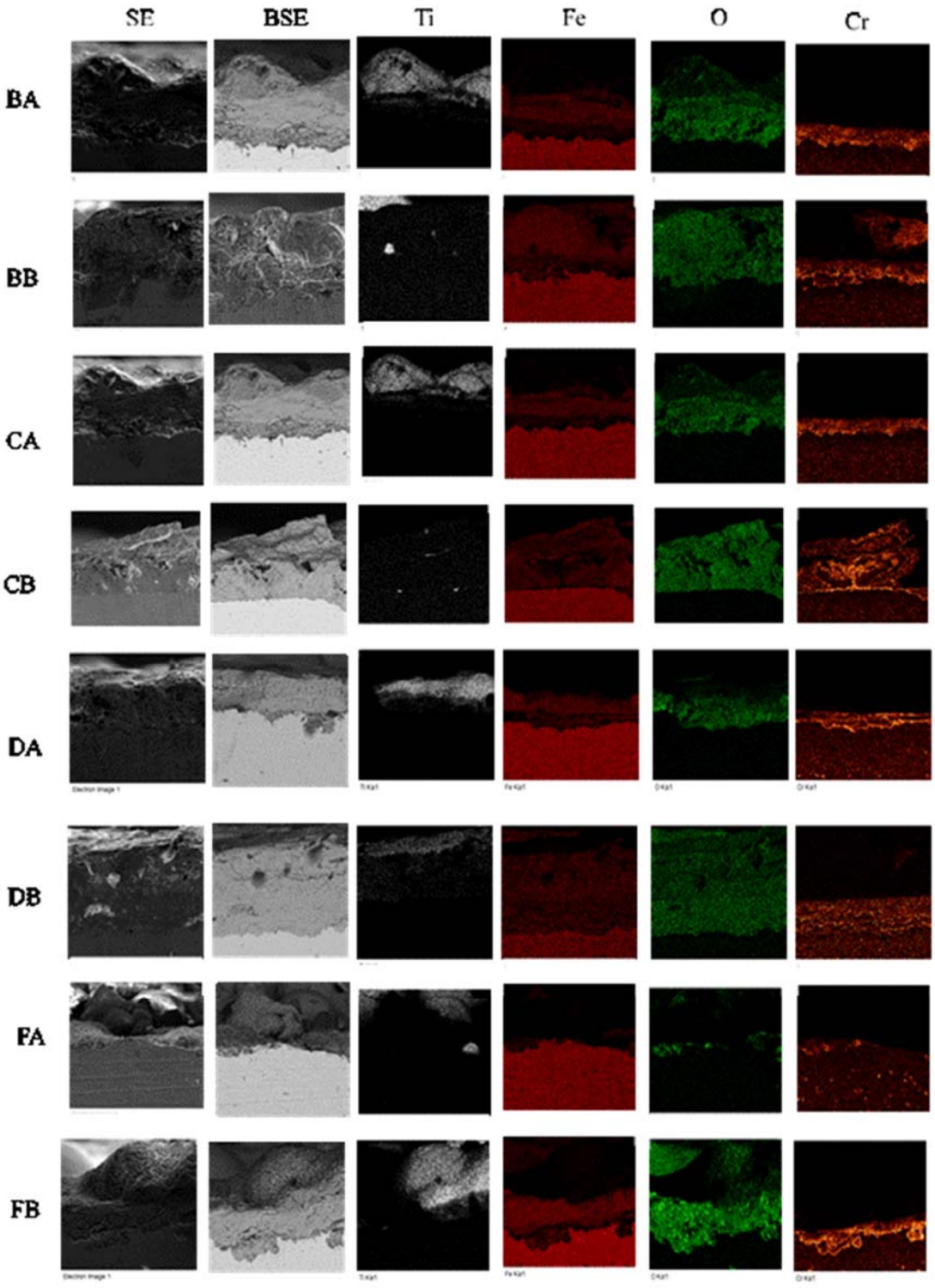

Figure 174. SEM- Secondary Electron (SE), Backscattering Electron (BSE) images and EDS mapping results of cross section of substrate BA, BB, CA, CB, DA, and DB after steam and air corrosion test at 700 ^{0}C for 180 hrs

Air oxidation study at 700 ^{0}C for 180 hrs

Pristine P91 substrates air oxidation at 700°C

SEM analysis results and corresponding EDS mapping results for surface of pristine P91 substrates with and without surface roughening (A and E) after 180 hrs of air oxidation test at 700°C is as shown in Figure 175. Compared to pristine substrates tested in steam and air environment surface of the pristine P91 substrates after air oxidation test are considerably smoother. The large iron oxide observed on the surface of the pristine substrates after steam and air corrosion test was not observed on this batch of substrate. No significant surface scale formation was observed for substrate A. Some iron oxide scale was observed on surface of substrate E. According to EDS analysis, higher amount of oxygen was observed on the surface of substrate E (57.75%) compared to the oxygen amount on surface of substrate A (49.58%). Lower amount of Cr content was observed on substrates E (6.31%) compared to substrate A (9.19%). This can be due to the iron oxide scale observed on the surface of substrate E. From the EDS mapping results, a uniform distribution of O, Fe, and Cr was observed on the surface of substrate A.

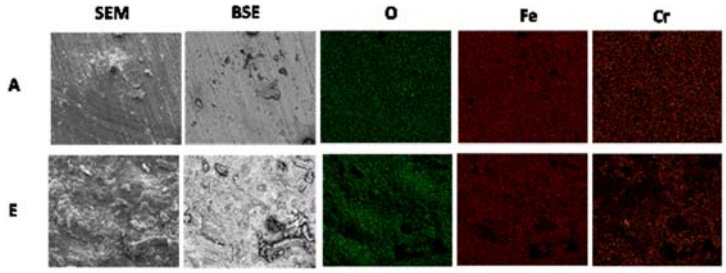

Figure 175. SEM images (Secondary and Backscattering electron) and corresponding EDS mapping results for surface of pristine P91 substrates with and without surface roughening (A and E) after 180 hrs of air oxidation test at 700°C.

Table 16. Elemental composition of pristine P91 substrates with and without surface roughening (A and E) after 180 hrs of air oxidation test at 700°C

Substrate A		Substrate E	
Element	Atomic%	Element	Atomic%
O K	49.58	O K	57.75
Cr K	9.19	Cr K	6.31
Mn K	3.2	Mn K	1.47
Fe K	38.02	Fe K	34.46

Cross sectional SEM/ EDS analysis of substrate A and E are as shown in Figure 176. A uniform distribution of iron and chromium was observed on substrate A. On substrate E, a pit at the surface had led to penetration of oxygen, and formation of corresponding chromium oxide layer in the penetrated channel. Oxidation penetration is in general, much less compared to the penetration observed on pristine substrates after steam and air corrosion test at 700 ^{0}C for 180 hrs.

Ti coated P91 substrates after 180 hrs corrosion test in air at 700°C

Figure 177 shows the SEM analysis results for P91 substrate coated using Ti metal. Dense layer of Ti coating can be seen on the surface of the substrate from both SEM top view and cross section images. Overlapping of Ti coating was also observed from the SEM top view image. Uniform Ti distribution can also be observed from the Ti EDS mapping. Similar to other Ti coated substrates, iron and chromium were only observed at areas not covered by the Ti coating. Cross section EDS mapping results shows oxygen distribution within the Ti coating. A thin high chromium content

layer was observed at the interface of the Ti coating and the P91 matrix. Several local area of high chromium content can also be observed from the cross sectional Cr map. A dense Ti coating was observed on surface of substrate CB, while P91 matrix can still be seen on the surface of substrate CA. Localized oxidation scale with high concentration of Fe, O, and Cr can be observed at area not being coated with the Ti coating. On the surface of substrate CB, Ti coating was covering most of the analyzed area. EDS mapping results shows higher concentration of Fe, O, and Cr only at area not being covered by Ti. However, part of the Ti coating was partially separated from the surface according to the secondary electron image.

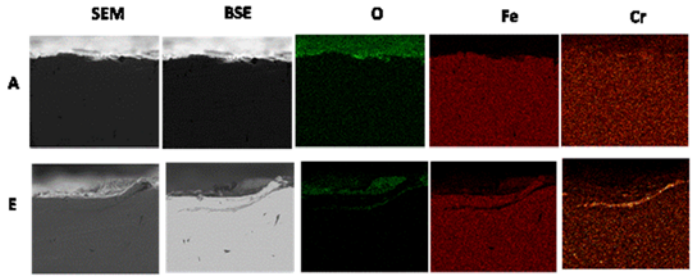

Figure 176. SEM images and corresponding EDS mapping results for cross section of pristine P91 substrates with and without surface roughening (A and E) after 180 hrs of air corrosion test at 700°C.

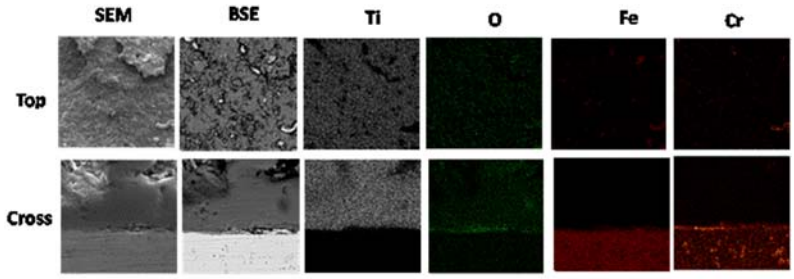

Figure 177. SEM images and corresponding EDS mapping for surface and cross section of P91 substrate coated using Ti metal after 180 hrs of air corrosion test at 700°C.

TiC coated P91 substrates after 180 hrs corrosion test in air at 700°C

SEM analysis was conducted for the P91 substrate coated using TiC nanoparticles after 180 hrs of air corrosion test at 700°C, and the results for surface and cross section as well as corresponding EDS maps are shown in Figure 178. From the SEM top view images and the Ti mapping, a uniform Ti coating can be observed. Small amount of iron and chromium can be observed at areas not coated with the Ti coating. Iron and chromium were absent at Ti coated areas. Cross section analysis results show a dense layer of Ti coating with thickness of (~35 µm) on the P91 substrate. From the oxygen map, it can be observed that oxygen was distributed within the Ti coated area. A thin layer of high chromium content was observed at the interface of the Ti coating and the P91 matrix, but no iron oxide layer was observed. The Ti coating on both substrate BA and BB consisted of particular Ti base coating particles. Better coverage of Ti coating can be observed on substrate BA when compared to substrate BB. Oxidation scales can be observed near the edges of the Ti coating but the growth of extruding scales covering Ti coating reported on substrates tested under steam and air corrosion environment at 700 ^{0}C were not observed on this set of substrates.

A different surface morphology of the Ti coating on substrate DA and DB compared to substrate C can be observed from the SEM images. Ti coating on substrate DA and DB consisted of coating particles. Multiple overlapping layers of coating can also be observed. The Ti coating appeared to

be still intact onto the substrates after the corrosion test, with substrate DA having better Ti coverage at the analyzed area when compared to substrate DB. Oxidation of the substrates can be observed at area not coated with Ti as well as formation of chromium oxide dendrites at the edge of the coating, but EDS mapping showed consistent Ti dominant elemental distribution on the Ti coated area.

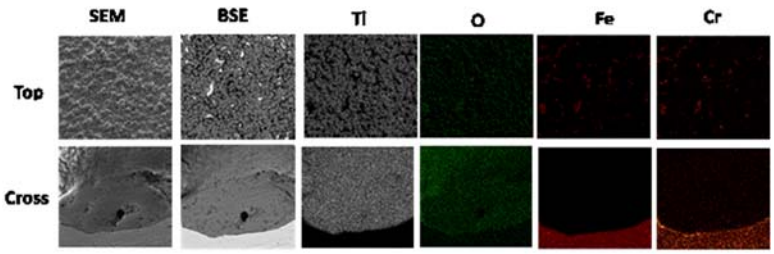

Figure 178. SEM images (and corresponding EDS mapping results for surface and cross section of P91 substrate coated using TiC nanoparticles after 180 hrs of air corrosion test at 700°C.

Figure 179 shows the combination of XRD analysis results for surface of pristine and Ti coated P91 substrates after 750 ^{0}C simulated flue gas corrosion test, 700 ^{0}C steam and air corrosion test, and 700 ^{0}C air corrosion test. For all the pristine substrates, Hematite was the major phase presented. Fe-Cr peak can also be observed on the pristine substrates as the characteristic peaks for the P91 substrates. The Fe-Cr peaks were more pronounced on pristine substrate after air corrosion test when compared to pristine P91 substrates after simulated flue gas test and steam and air corrosion test. Hematite peaks were also not as pronounce according to XRD results of the pristine P91 after air corrosion test. This should be due to the less oxidation attack from the air corrosion test leading to smaller amount of iron oxide (Hematite) formed. Rutile peaks as observed from the surface of Ti coated substrate indicated that the TiC coating had converted to TiO_2 (rutile) after corrosion tests.

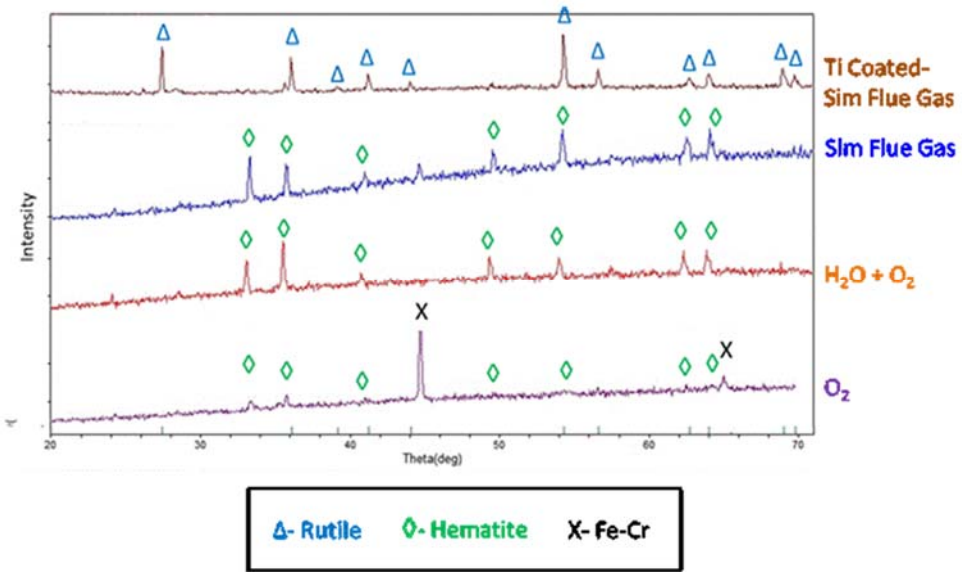

Figure 179. XRD analysis results for surface of pristine and Ti coated P91 substrates after high temperature simulated flue gas corrosion test, steam and air corrosion test, and air corrosion test.

Substrates F after 180 hrs air Corrosion test at 700°C

Substrate F was glass blasted P91 substrate (substrate E) with TiC powders, with low N_2 carrier flow for substrate FA, and high carrier flow for substrate FB. Both coated for 12 minutes. SEM secondary, back scattering electron images and EDS mapping results for substrate FA and FB after 180 hrs air corrosion test at 700°C are as shown in Figure 180.

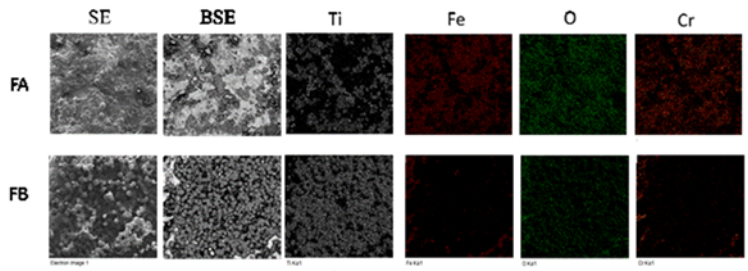

Figure 180. SEM images and corresponding EDS mapping results for surface of substrate FA and FB after air corrosion test at 700 0C for 180 hrs.

Ti coating on substrate FB showed Ti coating consisted of Ti particles while on the surface of substrate FA, a smoother Ti coating along with Ti coating particles was observed after the corrosion test. Multiple overlapping layers of Ti coating was observed on the surface of substrate FB. With the better coverage of Ti, at analyzed area of surface of substrate FB, higher concentration of Fe and Cr only occurred at area not coated with Ti. The Ti coating on both substrate FA and FB were both intact after the corrosion test. Cross section SEM/ EDS analysis for the titanium coated substrates (substrate B, C, D, and F) after 180 hrs air Corrosion test at 700 ^{0}C was performed. Results for the analysis are as shown in Figure 180. Uniform Ti coating layer can be observed from the cross section analysis of substrates BA, CA, CB, DA, DB, and FB. A thin layer of higher Cr concentration can be observed below the Ti coating layer and significantly lower traces of oxygen was observed below the Cr rich layer. This is a good indication of the dense Ti layer retarding oxygen penetration. For substrates BB and FA, significant lower amount of oxygen was observed at the Ti coated area when compared to the surrounding oxidized area. The duplex iron oxide- chromium oxide oxidation layer observed from substrates after 700^{o}C steam and air corrosion test was also only observed from substrate BB and FA, of which the titanium layers were not fully covering the entire surface. From the cross section of substrate CA, chromium distribution was observed near the surface of the substrate, while for substrate CB, localized area with high Cr concentration was observed in the P91 matrix below the thin chromium oxide layer.

During this study, it was observed that oxidation penetration can be effectively blocked when a dense titanium coating was formed on the surface of the P91 substrate. The Ti coating protected the coated substrates from oxygen attack in three of the high temperature corrosion conditions tested: simulated flue gas test, steam and air corrosion test, and air oxidation test. Similar protection against oxidation attack was observed for both substrates coated using Ti metal and using the synthesized TiC nanoparticles. With Ti metal being more than 10 times more expensive than the synthesized TiC nanoparticles, the benefit of using the synthesized TiC nanoparticles for coating material has become obvious not only due to the economic reason but also for the outstanding corrosion resistance performance.

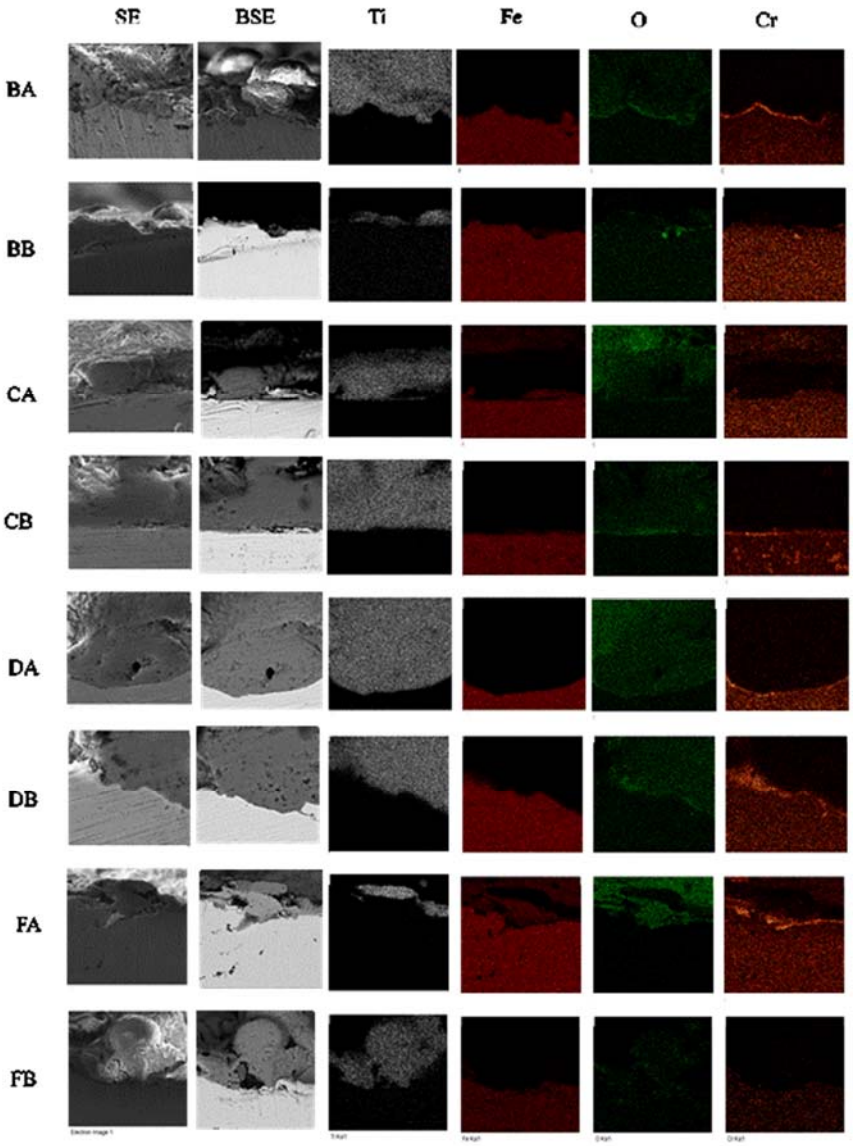

Figure 181. SEM- images and EDS mapping results of cross section of substrate BA, BB, CA, CB, DA, and DB after air driven oxidation at 700 ^{0}C for 180 hrs.

CONCLUSIONS

The project encompassed three aspects for the development of corrosion protection coatings for use in boiler and turbine parts in advanced ultrasupercritical cycles:- namely TiC and TiB_2 powder synthesis, HVOF coating of these powders on three steel substrates (304H, 430 and P91) and characterization of the corrosion resistance improvements due to these coatings against corrosive environments existing in the fireside and steam side operations in a boiler.

The TiC and TiB_2 powders were synthesized using a patented low temperature carbon coated precursor based carbothermal process. Initial HVOF thermal spray coating of these powders indicated the need for narrowing the particle size distribution range. Further experimentation with the carburizing conditions and carbon loading on the precursor was conducted the develop nano sized powders with suppression of agglomeration to obtain a narrow particle size distribution. It was found that carburizing at 1400 ^oC with 33% C coated TiO_2 carburized for 2 hrs provides the best results in times of finer sizes and narrower size distribution of the TiC powder. For TiB_2, higher %C coated TiO_2 provides more complete conversion to the product. Shorter carburizing times led to incomplete conversion to the non-oxide Ti ceramics and higher temperatures led to increased agglomeration

The optimization methodology adopted aimed at choosing the fastest path for achieving the most uniform coating. The coating process was not completely optimized by the end of the project and needs further tuning. The primary variables for the coating process can be divided into three parts: a) the properties of the coating material and substrate, b) the choice of the oxidant fuel mixture and d) the coating process parameters such as the velocity, carrier flow rate, distance from the gun and coating time. These parameters have significant interaction effects that need to be properly characterized in order to fine tune the process. In addition to the TiC and TiB_2 synthesized powders, commercially available Ti metal powders were also used for coating. At the end of the project, it was determined that H_2/O_2 mixture as the fuel oxidant mixture provides better coating than acetylene air or H_2/air. The flame temperature of the H_2/O_2 mixture was 2500 ^oC. The coating distance of 27 cm. However, the carrier gas flow, the velocity and the time of coating needs to be optimized. In some cases, the particles were bouncing off the substrate while in others the particles were not sufficiently distributed leading to localized dense coating with several locations left bare. Compared to samples coated with Ti metal, the TiC coating exhibited this phenomenon. This localized coating morphology may be a result of small particles used as source coating materials. At higher magnifications, coatings were also found to be porous in parts of the coated area, which was not observed from coatings from Ti metals. The XRD of the coatings show that irrespective of the source of Ti, some of the Ti is oxidized during the coating process.

Corrosion studies conducted under this project included air oxidation studies, steam and air oxidation studies to simulate both steam side and air side corrosion and ash corrosion studies and flue gas corrosion studies to simulate the fireside corrosion conditions. The TiC, TiB_2 and the Ti metals were successful in retarding substrate deterioration (irrespective of the substrate composition) due to the corrosive environment they were exposed to during these tests. However, coated 304 H was more resistant followed by coated 430 and finally the coated P91. The most corrosive environment was that of the simulated ash followed by the simulated flue gas conditions. Of the three coating choices, TiB_2 consistently provided the least protection although the

difference was not significantly low. In spite of more uniform coatings obtained when Ti metal was used, the TiC and the Ti metal coatings performed equally well. Since Ti metal is more than 10 fold more expensive than the synthesized TiC nanoparticles, TiC synthesized from 32 % or 33 % C coated TiO_2 and carburized for two hours at 140 or 1500 ^oC is recommended as the coating for these materials.

The coatings limited the penetration of oxygen into the substrates ranged from negligible to a few micrometers even after 800 hrs of exposure while oxygen penetration into the uncoated substrates, especially the ferritic steels, were several micrometers after 180 hrs of exposure. In the coated substrate, the oxygen penetration was largely due to the non-uniform coating applied. In most of these cases (even the low Cr steel), the oxygen penetration progress was additionally retarded by the diffusion of chromium towards the surface and forming a protective chromium oxide layer. The presence of the titanium based coating on the surface prevented the evaporation of the chromium and thus acting not only as a barrier to the oxygen from attacking the substrate but providing a second line of defense by not allowing the protective chromium to be lost. As a result, little or no difference in the oxidation between the 180 hr and 800 hr exposures was observed in many cases. The presence of both steam and oxygen was found to be more corrosive than high temperature air alone. The TiC coated materials showed little deterioration in terms of surface roughening, coarsening, spalling, and oxygen penetration, when compared to the bare substrates or with the ones coated with Ti metal or TiB_2. There is an increase in the oxygen content in the coating after exposure although TiC is also identified as a phase in the post exposure coats when TiC was used as the coating material. Based on the several tests, it is hypothesized that the coating itself may be oxidized initially but the oxide layer is non-porous and does not allow further penetration of the oxygen.

In the case of sulfur attack, whether due to the sulfates in the ash or the SO_2 in the flue gas, it was found that the sulfur tends to associate with the iron where it is not exposed to the oxygen. For example, in P91 samples, the Fe showed a duplex layer, one in the spalling top surface and one below the concentrated chromium layer (although Fe was also present in the concentrated Cr layer). It was found that the sulfur tended to concentrate towards the lower half of the concentrated Cr layer and the top of the second Fe layer. This observation was independent of the presence of coating. It should be noted here that the more uniform coatings prevented the duplex formations of Fe. In addition, it should also be noted that this observation is consistent only in cases where sulfur attack affected the substrate since there were several cases in which the coatings prevented deterioration. In coated substrates with bare surfaces, it was found that the sulfur was associated with the iron on the surface but that the sulfur was concentrated to the edges of the coated section bonded with the iron. In terms of sulfur penetration into the substrate, TiB_2 was found to be the most effective preventive coating. Thus, a uniform dense coating should prevent corrosion due to sulfur based components. The most exciting finding was that coatings performed extremely well against the attack by the sulfates, chlorides, sulfates and trisulfates of alkali metals. The bare substrates formed micro cracks in the early stages of the attack and completely disintegrated by 800 hrs, the coated substrates were not deteriorated.

The lower temperature $<700^oC$ studies showed significantly improved protection against corrosion by these coatings while the uncoated substrates showed signs of significant deterioration these lower temperatures. Thus, once the coating process is optimized, the TiC based coatings should provide long term robust protection to these stainless steels when exposed to the corrosive atmosphere in coal burning, AUSC boiler and turbine conditions.

TABLE OF FIGURES